Regulation of circular RNAs and micro RNAs in hippocampal neurons

Dissertation
zur Erlangung des Doktorgrades
der Naturwissenschaften

vorgelegt am Fachbereich Biowissenschaften
der Johann Wolfgang Goethe - Universität
in Frankfurt am Main

von

M.Sc. Mantian Wang
aus Lan Zhou (VR China)

Frankfurt 2020
(D30)

vom Fachbereich Biowissenschaften der

Johann Wolfgang Goethe - Universität als Dissertation angenommen

Dekan:	Prof. Dr. Sven Klimpel
Gutachter:	Prof. Dr. Erin Schuman
	Prof. Dr. Michaela Müller-McNicoll

Datum der Disputation: 04. Dezember 2020

The work presented in *Chapter II* of the thesis was published in Nature Neuroscience and iScience:

You, X.*, Vlatkovic, I.*, Babic, A.*, Will, T.*, Epstein, I.*, Tushev, G.*, Akbalik, G.*, **Wang, M**., Glock, C., Quedenau, C., et al. (2015). Neural circular RNAs are derived from synaptic genes and regulated by development and plasticity. Nat Neurosci 18, 603-610

- = Authors contribulted equally

Wang, M., Hou J., Müller-McNicoll M., Chen W., Schuman EM. (2019). Long and repeat-rich intronic sequences favor circular RNA formation under conditions of reduced spliceosome activity. iScience 20, 237-247

TABLE OF CONTENTS

ACKNOWLEDGEMENTS

First and foremost, I would like to thank my Ph.D. advisor Prof. Dr. Erin Schuman for being a great mentor, and for the continuous support and encouragement I received from her during my time in the lab. I am especially grateful to have had the opportunity to work on such a broad range of exciting projects and to get hands-on-experience on so many techniques. I have learned so much during my Ph.D. and it would not have been possible without her.

Next, I would like to thank the members of my thesis committee: Prof. Dr. Erin Schuman, Prof. Dr. Michaela Müller-McNicoll, Prof. Dr. Virginie Lecaudey and Prof. Dr. Helge Bode.

I would also like to thank the members of my Thesis Advisory Committee (TAC): Prof. Dr. Erin Schuman, Prof. Dr. Michaela Müller-McNicoll and Prof. Dr. Amparo Acker-Palmer for their guidance and support which helped to develop and shape my Ph.D. projects.

Furthermore, I am grateful to Arjan Vink and Irina Epstein for their great work as IMPRS graduate program coordinators. Many thanks for involving me in outreach activities of the MPIBR, I enjoyed them a lot!

I thank all of the Schuman lab members, both past and present. You made me feel welcome from the first minute I entered the lab and I feel honored to have been a part of this big family. I would like to particularly thank Claudia Fusco, Julio Perez, Maximillian Heumüller and Irina Epstein for always being there for me. Thank you all for sharing your expertise, giving me advice and guidance over the past years – I truly could not have wished for better colleagues and friends. I highly value and am very grateful for the administrative work of Nicole Thomsen, Sara Gil-Mast, Anita Kulak and Susanne tom Dieck.

Many thanks to our amazing prep team, Ina Bartnik, Nicole Fürst, Anja Stab, Christina Thum and Dirk Vogel, who have provided us with the most beautiful neuron cultures in all these years.

Moreover, I would like to thank Wei Chen and his entire team at the Max Delbrück Center in Berlin for the fruitful collaborations on the circular RNA projects. A special thank you also goes to David Unzué for his support on the bioinformatic analysis for the circRNA project. Moreover, I would like to thank the amazing chemists Alexander Heckel, Thomas Goldau and Robin Klimek – it was my pleasure to work with all of you on the antimiR project. You taught me a lot!

Through the past years I have received great support from our core facilities at the MPIBR, including the imaging facility, scientific computing, the proteomics facility, the IT, our animal caretakers, the administrative department and our facility management. And I am especially grateful for the valuable discussions and help of Stephan Junek and Claudio Polisseni.

For critical reading and comments on my dissertation I am thankful to Erin Schuman, Tamas Dalmay, Maximillian Heumüller and Irina Epstein.

Last but not least, I would like to express my deep gratitude and love to my family and friends for their never-ending support and encouragements in any situation. You gave me so much strength over the past years!

ZUSAMMENFASSUNG

Das menschliche Gehirn besteht aus einem komplexen Netzwerk aus hundert Milliarden Nervenzellen und die Informationsweitergabe zwischen einzelnen Neuronen geschieht an ihren Kontrapunkten, den Synapsen. Eine der wichtigsten Eigenschaften des Gehirns ist seine Lernfähigkeit und die Gedächtnisfunktion, die auf die Modifikation der Komposition, Form und Stärke individueller synaptischer Verbindungen beruhen – ein Prozess, der synaptische Plastizität genannt wird. Um jedoch eine langfristige Änderung der Synapsen zu ermöglichen, benötigt es der Synthese von neuer Boten-RNA und neuen Proteinen. Während lange Zeit der Zellkörper als einzige Quelle der Proteinproduktion galt, wissen wir heute, dass die lokale Proteinsynthesis in neuronalen Fortsätzen einen wichtigen Bestandteil neuronalen Plastizität darstellt. So wurde, zum Beispiel, im dendritischen Neuropil des Ratten Hippokampus über 5000 Boten-RNAs lokalisiert, die dezentralisiert für die Synthesis von Proteinen verwendet werden. Um die korrekte Translokation und Translation dieser Boten-RNA in Dendriten und Axonen sicherzustellen, greifen Neuronen auf eine Vielzahl an Regulationsmechanismen zurück. Eine dieser Regulatoren sind nicht-kodierende RNAs, die nicht als Vorlage zur Proteinproduktion dienen. Stattdessen fungieren diese als biologischen Katalysatoren. Mit der Weiterentwicklung von RNA-Sequenzierungsmethoden Anfang des 21. Jahrhunderts erkannte man, dass eigentlich der Großteil des Säugergenoms in tausende nicht-kodierende RNAs transkribiert wird. Diese unterschiedlichen Arten an nicht-kodierender RNA können die Genexpression auf vielfältige Art und Weise beeinflussen und spielen eine wichtige Rolle in der Funktion des Zentralnervensystems. Die kürzlich wiederentdeckte Familie der zirkulären RNA stellt eine außergewöhnliche Gruppe an regulatorische und nicht-kodierender RNA dar. Zwar kennen wir bereits einige wenige biologische Funktionen und Wirkmechanismen von zirkulärer RNA, jedoch fehlt bisher ein umfassendes Verständnis über die Expression und Biogenese dieser speziellen RNA Spezies in Neuronen und ihre Funktion in lokaler Translation und

Synaptischer Plastizität. Eine andere Familie an nicht-kodierender RNA, die ebenfalls eine wichtige Rolle in der Funktion von Nervenzellen spielt, sind mikroRNAs. Diese kurzen RNA Fragmente binden an Ziel-Boten-RNAs und können so deren Translation blockieren. Aufgrund der Expression von mikroRNAs in Dendriten und Axonen gelten mikroRNAs als ideale Regulatoren von lokaler Proteinsynthese und Synaptischer Plastizität. Um jedoch ihre Rolle in diesen Vorgängen genau zu untersuchen, bedarf es der Entwicklung einer Methode um speziell die lokale Population von mikroRNAs zu inaktivieren.

Die dynamische Landschaft der zirkuläre RNA in synaptischem Gewebe und nach Homeostatischer Plastizität

Zirkuläre RNAs stammen von linearen Boten-RNAs ab. Aber anders als diese sind zirkuläre RNA geschlossenen RNA Moleküle, die durch die Bildung einer speziellen Kopf-zu-Fuss (head-to-tail) Spleißverbindung geformt werden. Durch das Fehlen eines 5‘ Caps und eines 3‘ Poly-A Schwanzes weisen zirkuläre RNAs eine höhere Stabilität als lineare Boten-RNAs auf. Um die Expression von zirkulärer RNA zu bestimmen, isolierten wir RNA von fünf unterschiedlichen Mausgeweben und führten eine Sequenzierung durch. Dabei nutzten wir die Detektion der Kopf-zu-Fuss Spleißverbindung um die Expression von zirkulärer RNA zu quantifizieren. Verglichen mit allen anderen Gewebeproben, wie zum Beispiel dem Herz oder der Lunge, fanden wir die größte Anreicherung an zirkulärer RNA im Gehirn. Dabei stammten die meisten zirkulären RNAs von Boten-RNAs ab, die synaptischen Proteine kodierten und waren zudem verstärkt in synaptischem Gewebe, wie dem Hippokampalen Neuropil, zu finden. Diese Ergebnisse deuten auf eine mögliche regulatorische Funktion der zirkulären RNA in Synapsen hin.

Um zu untersuchen, ob zirkuläre RNA tatsächlich synaptische Funktionen regulieren, quantifizierten wir die Expression von zirkulärer RNA über verschiedene Entwicklungsstufen des Maushippokampus, angefangen von

Embryonalstadium E18 bis zum postnatalen Stadium P30. Hier fanden wir eine Hoch- und Runterregulierung von vielen zirkulären RNAs, die interessanterweise mit dem Zeitpunkt der Synaptogenese übereinstimmte. Viele dieser zirkulären RNAs zeigten eine veränderte Expression, die unabhängig von der ihrer verwandten linearen Boten-RNA war. Als nächstes testeten wir ob die Induktion von Homeostatischer Plastizität die Expression von zirkulären RNA beeinflussen kann, indem wir die Neuronen mit Bicucullin, einem $GABA_A$-Rezeptor-Antagonist behandelten. Hier fanden wir ebenfalls eine dynamische Veränderung der zirkulären RNA Population. Zusammenfassend deuten diese Ergebnisse darauf hin, dass zirkuläre RNAs eine wichtige Rolle in der Funktion und Regulation von Synapsen besitzen.

Das Spleißosom und intronische Sequenzen bestimmen die Synthese von neuronaler zirkulärer RNA

Wie aber werden neuronale zirkuläre RNAs generiert? Um diese Frage zu beantworten untersuchten wir die Spleißenden der Exone. Dabei fanden wir, dass die Kopf-zu-Fuss Spleißverbindung eine höhere Konservierung aufwies als andere Spleißverbindung, die ebenfalls in der verwandten linearen Boten-RNA gefunden werden konnte. Dies deutete auf eine Wichtigkeit der Kopf-zu-Fuss Spleißverbindung und die Möglichkeit, dass das Spleißosom eine tragende Rolle in der Ausbildung von zirkulärer RNA spielen könnte. Um diese Hypothese zu untersuchen, behandelten wir primären Neuronen vom Ratten Hippokampus mit Isoginkgetin, einem Spleißosominhibitor, und sequenzierten die gewonnene RNA. Eine Überexpression unreifer Boten-RNA nach Behandlung mit Isoginkgetin deutete auf eine erfolgreiche Inhibierung des Spleißosoms hin. Insgesamt detektieren wir über 700 robust exprimierte zirkulärer RNAs. Wenn das Spleißosom für die Generierung von zirkulärer RNA benötigt wird, so würde man nach Spleißosominhibierung eine Reduktion an zirkulärer RNA Expression erwarten. Überraschenderweise jedoch zeigten rund 140 zirkuläre RNAs eine gesteigerte Expression nach Inhibierung des Spleißosoms und nur sehr wenige

zirkuläre RNAs wiesen eine Runterregulierung auf. Die meisten zirkulären RNAs änderten ihre Expression unabhängig von der der verwandten linearen Boten-RNA.

Wie also führte die Inhibierung des Spleißosoms zur gesteigerten Generierung von zirkulärer RNA? Wenn nach der Isoginkgetinbehandlung die Spleißseiten von zirkularisierenden Exone in eine räumliche Nähe zueinandergekommen wären, könnte so die Produktion von zirkulärer RNA begünstigt werden. Daher untersuchten wir als nächstes die Intronsequenzen, die zirkularisierende Exone flankieren, nach Charakteristika, die eine Interaktion zueinander begünstigen. Interessanterweise fanden wir, dass zirkuläre RNA, die eine gesteigerte Expression nach der Inhibierung des Spleißosoms aufwiesen, die längsten flankierenden Introne besaßen. Zudem befanden sich in diesen ungewöhnlich langen Intronen eine signifikant höhere Anzahl an revers-komplementären Wiederholungssequenzen, die unter Bedingungen von reduzierter Spleißosomaktivität eine vermehrte Interaktion der langen Introne begünstigen können. Diese Ergebnisse deuten auf die Wichtigkeit des Spleißosoms und Intronsequenzen zur Generierung von zirkulärer RNA in Neuronen hin.

Die Entwicklung einer molekularen Sonde zur gezielten lokalen Inaktivierung von mikroRNA 181-a in Dendriten und Synapsen mittels Lichtpulsen

Ähnlich wie andere RNA Spezies, sind mikroRNAs in neuronalen Fortsätzen angesiedelt und stellen einen potentiellen Regulator für lokale Proteinsynthese und Synaptische Plastizität dar. Um die Rolle von mikroRNAs auf die lokale Boten-RNA Regulation zu untersuchen, bedarf es jedoch einer Methode mit der man lokale mikroRNA-Aktivität unterbinden kann. Da es bisher jedoch keinen Methodenansatz in dieser Richtung gibt, entwickelten wir gemeinsam mit der Arbeitsgruppe von Prof. Alexander Heckel (Goethe

Universität Frankfurt) eine Licht-aktivierbare Sonde um die endogene mikroRNA 181-a zu inaktivieren. Wir nannten diese Sonde das AntimiR. Das AntimiR beruht auf der Antisense-Oligonukleotid Technologie, in der ein modifizierter RNA-Strand komplementär zur Ziel-mikroRNA eingesetzt wird um diese zu binden und somit zu inaktiveren. Um die Sonde zeitlich und räumlich in ihrer Funktion zu kontrollieren, wurden fotospaltbare Linker eingebaut mittels welcher die Sonde nun mit Licht aktivierbar ist. Zudem besitzt das AntimiR einen Verfolgungsfluorophor, der kontinuierlich leuchtet und somit eine zeitaufgelöste Beobachtung des AntimiR in Neuronen ermöglicht. Um eine erfolgreiche Bindung zwischen dem AntimiR und der Ziel-mikroRNA 181-a zu detektieren, wurde ein Hybridisierungsfluorophor eingesetzt, der vor Belichtung und mikroRNA-Bindung durch einen Quencher gelöscht wird. Wir testeten zwei Sondenmodelle, die alle oben genannten Anforderung erfüllen: Die Hairpin-Sonde und den Molekularen Beacon. Die Hairpin-Sonde besteht aus einem Doppelstrang, in dem ein Strang komplementär zur mikroRNA 181-a Sequenz ist. An einem Ende wurde eine Verfolgungsfluorophor und am anderen ein Hybridisierungsfluorophor installiert. Der zweite RNA-Strang, der Gegenstrang, trägt den Quencher und ist mit einer Vielzahl von fotospaltbaren Gruppen durchzogen. Dieser Gegenstrang soll die Bindung von mikroRNA 181-a vor Fotoaktivierung verhindern. Der Molekulare Beacon besteht aus einem einzigen Strang und trägt den Hybridisierungsfluorophor an einem und den Quencher am anderen Ende. Vor der Bindung zu mikroRNA 181-a befinden sich der Hybridisierungsfluorophor und Quencher aufgrund von Nukleotidpaarungen in räumlicher Nähe zueinander. Die offene Schleifenregion ist komplementär zur mikroRNA 181-a Sequenz und wird vor der Belichtung mittels fotospaltbaren Gruppen an einer Bindung gehindert. In der Schleifenregion befindet sich zudem der Verfolgungsfluorophor.

Beide Sonden wurden auf ihr Verhalten hinsichtlich des Hybridisierungssignals nach Fotoaktivierung im Zellkern und Dendriten von primären Neuronen untersucht. Wir beobachteten ein rasches Erscheinen des Hybridisierungssignals nach dem ersten Lichtpuls, was auf eine erfolgreiche

Bindung und Inaktivierung von mikroRNA 181-a hinweist. Eine Steigerung der Hybridisierungsintensität wurde nach wiederholter Belichtung beobachtet und erreichte ihren Plateau nach ungefähr fünf Lichtpulsen. Da die Hairpin-Sonde stabilere Hybridisierungsanstiege über mehrere biologischen Replikate aufwies als der Molekulare Beacon, wurden die nachfolgenden Untersuchungen ausschließlich mit der Hairpin-Sonde durchgeführt. Als nächstes untersuchten wir, welche Auswirkungen die lokale Inaktivierung von mikroRNA 181-a auf die lokale Proteinsynthese von ihrer Ziel-Boten-RNA *Camk2a* in Dendriten hat. Wenn mikroRNA 181-a die lokale *Camk2a* Translation inhibiert, sollte sich nach der lokalen Inaktivierung der mikroRNA 181-a mittels der Hairpin-Sonde mehr Camk2a Protein gebildet haben. Um diese Hypothese zu untersuchen kombinierten wir eine Live-Zell-Bildgebungsmethode mit der metabolischen Färbung von neu-synthetisiertem Camk2a Protein. Wir quantifizierten die Menge an neuem Camk2a Protein um Hybridisierungspunkte und fanden, dass sich in einem Radius von 2.5 μm um jeden Hybridisierungspunkt mehr neu-synthetisiertes Camk2a Protein befindet als um Kontrollpunkte. Diese Ergebnisse deuten darauf hin, dass unter basalen Bedingungen, mikroRNA 181-a in einem Radius von 2.5 μm die Translation seiner Ziel-Boten-RNA unterbinden kann. Ob und in welchem Ausmaß sich die zeitliche und räumliche Regulation von lokaler Camk2a Translation durch mikroRNA 181-a nach neuronaler Stimulation verändert, sollte anhand weiterer Studien bestätigt werden.

ABSTRACT

Synaptic plasticity is the activity dependent alteration of the composition, form and strength of synapses and believed to be the underlying mechanism of learning and memory formation. While initial changes in synaptic transmission are caused by second messenger signaling pathways and rapid modifications in the cytoskeleton, to achieve stable and persistent changes at individual synapses, the expression of new mRNAs and proteins is required. The central dogma postulated that the cell body is the only source of newly synthesized proteins. For neurons, with their unique morphology, this meant that proteins would need be transported long distances, often hundreds of microns, to reach their destined locations in dendrites and at spines. To overcome this limitation, neurons have developed a strategy to regulate protein synthesis locally by distributing thousands of mRNAs into neuronal processes and use them for local protein synthesis. Ample research has demonstrated the importance of local protein synthesis to many forms of long-term synaptic plasticity. One potential regulator of mRNA localization and local translation in neurons are non-coding RNAs. Intensive work over the past decades has highlighted the importance of non-coding RNAs in many aspects of brain function. The aim of this thesis is to obtain a better understanding of the role of non-coding RNAs in synaptic function and plasticity in the murine hippocampus. For this, we focused our studies on two classes of non-coding RNAs.

In the first part of my thesis, I describe our efforts on characterizing circular RNAs, a novel and peculiar family of non-coding RNAs, in the murine hippocampus by combining high throughput RNA-Sequencing with fluorescence *in situ* hybridization. Furthermore, we investigated the mechanisms of circular RNA biogenesis in hippocampal neurons by temporarily inhibiting spliceosome activity and analyzing the differentially regulated circular RNAs.

The second aim of my thesis was to develop a molecular tool – which we called the antimiR – to spatio-temporally control endogenous microRNA activity in order to study microRNA-mediated regulation of local protein synthesis and synaptic plasticity. Using live-cell imaging and metabolic labelling of newly synthesized proteins we studied the effect of local miR-181a inactivation on local Camk2a protein synthesis in distal dendrites.

Chapter I

INTRODUCTION

The complexity of the brain

The brain is the most complex organ in our body and comprises billions of neurons. For centuries the brain has captured the curiosity of scientists who try to understand how individual neurons cooperate in ensembles to exert central control over all our actions. Moreover, the brain is plastic – changing continuously throughout our lifetime, enabling us to adapt to ever-changing environmental cues. The complexity of the brain is reflected on multiple levels. At the macro level, the brain consists of neuronal networks formed by thousands of neurons that are densely connected to each other via synapses – the contact points between individual neurons that receive and process information. Often these connections stretch over large distances and aberrant connectivity can cause severe pathologies of the brain (Ellison-Wright & Bullmore, 2009; Kubicki et al., 2007). At the cellular level, the brain is formed by a myriad of different neuronal and non-neuronal cell types, each with complex morphology and functions. We are only beginning to uncover the cellular heterogeneity of the vertebrate brain, as the advent of single-cell sequencing has led to the discovery of hundreds of novel neuronal subclasses (Darmanis et al., 2015; Fuzik et al., 2016; La Manno et al., 2016; Rheaume et al., 2018; Usoskin et al., 2015). At the molecular level, the brain faces the challenge of creating functional diversity between the many different neuronal cell types. Transcriptomic diversity between neurons is achieved through mechanisms such as alternative splicing and RNA editing, which are most prevalent in the nervous system compared to other tissues (Blow, Futreal, Wooster, & Stratton, 2004; Furlanis, Traunmüller, Fucile, & Scheiffele, 2019; Ramsköld, Wang, Burge, & Sandberg, 2009). However, the functional diversity within a single neuron through sub-cellular compartmentalization is equally crucial. Neurons have a unique morphology with processes – an axon and multiple dendrites – stretching vast distances away from the cell soma and taking up to 99% of the entire cytoplasmic volume (Holt, Martin, & Schuman, 2019). While axons can extend over a hundred centimeters in length, the dendritic tree is elaborately branched and can, in the case of a rat hippocampal

pyramidal neuron, stretch a total distance in the range of 13.5 millimeters (Figure1) (Holt et al., 2019; Ishizuka, Cowan, & Amaral, 1995). Moreover, an average excitatory neuron receives information from 1-10,000 other neurons and transmits information to 50-100,000 neurons (Holt et al., 2019). To fully appreciate the dimensions between the length of the neuron soma to the dendrites, imagine a human (1.70 m) trying to process information that was received hundreds of meters away, at the top of the highest building of the world, the Burj Khalifa (829.8 m).

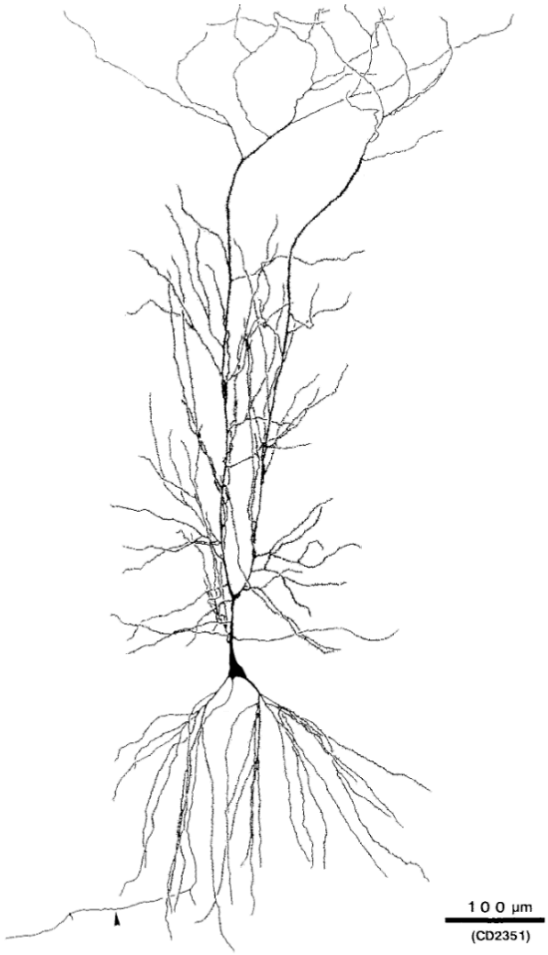

Figure 1. Dendritic morphology of CA1 pyramidal neurons.
Illustration of a CA1 pyramidal neuron from rat hippocampus with an average soma size of 15 - 20 μm and total dendritic length of 13.500 μm. The axon is indicated with an arrowhead. Scale bar = 100 μm. Modified from Ishizuka et al. (1995).

Slowly we can understand how important functional regulation locally at the site of information transfer is for neurons. How do neurons coordinate cellular processes at such distances far away from the cell body? A well-suited structure to study this question is the hippocampus.

The hippocampus and its role in learning and memory

The hippocampus is a major component of the brain of humans and other vertebrates. Bilaterally located under the cerebral cortex in the allocortex, the hippocampus is part of the limbic system and plays an important role in memory formation and consolidation (Roxo, Franceschini, Zubaran, Kleber, & Sander, 2011). Together with the dentate gyrus (DG), subiculum and entorhinal cortex (EC) the hippocampus is part of a functional brain formation called hippocampal formation. The hippocampus itself is subdivided into three regions: CA1, CA2 and CA3 (CA = *Cornu ammonis*). There are four main synaptic pathways of the hippocampal circuitry (Figure 2). Axons of layer II and III neurons of entorhinal cortex (EC) project to the dentate gyrus (DG) and the CA3, forming the major input to the hippocampus, the perforant pathway. Principal neurons of the DG, the granule cells, connect to the CA3 pyramidal neurons via the mossy fiber pathway. CA3 pyramidal neuron axons project the information to CA1 pyramidal neurons via the Schaffer collateral. Here, the axons either come from neurons in the same hemisphere (*ipsilateral*) or from the other hemisphere (*contralateral*), crossing the corpus callosum. Additionally, CA1 neurons can also receive direct input from EC layer III via the temporoammonic pathway. The projections from the CA1 to the subiculum (S) and on to the deeper layers of the entorhinal cortex (EC) form the principal output from the hippocampus – closing the hippocampal loop that originated in the superficial layers of the EC and concludes in its deep layers (T. Bliss, 2007; Deng, Aimone, & Gage, 2010).

Moreover, the hippocampus displays a laminar organization consisting of four layers (Figure 3): *Stratum pyramidale* is composed of the cell bodies of CA1,

CA2 and CA3 pyramidal neurons and synapses from the mossy fibers in CA3. While *stratum oriens* contains the basal dendrites of the principal neurons and cell bodies of inhibitory cells, the *stratum radiatum* harbors apical dendrites of pyramidal neurons and Schaffer collateral fibers from CA3. Finally, the *stratum lacunosum-moleculare* is composed of distal dendrites of CA1 neurons, interneuron cell bodies and processes, and axons from EC.

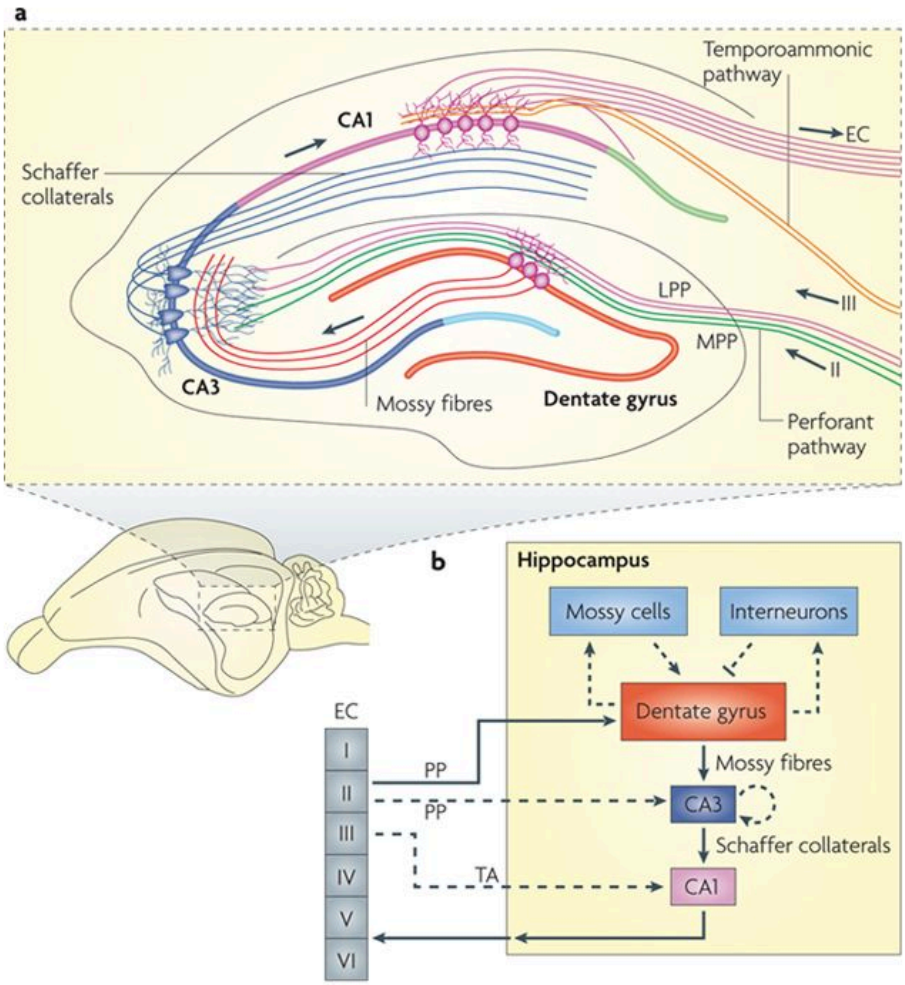

Figure 2. The neural circuitry in the rodent hippocampus.
A. Location of the hippocampus in the rodent brain and illustration of the hippocampal circuitry. **B.** Diagram of the hippocampal neural network. The axons of layer II and III neurons in the entorhinal cortex (EC) project to the dentate gyrus through the perforant pathway (PP), including the lateral and medial perforant pathway (LPP and MPP). The dentate gyrus sends projections to the pyramidal neurons in CA3 through mossy fibers. CA3 pyramidal neurons relay the information to CA1 pyramidal neurons through Schaffer collaterals. CA1 pyramidal neurons send projections into deep-layer neurons of the EC. CA1 also receives direct input from EC layer III neurons through the temporoammonic pathway (TA). Adapted from Deng et al. (2010).

The first link between the hippocampus and memory arose from reports by Scoville and Milner (1957) describing patient H.M., whose hippocampi, amygdala, and associated cortical areas were surgically removed in an attempt to cure his epileptic seizures. Although the surgery was partially successful in controlling his epilepsy, as a severe consequence, H.M. was no longer able to form new long-term memories. While his short-term memory was not affected, he was unable to form new memories of facts and events after the surgery (anterograde amnesia) and recall episodic experiences for a limited time before the operation (temporally-graded retrograde amnesia). Later lesion studies confirmed the dependence of certain types of memory on the integrity of the hippocampus (Squire & Zola-Morgan, 1991).

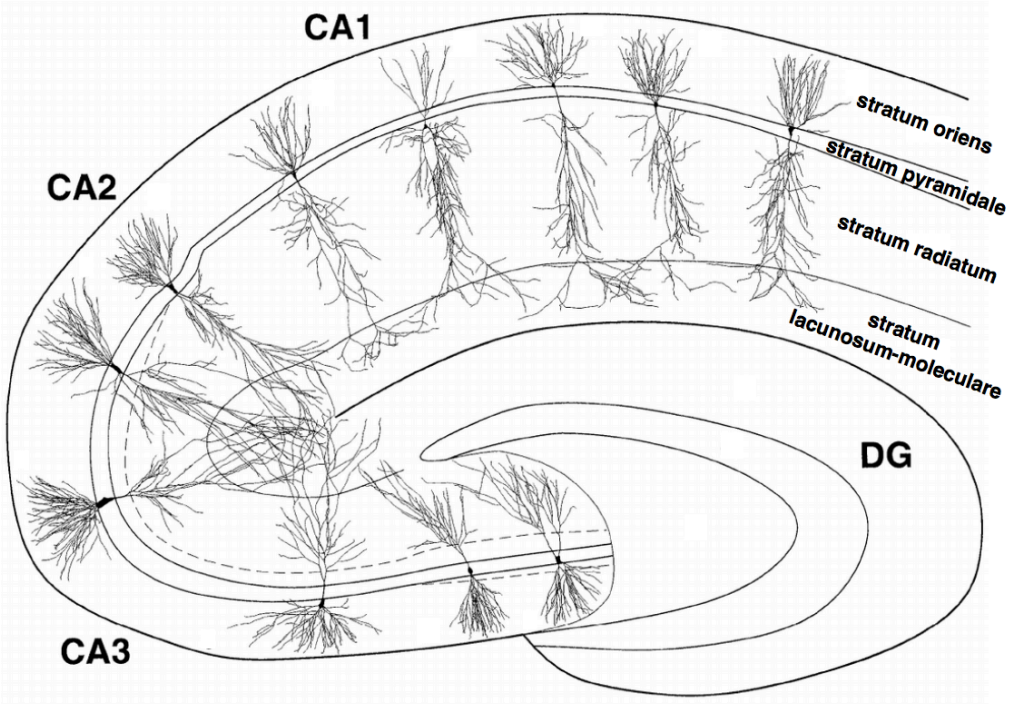

Figure 3. Laminar organization of the hippocampus.
The *stratum pyramidale* contains the cell bodies of CA1, CA2 and CA3 pyramidal neurons, while *stratum oriens* the basal dendrites of the principal neurons and cell bodies of inhibitory cells. The *stratum radiatum* harbors apical dendrites of pyramidal neurons and Schaffer collateral fibers from CA3 to CA1 interneurons and the *stratum lacunosum-moleculare* is composed of dendrites of the granule, basket and polymorphic cells and axons from EC. Modified from Ishizuka et al. (1995).

Moreover, other studies have demonstrated the role of the hippocampus in spatial memory (Morris, Garrud, Rawlins, & O'Keefe, 1982; Squire & Zola-Morgan, 1991; Tsien, Huerta, & Tonegawa, 1996). Spatial positioning of animals is encoded in the firing pattern of distinct cells of the hippocampus, the place cells (O'Keefe & Dostrovsky, 1971). Later, grid cells were discovered, neurons in the entorhinal cortex that fire at regular intervals as the animal navigates an open area (Hafting, Fyhn, Molden, Moser, & Moser, 2005). Together these studies highlight the presence of the cognitive map in the hippocampus. Furthermore, synaptic plasticity at the dendrites of hippocampal pyramidal neurons is a key mechanism for the induction of spatial representation in place cells (M. E. Sheffield & Dombeck, 2015; M. E. J. Sheffield, Adoff, & Dombeck, 2017).

Synaptic plasticity

What are the mechanisms enabling us to learn new tasks and replace old knowledge with new knowledge? It is now generally accepted that learning and memory involves a long-lasting modification of the contact points between neurons, the synapses. Synapses are essential for information flow between neurons, where electrical signal is passed from presynaptic neuron to the postsynaptic neuron. At many synapses, the presynaptic part is located on an axon and the postsynaptic part on a dendrite or soma (Sheng & Hoogenraad, 2007). We distinguish between two fundamentally different types of synapses (Figure 4). At chemical synapses, a wave of electrical current called the action potential arrives at the pre-synapse and leads to a probabilistic release of chemicals, called neurotransmitters, upon depolarization. These neurotransmitters are detected by ionotropic and/ or metabotropic receptors on the postsynaptic membrane, resulting in the activation of these receptors and the formation of excitatory or inhibitory postsynaptic currents (EPSCs or IPSCs). These currents are summed, integrated in the dendrites and propagated towards the cell soma. The balance of excitatory and inhibitory synaptic inputs determines the likelihood of a neuron firing an action potential (Stuart, Spruston, Sakmann,

& Häusser, 1997). If the summation of EPSCs passes a critical threshold, an action potential may be elicited at the axon initial segment and propagate towards the axon terminals (Clark, Goldberg, & Rudy, 2009; Colbert & Johnston, 1996; Stuart et al., 1997). As chemical synapses pass information directionally, structural and functional asymmetry is found between pre- and post-synapse. At electrical synapses, electrical current is transmitted bidirectionally by intercellular channels called gap junctions. Different from chemical synapses, electrical synapses do not amplify or transform the presynaptic signal and can coordinate the activity of interconnected neurons (Bennett, 2000; Curti, Hoge, Nagy, & Pereda, 2012; Galarreta & Hestrin, 2001; Getting, 1974).

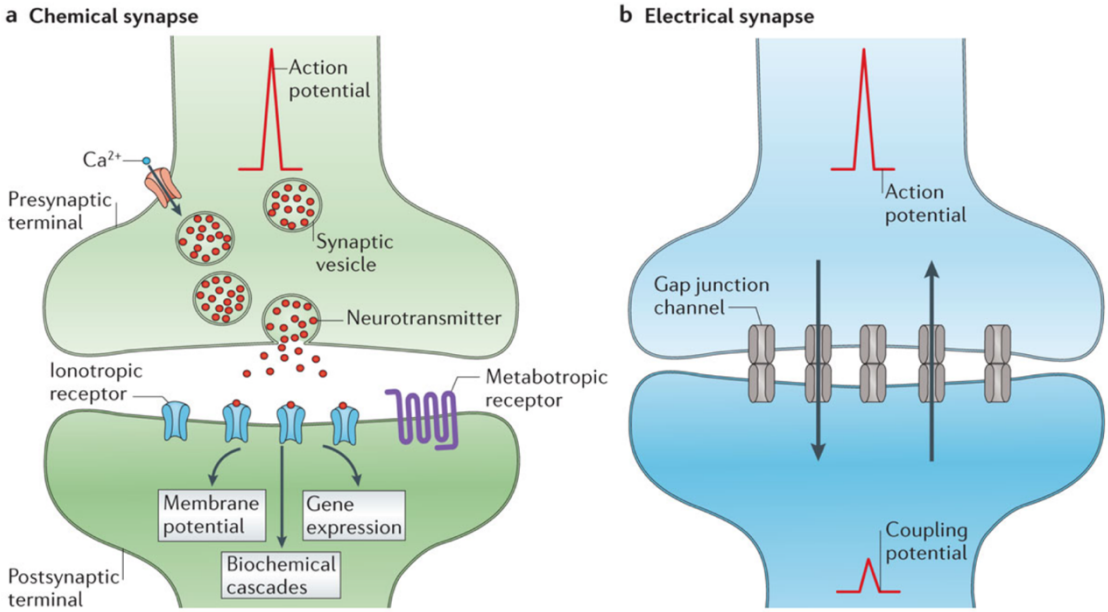

Figure 4. The two main modalities of synaptic transmission.
A. Chemical transmission requires sophisticated presynaptic molecular machinery that regulates neurotransmitter release in a probabilistic manner upon depolarization of the presynaptic terminal and the activation of voltage-gated calcium channels (VGCCs). Ionotropic and metabotropic receptors in the postsynaptic membrane detect and translate the presynaptic message in the form of neurotransmitters in postsynaptic events, such as changes in membrane potential, induction of gene expression or activation of biochemical cascades. **B.** Electrical transmission is mediated by intracellular junctions calls gap junctions that connect the two synapses and thereby enable the bidirectional passage of electrical currents. Adapted from Pereda (2014).

Here, I describe in more detail the structure of an excitatory glutamatergic synapse, as work in this thesis is focusing on hippocampal pyramidal neurons (Figure 5). The presynaptic axon terminal, or synaptic bouton, is characterized

by hundreds to thousands of glutamate-filled synaptic vesicles and the active zone, the specialized site of the presynaptic membrane where synaptic vesicles dock, fuse and release neurotransmitter into the synaptic cleft. The active zone is made up of an electron-dense matrix of proteins, containing voltage-gated calcium channels (VGCCs), presynaptic cytoskeletal scaffolding molecules like bassoon, piccolo and Rim, and SNARE proteins, a large protein complex to mediate vesicle fusion (Martens & McMahon, 2008; Ziv & Garner, 2004). The pre- and post-synapse are held together by a number of synaptic adhesion molecules, such as cadherins, integrins and neurexins (Jang, Lee, & Kim, 2017; Missler, Südhof, & Biederer, 2012). These adhesion molecules are not only involved in the formation and stabilization of synapses but also dynamically regulated during plasticity (Bruns & Jahn, 1995; Scheiffele, 2003; Sheng & Hoogenraad, 2007; Yamagata, Sanes, & Weiner, 2003). At the post-synapse, scaffolding proteins such as Homer1, Shanks and PSD-95 anchor the transmembrane adhesion molecules to the actin cytoskeleton. Furthermore, postsynaptic scaffolding proteins interact with receptors (Lim et al., 1999; Sala, Vicidomini, Bigi, Mossa, & Verpelli, 2015; Sheng & Kim, 2011). Ionotropic receptors, such as AMPA, NMDA and Kainate receptors, lead to ion influx, while metabotropic glutamate receptor (mGluRs) activation triggers an intracellular signal cascade by phosphorylation of target proteins. As this region of the post-synapse is densely packed with proteins and appears as an electron dense part of the synapse in EM images, it is called the post-synaptic density (PSD). Importantly, the myriad components of the pre and post-synapse are dynamically regulated, enabling the rapid remodeling of both synapse structure and function.

In the late 1940s Donald Hebb postulated that associative memory is formed in the brain by a process of synaptic modifications that strengthen connections when presynaptic activity correlated with postsynaptic firing:

“ When an axon of cell A is near enough to excite a cell B and repeatedly or persistently takes part in firing it, some growth process or metabolic change

takes place in one or both cells such that A's efficiency, as one of the cells firing B, is increased."

The first experimental support came 30 years later by Bliss and Lomo, who showed that repeated high-frequency stimulation of the perforant path in the hippocampus of anesthetized rabbits caused long-term potentiation (LTP) of synaptic strength lasting for hours or even days. Shortly after, it was found that the modulation of synaptic efficacy is bidirectional as low-frequency stimulation produces synaptic weakening, or long-term depression (LTD) (Dudek & Bear, 1992; Lynch, Dunwiddie, & Gribkoff, 1977). This marked the beginning of the search for molecular mechanism underlying synaptic plasticity. Over the past decades studies have identified key events involved in the activity-dependent changes in neuronal connectivity, such as presynaptic synaptic vesicle release and recycling, neurotransmitter receptor trafficking and modulation, and changes in the dynamic ultra-structure of synapses (Barria, Muller, Derkach, Griffith, & Soderling, 1997; Cesca, Baldelli, Valtorta, & Benfenati, 2010; Collingridge, Isaac, & Wang, 2004; Engert & Bonhoeffer, 1999; Granger, Shi, Lu, Cerpas, & Nicoll, 2013; C. G. Lau & Zukin, 2007). Today, we know that experience-dependent long-term synaptic plasticity is a major cellular substrate for learning, memory and behavioral adaptation (Bi & Poo, 2001; T. V. Bliss & Collingridge, 1993; Collingridge, Peineau, Howland, & Wang, 2010; Hughes, 1958; Sjöström, Rancz, Roth, & Häusser, 2008).

Local protein synthesis and mRNA localization enabling long-term synaptic changes

The establishment and maintenance of long-lasting changes at individual synapses requires new RNA and protein synthesis (H. P. Davis & Squire, 1984; Sutton & Schuman, 2006). There are two distinct phases of conventional LTP and LTD. While the early phase (1-3 h) is protein-synthesis independent, the late-phase (> 3h; L-LTP) requires transcription and new protein synthesis (T. V. Bliss

& Collingridge, 1993; Bolshakov, Golan, Kandel, & Siegelbaum, 1997; Frey, Krug, Reymann, & Matthies, 1988; Nguyen, Abel, & Kandel, 1994; Sutton & Schuman, 2006). The first direct evidence that memory depends in part on *de novo* protein synthesis *in vivo* was provided by Flexner et al (1963). Injection of the protein synthesis inhibitor puromycin in the temporal lobe of mice from day 1 to 3 after learning effectively blocked long-term memory formation for the location where an electric shock was received in a Y-maze. When injections were made later than 3 days after training, no memory deficit was detected. Subsequent work further strengthened the hypothesis that memory formation is disrupted by protein synthesis inhibition and an interference with L-LTP (Agranoff, Davis, & Brink, 1965; Agranoff, Davis, Casola, & Lim, 1967; Agranoff & Klinger, 1964; Banko, Hou, Poulin, Sonenberg, & Klann, 2006; Barondes & Cohen, 1966; Cohen, Ervin, & Barondes, 1966; Costa-Mattioli, Sossin, Klann, & Sonenberg, 2009; McGaugh & Izquierdo, 2000). But how is the soma of neurons capable of providing all the newly synthesized proteins required?

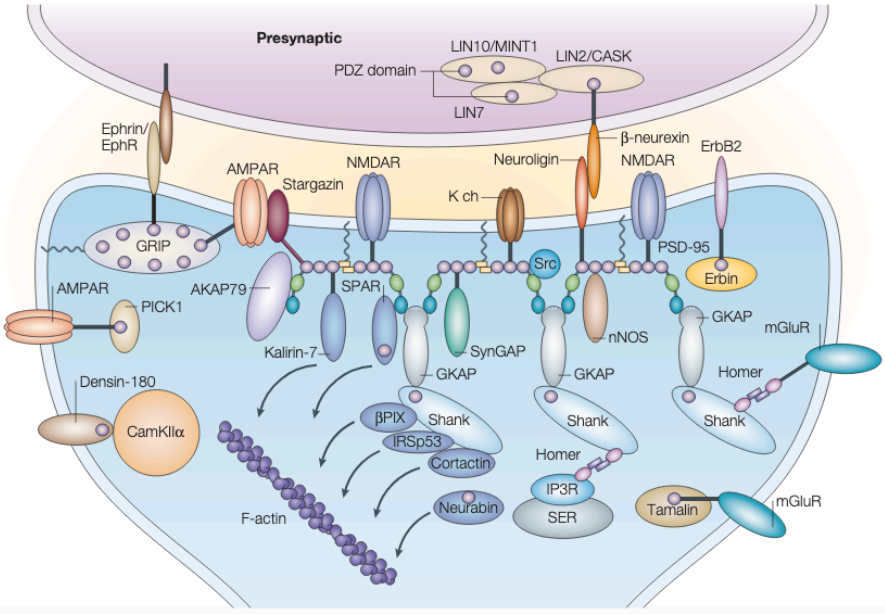

Figure 5. A schematic diagram of the PSD-protein organization at an excitatory synapse. The postsynaptic density (PSD) is composed of many proteins involved in the regulation of synaptic function. Key proteins among these, are scaffolding proteins (PSD-95, Homer1, Shank), cell adhesion molecules (neuroligin), receptors (NMDA receptors, AMPA receptors), diverse set of signaling molecules (Camk2a) and actin-cytoskeleton. Many of the proteins contain a PSZ domain which is indicated as purple circle. Adapted from Kim and Sheng (2004).

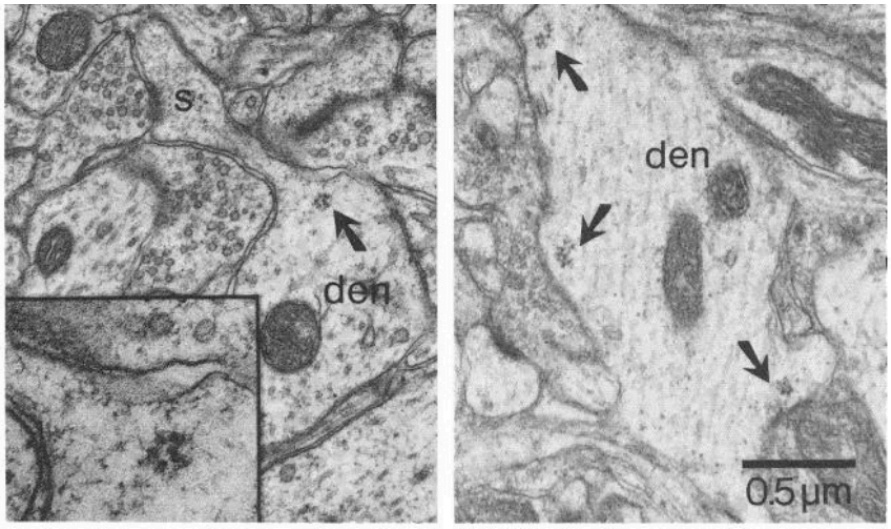

Figure 6. Distribution of polyribosomes at the base of spines.
Polyribosomes (arrow) were detected beneath spines in mid proximo-distal locations along the dendrites (left) or under mounds in the dendritic shaft (right) of granule cells of the dentate gyrus using EM microscopy. Inset illustrates the polyribosome cluster magnified three times. Scale bar = 0.5 μm. Modified from Steward and Levy (1982).

For a long time, the central dogma that the cell body is the source of all newly synthesized protein dominated the field. For a neuron this would mean that distally required proteins are synthesized in the soma and then transported into distal processes. It was the discovery of polyribosomes beneath spines in distal dendrites in electro micrographs (Figure 6) (Steward & Levy, 1982) and the radioactive labeling of de novo proteins within dendrites and axons (Feig & Lipton, 1993; Rao & Steward, 1991) that sparked the idea that protein synthesis takes places locally in neuronal processes, independent from the soma. The first functional role for local protein synthesis for synaptic plasticity was provided by Kang and Schuman (1996). By surgically separating the cell body of CA1 pyramidal neurons in rat hippocampal slices, they demonstrated that local protein synthesis in dendrites is crucial for BDNF (brain-derived neurotrophic factor) - induced LTP at CA3 – CA1 synapses (Figure7). Later it was shown, that local protein synthesis in dendrites contributes greatly to many forms of long-term synaptic plasticity: L-LTP (Bradshaw, Emptage, & Bliss, 2003; Cracco, Serrano, Moskowitz, Bergold, & Sacktor, 2005; Miller et al., 2002), mGluR-dependent LTD (Huber, Kayser, & Bear, 2000), NMDAR-dependent L-LTP (Vickers, Dickson, & Wyllie, 2005), L-LTP independent of transcription (Y. Y. Huang & Kandel, 2005),

dopamine-induced plasticity (W. B. Smith, Starck, Roberts, & Schuman, 2005) and homeostatic forms of synaptic plasticity (Sutton et al., 2006; Sutton, Taylor, Ito, Pham, & Schuman, 2007; Sutton, Wall, Aakalu, & Schuman, 2004). Moreover, clear evidence demonstrates the role of presynaptic translation in developing and mature axons (Campbell & Holt, 2001; Hafner, Donlin-Asp, Leitch, Herzog, & Schuman, 2019).

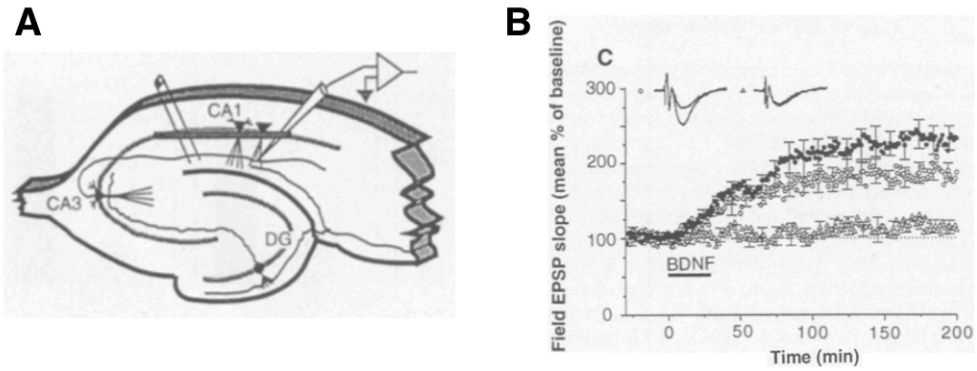

Figure 7. Requirement of local protein synthesis for BDNF-induced potentiation.
A. Schematic representation of a hippocampal slice showing the placement of a microlesion to isolate CA1 cell bodies from their dendrites, where electrophysiological recordings were made. **B.** Field EPSP recordings over time. Filled circles indicate enhancement obtained in sham-lesioned slices after the application of BDNF. Open circles indicate the enhancement obtained in CA1 somata-isolated slices. Open triangles show that pretreatment of the slices with anisomycin prevented the BDNF-induced plasticity at CA1 somata-isolated synapse. Calibration bars, 1 mV and 20 ms. Modified from Kang and Schuman (1996).

The finding that local translation is required for neuronal development and plasticity set the beginning of the search for messenger RNAs (mRNAs) in subcellular compartments. Initially a handful of mRNAs were detected and visualized in dendrites and axons, including the Ca^{2+}/calmodulin-dependent kinase alpha subunit, Camk2a (Bassell et al., 1998; Burgin et al., 1990; Mayford, Baranes, Podsypanina, & Kandel, 1996), microtubule-associated protein 2 (MAP2) (Garner, Tucker, & Matus, 1988), SH3 and multiple ankyrin repeat domains, Shank (Böckers et al., 2004) and beta-actin (Tiruchinapalli et al., 2003) using *in situ* hybridization techniques. The advent of microarray and RNA-sequencing provided an overview of the local transcriptome. Initial microarray

studies estimated the presence of between 70 – 285 mRNAs locally in processes (Lein et al., 2007; Poon, Choi, Jamieson, Geschwind, & Martin, 2006; Zhong, Zhang, & Bloch, 2006). However, a surprisingly small number of mRNAs overlapped between these studies, indicating that the so far discovered local transcriptome was not yet complete (Cajigas et al., 2012). It was later studies that led to the identification of thousands of mRNA species in the hippocampal neuropil (Biever et al., 2020; Cajigas et al., 2012; Tushev et al., 2018) and in axons (Gumy et al., 2011; Hafner et al., 2019; Zivraj et al., 2010). These local mRNAs represent a local tool box, as they encode for nearly all proteins important for the function and maintenance of dendritic spines, including ionotropic and metabotropic receptors, cell-adhesion molecules, scaffolding proteins, calcium signaling molecules and components of the translation machinery (Figure 8) (Cajigas et al., 2012).

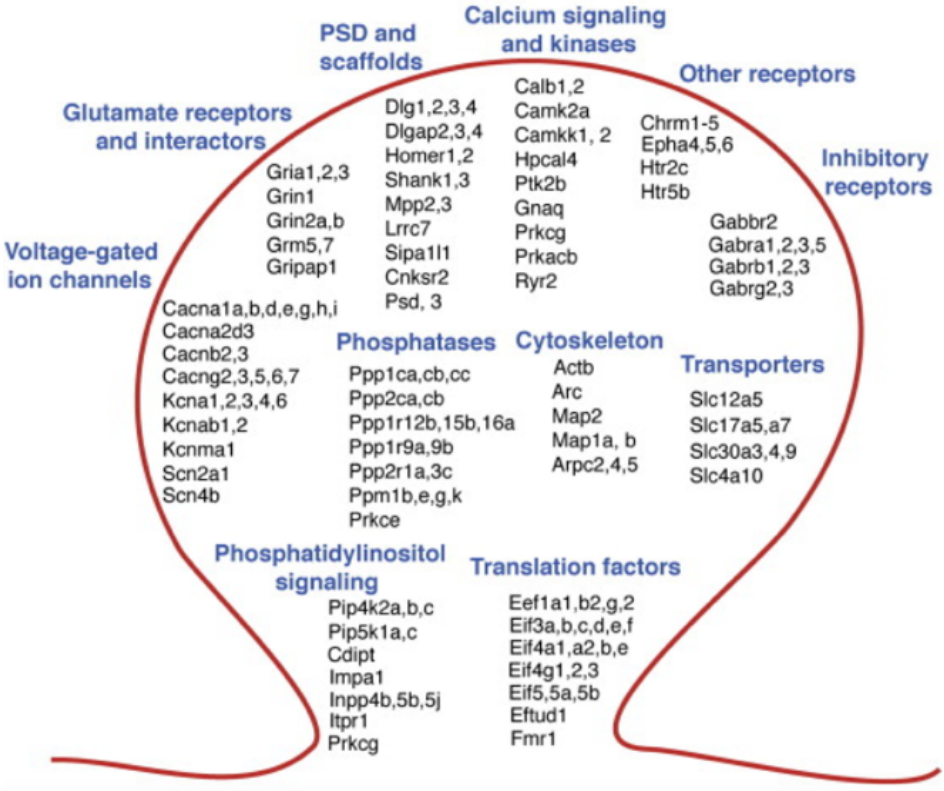

Figure 8. The local transcriptome of the rat hippocampal CA1 neuropil.
Schematic representation of a postsynaptic compartment highlighting some of the transcript families and mRNAs identified in the neuropil. Adapted from Cajigas et al. (2012).

The localization of many mRNAs is regulated by cis-acting motifs in the 3' untranslated region (UTR). Sequences within the 3'UTR are recognized by trans-acting RNA-binding proteins (RBPs) involved in the transport, localization, stability and translation of the mRNA (Darnell, 2013; St Johnston, 1995; Tian & Manley, 2017; Tushev et al., 2018). For example, beta-actin mRNA expresses a zip-code element in its 3'UTR which is recognized by zipcode binding protein 1 (ZBP1) and essential for the transport of the beta-actin mRNA (Condeelis & Singer, 2005; Hüttelmaier et al., 2005). The long 3'UTR of Camk2a is essential for the dendritic targeting, as mutation of the long 3'UTR leads to a restriction of the Camk2a mRNA in the soma (Mayford et al., 1996; Miller et al., 2002). In order to be transported, the mRNA along with RBPs, ribosomes and other RNA species are sorted into motile, heterogenous structures, called RNA granules (Kiebler & Bassell, 2006; Knowles et al., 1996). It is believed that the mRNA cargo is in a translationally silenced state while it is carried along the microtubules by motor proteins (Bullock, Nicol, Gross, & Zicha, 2006; Czaplinski & Singer, 2006; Krichevsky & Kosik, 2001). A recent report suggested an alternative model whereby synaptic mRNAs are transported on stalled ribosomes, paused at the level of translation elongation and only re-activated upon synaptic plasticity (Graber et al., 2013).

The non-coding RNA world

Much of the emphasis was placed onto mRNAs as they serve the role of relaying the genetic information for the protein output. However, it became evident as early as in the 50s that not all transcribed RNAs encode for proteins, some are "non-coding". These non-coding RNAs carry out important regulatory functions (Hoagland, Keller, & Zamecnik, 1956; Zamecnik & Keller, 1954). It was the efforts of next generation sequencing (NGS) studies of the 2000s that truly marked the beginning of a new era in the non-coding RNA field. One significant finding has been the discovery that the vast majority of the mammalian genome

is transcribed into tens of thousands of non-coding transcripts (Carninci et al., 2005; Derrien et al., 2012; Djebali et al., 2012; Okazaki et al., 2002).

Interestingly, while higher organisms show a relatively comparable number of protein-coding genes, the biodiversity and complexity of organisms expanded greatly with the relative amount of the genome transcribed into non-coding sequences (Table 1) (Frith, Pheasant, & Mattick, 2005; Mattick, 2001; Taft, Pheasant, & Mattick, 2007).

Table 1. Increase in the non-coding transcriptome in metazoan.
Adapted from Frith et al. (2005).

			Coding sequences		*UTR sequences*		*Total transcribed noncoding sequences*		
Organism	***No. of protein-coding genes***	***Genome size (Mb)***	***Mb***	***%***	***Mb***	***%***	***Mb***	***%***	***Ratio of noncoding to coding sequences***
Whole genome									
Human	~20–25 000	2851	34	1.2	32	1.1	1619	57	47:1
Mouse	~20–25 000	2490	31	1.3	26	1.1	1339	54	43:1
Fruit fly	~13 500	120	22	18	6.4	5.3	53	44	2.4:1
Nematode	~19 000	100	26	26	0.4	0.4	33	33	1.3:1
Nonrepetitive portion of genome only									
Human		1455	33	2.3	26	1.8	867	60	27:1
Mouse		1422	29	2.0	22	1.6	811	57	28:1
Fruit fly		109	21	20	6.2	5.7	48	44	2.2:1
Nematode		86	25	29	0.3	0.4	26	31	1.1:1

Non-coding RNAs are versatile catalysts of a remarkable variety of biological reactions and have become recognized as critical regulators of gene expression and genome maintenance. More importantly, the discovery of each member of the non-coding RNA family has revolutionized our way of thinking about the functional capacity of RNAs. Detailed lists of important members of the RNA world and their estimated content in mammalian cells is provided in Table 2 and Table 3.

Table 2. Selected classes of RNA and their sizes and functions.
Modified from Cech and Steitz (2014).

RNA	Definition	Function	Size
rRNA	Ribosomal RNA	RNA component of the small or large ribosomal subunit; the largest is a ribozyme	120, 160, 1,868, 5,025 nt, human; 120, 1,541, 2,904 nt, *E. coli*
tRNA	transfer RNA	RNA adaptor connecting an mRNA codon and the activated form of the cognate amino acid during protein synthesis on the ribosome	70–90 nt
mRNA	messenger RNA	contains a coding region that directs synthesis of a protein product; typically has both 5′- and 3′-untranslated sequences	2–5 kb
hnRNA	heterogeneous nuclear RNA	intron-containing pre-mRNA	2–40 kb
ciRNA	Circular RNA	Covalently closed nuclear and cytoplasmic RNA, can act as miRNA sponge	viroids 250-400nt; 250-900 nt in neurons
snRNA	small nuclear RNA	RNA localized in the eukaryotic cell nucleus, RNA component of the splicing machinery	100–300 nt
snoRNA	small nucleolar RNA; in vertebrates, most snoRNAs are processed intron fragments	essential for pre-rRNA processing or modification by serving as a guide RNA to direct a bound enzyme to either 2′-*O*-methylate or pseudouridylate a complementary sequence in rRNA	70 nt
miRNA	microRNA	RNA that, in complex with AGO protein, uses seed sequences near its 5′ end to base pair with a target mRNA to induce deadenylation and decay or translational regulation	22 nt
7SL	RNA component of the signal recognition particle (SRP)	scaffolds formation of a cytoplasmic RNP that enables transit of nascent proteins through the translocon and into the endoplasmic reticulum	300 nt
Xist	X-inactive-specific transcript RNA	coats one X chromosome in female mammals, triggering heterochromatization and transcriptional repression	17 kb
Other lncRNA	long noncoding RNA	autonomously transcribed RNA that does not encode a protein; often capped and polyadenylated; can be nuclear, cytoplasmic or both	>200 nt

piRNA	PIWI-associated RNA	RNA that directs the modification of chromatin to repress transcription; best characterized in the male germline	27 nt
riboswitch	RNA element within a mRNA that toggles between two conformations upon exposure to a small-molecule ligand or other stimulus	inhibits or promotes gene expression at the level of transcription, translation, or RNA splicing	40–140 nt

Table 3. Estimates of total RNA content in mammalian cells.
Adapted from Palazzo and Lee (2015).

Type	Percent of total RNA by mass	Molecules per cell	Average size (kb)	Total weight picograms/cell	Notes	Reference
rRNAs	80 to 90	3–10 × 10^6 (ribosomes)	6.9	10 to 30		Blobel and Potter (1967), Wolf and Schlessinger (1977), Duncan and Hershey (1983)
tRNA	10 to 15	3–10 × 10^7	<0.1	1.5 to 5	About 10 tRNA molecules /ribosome	Waldron and Lacroute (1975)
mRNA	3 to 7	3–10 × 10^5	1.7	0.25 to 0.9		Hastie and Bishop (1976), Carter et al. (2005)
hnRNA (pre-mRNA)	0.06 to 0.2	1–10 × 10^3	10*	0.004 to 0.03	Estimated at 2–4% of mRNA by weight	Mortazavi et al. (2008), Menet et al. (2012)
Circular RNA	0.002 to 0.03	3–20 × 10^3	~0.5	0.0007 to 0.005	Estimated at 0.1–0.2% of mRNA**	Salzman et al. (2012), Guo et al. (2014)
snRNA	0.02 to 0.3	1–5 × 10^5	0.1–0.2	0.008 to 0.04		Kiss and Filipowicz (1992), Castle et al. (2010)
snoRNA	0.04 to 0.2	2–3 × 10^5	0.2	0.02 to 0.03		Kiss and Filipowicz (1992), Cooper (2000), Castle et al. (2010)
miRNA	0.003 to 0.02	1–3 × 10^5	0.02	0.001 to 0.003	About 10^5 molecules per 10 pg total RNA	Bissels et al. (2009)
7SL	0.01 to 0.2	3–20 × 10^4	0.3	0.005 to 0.03	About 1–2 SRP molecules/100 ribosomes	Raue et al. (2007), Castle et al. (2010)
Xist	0.0003 to 0.02	0.1–2 × 10^3	2.8	0.0001 to 0.003		Buzin et al. (1994), Castle et al. (2010)
Other lncRNA	0.03 to 0.2	3–50 × 10^3	1	0.002 to 0.03	Estimated at 1–4% of mRNA by weight	Mortazavi et al. (2008), Ramsköld et al. (2009), Menet et al. (2012)

**The size for the average unspliced pre-mRNA is 17 kb; however, most pre-mRNAs are partially spliced at any given time, and the average size of hnRNA is estimated at 10 kb (Salditt-Georgieff et al., 1976).*
***Based on the finding that 1–2% of all mRNA species generate circular RNA, which is present at 10% of the level of the parental mRNA.*

Ribosomal RNA and transfer RNA

Identification of tRNA and rRNA marked the beginning of the ncRNA revolution. In the 50s, the Zamecnik lab demonstrated that RNA is involved in protein synthesis not as a messenger molecule, but as an adapter molecule for amino acids – or transfer RNAs (tRNAs) (Hoagland et al., 1956; Zamecnik & Keller, 1954). Soon after, the link between rRNA and ribosomes were established (Palade, 1955). While it was long believed that rRNA served as a scaffold for ribosomal proteins to assemble onto, it was experiments, such as those performed by Noller et al, showing that ribosomes digested with proteases could still stimulate peptide bond formation that proved the catalytic function of rRNA (Ban, Nissen, Hansen, Moore, & Steitz, 2000; Noller, Hoffarth, & Zimniak, 1992; Voorhees & Ramakrishnan, 2013; Wimberly et al., 2000; Yusupov et al., 2001). tRNA and rRNA are not only the first non-coding RNAs with established functions, but also make up the largest fraction of ncRNAs in the mammalian genome (Figure 9).

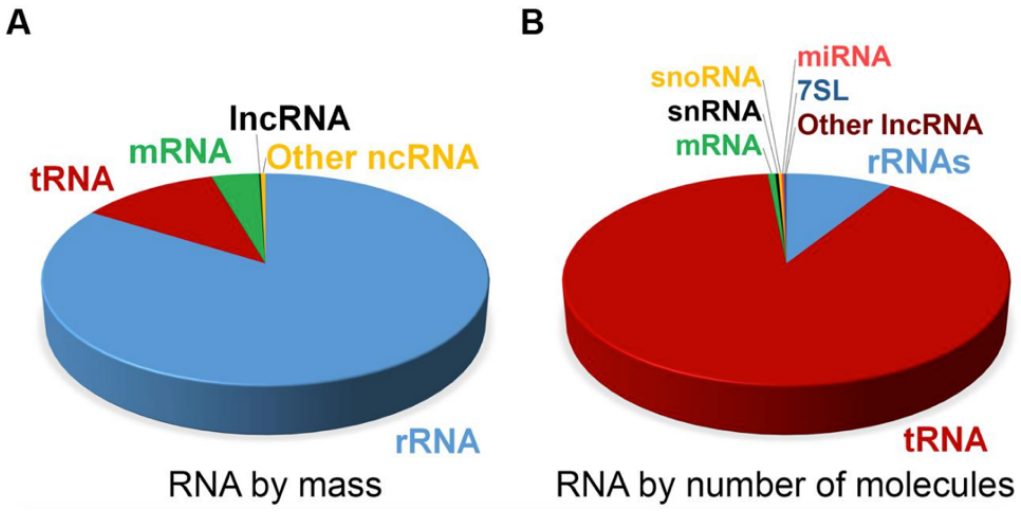

Figure 9. Estimate of RNA levels in a mammalian cell.
Proportion of the various classes of RNA in a mammalian somatic cell by total mass **A** and by absolute number of molecules **B**. Total number of RNA molecules is estimated at roughly 10^7 per cell. Other ncRNAs in **A** include snRNA, snoRNA and miRNA. Due to their relative size rRNA, mRNA and lncRNAs make up a larger proportion of the mass as compared to the overall number of molecules. Adapted from Palazzo and Lee (2015).

Small nuclear RNA and pre-mRNA splicing

The discovery of small nuclear RNA (snRNA) led to the finding of a key machinery for transcriptome diversity – the spliceosome. Protein coding regions of genes of higher organisms (exons) are intersected by regions that are not involved in protein expression (introns) (Berget, Moore, & Sharp, 1977). The spliceosome excises introns from the precursor mRNAs (pre-mRNAs) and recombines the exons. By including or excluding particular exons during this process, a single gene can give rise to multiple mRNA transcript isoforms and protein variants (alternative splicing) (Black, 2003).

The spliceosome consists of snRNAs, short and uridine-enriched RNAs that are found in the nuclei of vertebrate cells, and approximately 80 proteins (Busch, Reddy, Rothblum, & Choi, 1982; Matera, Terns, & Terns, 2007; Weinberg & Penman, 1968; Will & Lührmann, 2011). Based on common sequence features and associated protein factors, snRNAs are divided into two classes (Matera et al., 2007). Sm snRNAs U1, U2, U4, U4atac, U5, U11 and U12 are transcribed in the nucleus and transported into the cytoplasm through Cajal bodies (Fornerod, Ohno, Yoshida, & Mattaj, 1997; Izaurralde et al., 1994; Ohno, Segref, Bachi, Wilm, & Mattaj, 2000; K. P. Smith & Lawrence, 2000; Suzuki, Izumi, & Ohno, 2010). There they assembled with Sm proteins with the help of SMN and associated proteins, called GEMINIs (Massenet, Pellizzoni, Paushkin, Mattaj, & Dreyfuss, 2002; Meister, Eggert, & Fischer, 2002; Pellizzoni, Yong, & Dreyfuss, 2002). The formation of the Sm ring stabilizes snRNAs and initiates the nuclear import. After nuclear import, SMN dissociates from the snRNA Sm protein complex, called snRNPs, which continue their maturation in Cajal bodies (Schaffert, Hossbach, Heintzmann, Achsel, & Lührmann, 2004; Sleeman & Lamond, 1999; Trinkle-Mulcahy et al., 2008). In contrast, Lsm snRNA U6 and U6atac remain in the nucleus after their transcription and are bound by Lsm proteins (Matera et al., 2007). Matured spliceosomal snRNPs and their

associated factors localize to nuclear speckles, ready to carry out their function (Lamond & Spector, 2003; Matera et al., 2007).

Spliceosome assembly on a pre-mRNA is a stepwise process and the correct catalytic removal of introns is mediated by base pairing between spliceosomal snRNAs and pre-mRNAs as shown in Figure 10 (Madhani & Guthrie, 1994). As the first step, U1 snRNP binds the 5' splice site (ss) on the pre-mRNA and forms the early complex (complex E). U2 snRNP and associated factors, such as SF1 (splicing factor), U2AFs (U2 auxiliary factors) recognize the 3' ss around the branch point of the pre-mRNA. The interaction between U1 and U2 snRNP results in the formation of the pre-spliceosome (complex A). Then, U4-U6 and U5 snRNPs are recruited as preassembled tri-snRNP to form complex B. Through a series of compositional and conformational rearrangements the catalytically active complex B is established (complex B *). The first catalytic step of splicing generates complex C, resulting in a free exon1 and an intron-exon 2 lariat intermediate. After additional ATP-dependent rearrangements, the second catalytic step of splicing is carried out and leads to the generation of the post-spliceosomal complex with the intron lariat and spliced exons. Finally, U2, U5, U6 snRNPs are released from the mRNP particle and recycled for another round of splicing.

Whether an exon is included or excluded from the mature mRNA transcript is regulated by cis-regulatory RNA elements as well as intronic and exonic silencer and enhancer sequences. These splicing elements are recognized by trans-regulatory proteins, splicing activators and inhibitors (M. Chen & Manley, 2009; Licatalosi et al., 2008; Matera & Wang, 2014). The combinatorial or competitive effects of all splicing factors determines the pattern of pre-mRNA splicing (Bessonov, Anokhina, Will, Urlaub, & Lührmann, 2008; Hegele et al., 2012; Jurica & Moore, 2003; Zhou, Licklider, Gygi, & Reed, 2002). As splicing factors are often auxiliary proteins of the spliceosome, they most commonly affect the early and intermediate steps of spliceosome assembly along the pre-mRNA

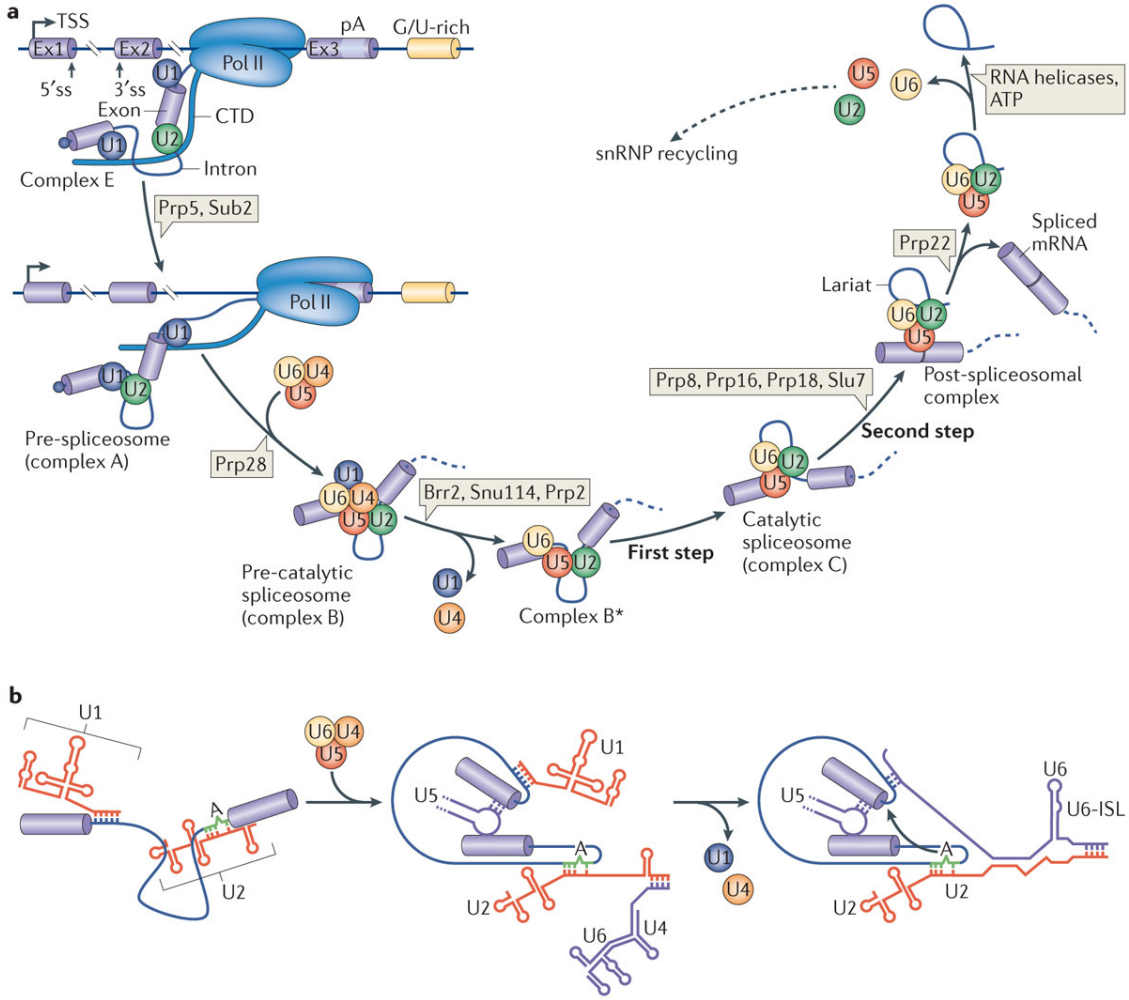

Figure 10. Step-wise assembly of the spliceosome and catalytic steps of splicing.
A. Spliceosome assembly on a pre-mRNA. U1 and U2 small nuclear ribonucleoproteins (snRNPs) recognize 5' and 3' splice and through their interaction form the pre-spliceosome complex (complex A). In a subsequent reaction catalyzed by Prp28, the preassembled tri-snRNP U4-U6-U5 is recruited to from the complex B. The resulting complex B undergoes a series of rearrangements to form a catalytically active complex B (complex B*), which requires multiple RNA helicases and results in the release of U4 and U1 snRNPs. Complex B* then carries out the first catalytic step of splicing, generating complex C, which contains free exon 1 (Ex1) and the intron–exon 2 lariat intermediate. Complex C undergoes additional rearrangements and then carries out the second catalytic step, resulting in a post-spliceosomal complex that contains the lariat intron and spliced exons. Finally, the U2, U5 and U6 snRNPs are released from the mRNP particle and recycled for additional rounds of splicing (dashed arrow). **B.** During splicing, RNA–RNA interactions are rearranged in a stepwise manner to create the catalytic center of the spliceosome. Initially, U1 and U2 small nuclear RNA (snRNA) pair with the 5′ss and the branch point sequence within complex A. Subsequently, complex A associates with the U4–U6-U5 tri-snRNP, leading to new base pairs between U2 and U6 snRNA and between U5 snRNA and exonic sequences near the 5′ss. The U4 snRNA is disassociated from U6 to expose the 5′ end of U6, which then base pairs with the 5′ss to displace U1 snRNA. In the end, an extensive network of base-pairing interactions is formed between U6 and U2, juxtaposing the 5′ss and branch-point adenosine for the first catalytic step of splicing. The central region of U6 snRNA forms an intramolecular stem-loop (the U6-ISL), which is essential for splicing catalysis. Adapted from Matera and Wang (2014).

(M. Chen & Manley, 2009; Fu & Ares, 2014). However, the activity of splicing factors and cis-acting splice recognition elements are highly context dependent. For certain splicing factors, such as hnRNP H, NOVA (a brain-specific splicing factor), SR splicing factors and hnRNP A1, their relative position on the pre-mRNA will determine their function as either splice activator or repressor (Borah, Wong, & Steitz, 2009; Chou, Rooke, Turck, & Black, 1999; McCullough & Berget, 1997; Ule et al., 2006; Y. Wang et al., 2013).

Most genes in higher eukaryotes undergo alternative splicing to produce multiple isoforms of an mRNA with distinct activity, generating functional diversity in the proteome at a cellular and tissue specific level (Nilsen & Graveley, 2010). In humans, more than 95% of all multi-exon genes undergo alternative splicing (Pan, Shai, Lee, Frey, & Blencowe, 2008; E. T. Wang et al., 2008) and dysregulation of splicing is associated with several human diseases (He et al., 2011; Padgett, 2012; Singh & Cooper, 2012; Tanackovic et al., 2011). Alternative splicing is particularly prevalent in the brain (de la Grange, Gratadou, Delord, Dutertre, & Auboeuf, 2010; Grosso et al., 2008; Yeo, Holste, Kreiman, & Burge, 2004), suggesting that splicing serves an important function in regulating the molecular and cellular diversity and specificity of the nervous system (Q. Li, Lee, & Black, 2007; Lipscombe, 2005). Ample studies have shown that alternative splicing contributes to the regulation of ion channel properties, cell surface interactions, neural signaling and other functions (Craig & Kang, 2007; Mu, Otsuka, Horton, Scott, & Ehlers, 2003; Norris & Calarco, 2012; Quesnel-Vallières, Irimia, Cordes, & Blencowe, 2015). For example, alternative splicing of the cell adhesion molecules neurexins and neuroligins determines not only the strength of the synapse but coordinates the appropriate excitatory or inhibitory specialization across the synaptic cleft (Boucard, Chubykin, Comoletti, Taylor, & Südhof, 2005; Chih, Gollan, & Scheiffele, 2006; Graf, Kang, Hauner, & Craig, 2006). Many splicing events that alter neuronal activity are themselves dynamically regulated by activity, such as the mRNA abundance and splice-variant distribution of the PSD scaffolding protein Homer1 after strong

potentiation (Bottai et al., 2002). Alternative splicing not only generates variability in the coding sequence, but is also responsible for the formation of alternative mRNA 3' ends that differ in the length and sequence of the 3' untranslated region (UTR) (Mayr, 2016). As described previously, neurons especially employ the 3' UTR complexity to regulated the sub-cellular localization, stability, translation and plasticity of synaptic mRNA transcript isoforms (Tushev et al., 2018). This is achieved by 3' UTRs functioning as a binding platform for not only RBPs, but also a specific family of ncRNAs, micro RNAs (miRNAs) (Bartel, 2009; Chi, Zang, Mele, & Darnell, 2009; Darnell, 2013; Lai, 2002; Licatalosi et al., 2008; Tushev et al., 2018).

The new member of the non-coding RNA family

In the 2000s, the revolution of ncRNAs gained a huge momentum with the discovery of miRNAs, small non-coding RNAs that act as post-transcriptional regulators of gene expression (Fire et al., 1998; Hamilton & Baulcombe, 1999; Lagos-Quintana, Rauhut, Lendeckel, & Tuschl, 2001; N. C. Lau, Lim, Weinstein, & Bartel, 2001; Lee & Ambros, 2001; Lee, Feinbaum, & Ambros, 1993; Ngô, Tschudi, Gull, & Ullu, 1998; Pasquinelli et al., 2000; Wightman, Ha, & Ruvkun, 1993). miRNAs are found in plants, animals and some viruses, and trigger the translational repression or decay of the target mRNA by base-pairing to its 3'UTRs (Bartel, 2009). A single mRNA transcript can be targeted by multiple miRNAs and the impact of a miRNA on gene expression correlates with its abundance (Ameres & Zamore, 2013). Compared to other tissues, the brain expresses the highest number of tissue-specific or -enriched miRNAs (Krichevsky, King, Donahue, Khrapko, & Kosik, 2003; Lagos-Quintana et al., 2002; Sempere et al., 2004). Neural miRNAs are subject to activity-dependent regulation and play a pivotal role in the regulation of synapse development and synaptic plasticity (Fineberg, Kosik, & Davidson, 2009; Hu & Li, 2017). The role of miRNA regulation on local protein synthesis is subject of this thesis and will be discussed in detail in *Chapter III*.

The advent of deep-sequencing further led to the discovery of long non-coding RNAs (lncRNAs) (Guttman et al., 2009; Guttman, Russell, Ingolia, Weissman, & Lander, 2013; Mercer, Dinger, Sunkin, Mehler, & Mattick, 2008; Rinn & Chang, 2012), a very heterogenous class of ncRNAs. Equally diverse is the rich repertoire of lncRNA functions, ranging from transcriptional and post-transcriptional regulation to the participation of protein scaffold formation (Geisler & Coller, 2013; Gong & Maquat, 2011; Kino, Hurt, Ichijo, Nader, & Chrousos, 2010; Latos et al., 2012; Tsai et al., 2010; Tseng et al., 2014). Moreover, lncRNAs have become relevant players in the nervous system as hundreds of lncRNAs were identified in mammalian brain, controlling functions such as synapse formation or local protein synthesis in dendrites (Bernard et al., 2010; Clemson et al., 2009; Tiedge, Fremeau, Weinstock, Arancio, & Brosius, 1991; Tripathi et al., 2010; H. Wang et al., 2005; H. Wang et al., 2002; Zalfa et al., 2003).

Recently, a special class of covalently closed circular RNAs (circRNAs) joined the ncRNA family. CircRNAs are generated from exonic or intronic sequences via back-splicing (Memczak et al., 2013; X. O. Zhang et al., 2014; Y. Zhang et al., 2016) and have been identified in various species over the past years (W. Chen & Schuman, 2016). Several functions of circRNAs have been proposed, including sequestration as miRNA sponges and scaffolding of proteins (Hentze & Preiss, 2013). Due to the heterogeneous nature of the brain and the dynamic regulation of neuronal function, the influence of circRNA is potentially extensive. Hence, a systematic characterization of circRNAs in the brain would provide valuable insight in the biogenesis and function of the new class of RNA regulators. In *Chapter II* of this thesis I describe our efforts to elucidate the circRNA landscape in the murine brain and to identify key biogenesis regulators of neuronal circRNAs.

The aim of the thesis

Proper neuronal function relies on the continuous modifications of the synaptic proteome over space and time. Given the elaborate morphology of neurons, the protein pool in neuronal processes cannot be fueled by somatic protein synthesis only. Local regulation on mRNA localization and translation are hence crucial. Scientific efforts over the past decades have highlighted the importance of non-coding RNA-mediated regulation on many aspects of brain function. The aim of my thesis is to obtain a better understanding of the role of non-coding RNAs in regulating local protein synthesis and synaptic function in the murine hippocampus. In particular, we focused our studies on two classes of non-coding RNAs.

The work presented in *Chapter II* of this thesis addresses on our attempt to provide an in-depth characterization of the circRNA landscape in mouse and rat hippocampus. By combining high throughput RNA-sequencing with fluorescence *in situ* hybridization we assessed the circRNA expression in the subcellular compartments of hippocampal neurons. Furthermore, we investigated the dynamic expression changes of circRNAs during neuronal development and upon induction of synaptic plasticity. In addition, we studied how the spliceosome regulates neuronal circRNA formation by temporarily inhibiting spliceosome activity and analyzing the differentially regulated circRNAs.

The second aim of my thesis is to investigate the spatio-temporal dynamics of miRNA-regulation on local protein synthesis in dendrites and spines. For this purpose, we developed in collaboration with the group of Prof. Dr. Alexander Heckel (Goethe University Frankfurt) a molecular probe, the antimiR, to control miR-181a activity using light. We combined a live-cell imaging approach with metabolic labelling of newly synthesized proteins using the Puro-PLA technique to study the effect of miR-181a sequestration on the local protein synthesis of Camk2a mRNA in space and time.

Chapter II

INVESTIGATING THE ROLE AND BIOGENSIS OF NEURONAL CIRCULAR RNAS IN THE MURINE HIPPOCAMPUS

INTRODUCTION

Circular RNAs are a new class of regulatory RNAs

Recently, circular RNAs (circRNAs) have re-emerged as a class of regulatory RNAs that are generated by the circularization of 3' and 5' end of exons and/ or introns of their host mRNAs. The covalently closed nature of circRNAs sets them strongly apart from the linear RNA classes expressed in the cell. Although the discovery of the first circRNAs as viroids dates back nearly 40 years (Hsu & Coca-Prados, 1979; Sanger, Klotz, Riesner, Gross, & Kleinschmidt, 1976), the rare expression of endogenous circRNAs led to the assumption that they are rather byproducts of aberrant splicing without any functional relevance (Cocquerelle, Daubersies, Majérus, Kerckaert, & Bailleul, 1992; Cocquerelle, Mascrez, Hétuin, & Bailleul, 1993; Nigro et al., 1991). With the advent of new high-throughput sequencing technologies, however, thousands of circRNAs were detected in metazoans, often highly conserved across species and displaying tissue and cell-type specific expression (Gruner, Cortés-López, Cooper, Bauer, & Miura, 2016; Guo, Agarwal, Guo, & Bartel, 2014; Hansen et al., 2013; Jeck et al., 2013; Memczak et al., 2013; Rybak-Wolf et al., 2015; Salzman, Gawad, Wang, Lacayo, & Brown, 2012; Venø et al., 2015; Westholm et al., 2014). The ubiquitous expression of circRNAs in nearly all species and tissues investigated so far highlights the potential importance of this class of RNA molecules and raises the question of the functionality of circRNAs.

The functional repertoire of circRNAs

Up to now, few functions of circRNAs have been described. Most prominently, two circRNAs were shown to act as modulators of miRNA function (Hansen et al., 2013; Memczak et al., 2013). CircRNA *CDR1as* possesses multiple binding sites and displays binding capacity for miR-7 (Hansen et al., 2013). The potential of *CDR1as* to regulate intracellular miR-7 expression level

or activity *in vivo* was verified as reduced stability of miR-7, and increased levels of miR-7 target genes is observed in *CDR1as* knock-out mice (Piwecka et al., 2017). Moreover, *CDR1as* was shown to form a regulatory network with lncRNA *Cyrano* to modulate the expression of miR-7 (Kleaveland, Shi, Stefano, & Bartel, 2018). The second circRNA, *circSRY,* was shown to bind miR-138 (Hansen et al., 2013). However, the physiological importance of their interaction has not yet been established (Hansen et al., 2013). Although some circRNAs have shown to act as miRNA sponges, studies have suggested that circRNAs, as a group, do not extensively bind to miRNAs (Guo et al., 2014; You et al., 2015). Another hypothesized function of circRNAs is to serve as templates for translation. Here the difficulty lies in the discrimination between parent mRNA translation and circRNA translation. Several groups tackled this question by using ribosome footprinting, cellular assays and mass spectrometry (Legnini et al., 2017; Pamudurti et al., 2017; Yang et al., 2017). Especially for the latter, the detection of peptides originating from the head-to-tail junction would provide direct evidence for the translation of circRNAs. Unfortunately, to date the data addressing this issue remain inconclusive. Another role of circRNAs is to act as transporters or scaffolds for RNA-binding proteins (RBPs) (Abdelmohsen et al., 2017; Du et al., 2016; Holdt et al., 2016). Together, these studies provided insight into possible roles of circRNAs. However, the full functional repertoire of this heterogeneous class of RNAs still awaits to be discovered.

Biogenesis factors for circRNAs

Another field of intensive investigation is the regulation of circRNA biogenesis. CircRNAs are generated by the formation of a head-to-tail junction, in which the 5' splice donor site of a downstream exon is covalently joined with the 3' splice acceptor site of an upstream exon. At least three factors seem to influence the formation of circRNAs. While mutations of distinct splice sites abolish circRNA formation, modulation of the spliceosome machinery results in either an increase or a decrease of circRNA levels (Ashwal-Fluss et al., 2014;

Kramer et al., 2015; Liang et al., 2017; Starke et al., 2015). These results suggest the involvement of the splicing machinery in circRNA formation. The production of circRNAs seems to further depend on intronic sequences that are enriched in reverse complementary motifs, such as Alu repeats (Ivanov et al., 2015; Jeck et al., 2013; Venø et al., 2015; X. O. Zhang et al., 2014). However, only around 40% of circRNAs are expressed from genes that contain Alu repeats in their flanking introns (Ivanov et al., 2015; Jeck et al., 2013; Venø et al., 2015), suggesting additional mechanisms of exon circularization. For example, several RBPs were found to modulate the expression of circRNAs, often binding to introns flanking the circularizing exons (Aktaş et al., 2017; Ashwal-Fluss et al., 2014; Conn et al., 2015; Errichelli et al., 2017; Ivanov et al., 2015; Kramer et al., 2015). The presence of intronic repeat sequences and binding of RPBs share the common mechanism of facilitating intron-intron interactions resulting in circRNA formation. Currently, biogenesis factors are tested individually for their effect on the generation of circRNAs, often using a candidate-based approach. As circRNA expression is highly dynamic across tissues and cell-states (Memczak et al., 2013; Salzman, Chen, Olsen, Wang, & Brown, 2013), it is likely that proper regulation is achieved by the synergistic activity of multiple biogenesis factors.

Studying the biogenesis and role of circRNAs in the mammalian hippocampus

The efficient regulation of cellular function and gene expression is especially important for neurons, due to their unique, polarized morphology. The discovery of mRNAs, miRNAs and more recently lncRNAs in neuronal somata and processes (Huntzinger & Izaurralde, 2011; Kye et al., 2007; Rinn & Chang, 2012) broadened the landscape for the complex regulatory network of RNA-mediated mechanisms in neurons. Although circRNAs have been previously identified in the brain (Memczak et al., 2013; Nilsen & Graveley, 2010; Rybak-Wolf et al., 2015; Westholm et al., 2014), a global and functional characterization of neuronal circRNAs is still missing. Hence, we set out to profile the neuronal circRNA landscape of the mammalian hippocampus. Furthermore, we

investigated changes in circRNA expression throughout developmental stages. As many RNAs are subject to activity-mediated regulation in neurons, we examined circRNA expression upon plasticity. To dissect the roles of distinct factors on neuronal circRNA biogenesis, we combined pharmacological inhibition of the spliceosome with RNA-sequencing and bioinformatic analyses. Understanding the biogenesis of neuronal circRNAs is crucial for the development of novel tools to manipulate the expression of not only individual candidates, but entire circRNA classes and will open up new avenues for investigating the functionality of circRNAs in the brain.

RESULTS

Previous data

CircRNAs are enriched in brain tissue

To investigate the pattern of circRNA expression across different mouse tissue, we performed rRNA-depleted total RNA-sequencing on brain, heart, liver, lung and testis samples. RNA-seq reads that mapped directly to the reference genome and canonical exon-exon junctions were used to determine the total transcriptional output from a given gene loci (TTO). Reads that span the head-to-tail junction, where the 5' and 3' splice site of exons mapped to the mouse genome in reversed order, were used to identify circRNAs. Using this pipeline, we identified thousands of circRNAs across all examined tissues, with the highest circRNA abundance detected in the brain, where 20% of the protein-coding genes gave rise to circRNAs. Our data suggested that two factors contribute to the high abundance of neuronal circRNAs: i) many host genes that produced circRNAs are exclusively expressed in brain and ii) host genes that produce circRNAs in multiple tissues give rise to more circRNAs in brain (Figure 11).

Using three independent methods we successfully validated the circularity of the detected circRNAs. As circRNAs do not possess poly(A) tails, we observed an expected depletion of circRNAs in poly(A)-enriched sequencing libraries. Second, due to their closed-loop structure all tested candidate circRNAs showed resistance to treatment with exonuclease RNase R. Furthermore, when we deep sequenced cDNA products obtained from 12 candidate circRNAs and for 11 of them, we detected reads corresponding to the rolling circle RT products that could not be detected in the cDNA from any linear RNAs (Figure 12).

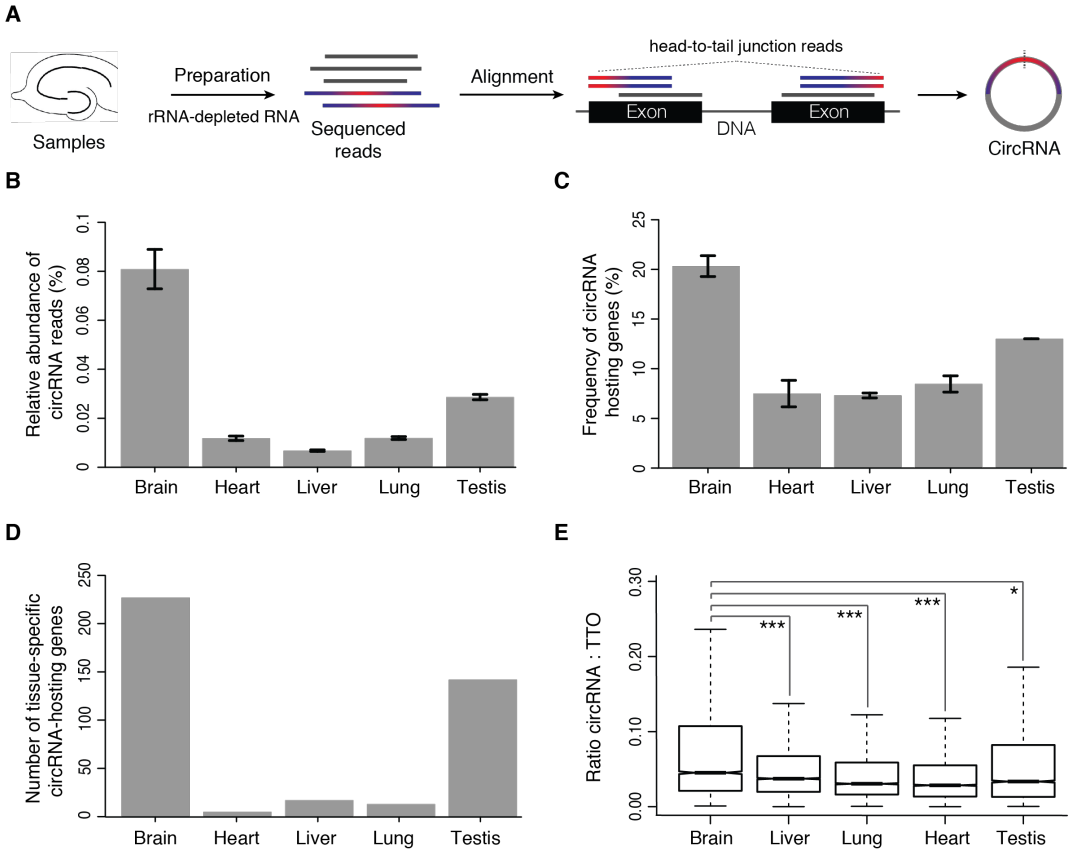

Figure 11. Compared to other tissues circRNAs are the most abundant in the brain.
A. Mouse tissue samples, such as the hippocampus, were isolated and rRNA-depleted total RNA was used for deep sequencing. Reads that mapped to the genome in a non-canonical order (red-blue lines) were used to identify head-to-tail junction reads that are unique to circRNAs. **B.** The percentage of head-to-tail junction reads to all mapped reads is shown for the tested tissues. The highest abundance of circRNAs was observed in the brain (0.075-0.087%). **C.** The percentage of all genes detected from a given tissue that produce circRNAs is shown. The highest fraction of circRNAs (20-21%) was found in the brain. **D.** The number of circRNA host genes that are exclusively found in one tissue. The brain expressed the most tissue-specific circRNAs. **E.** The relative contribution of circRNAs to the total transcriptional output (TTO) of a given gene loci. The highest contribution of circRNAs to the TTO is found in brain. The ratios of the relative contribution between brain and the other four tissues were significantly larger than 1 (***$p < 2.2 \times 10^{-16}$, two-sided one-sample t-test).
Modified from You et al. (2015).

CircRNAs are derived from synaptic genes and enriched at synapses

Are certain genes more likely to give rise to circRNAs than other genes? To answer this question, we performed a Gene Ontology analysis of genes that generate neuronal circRNAs. Interestingly, several functional groups related to

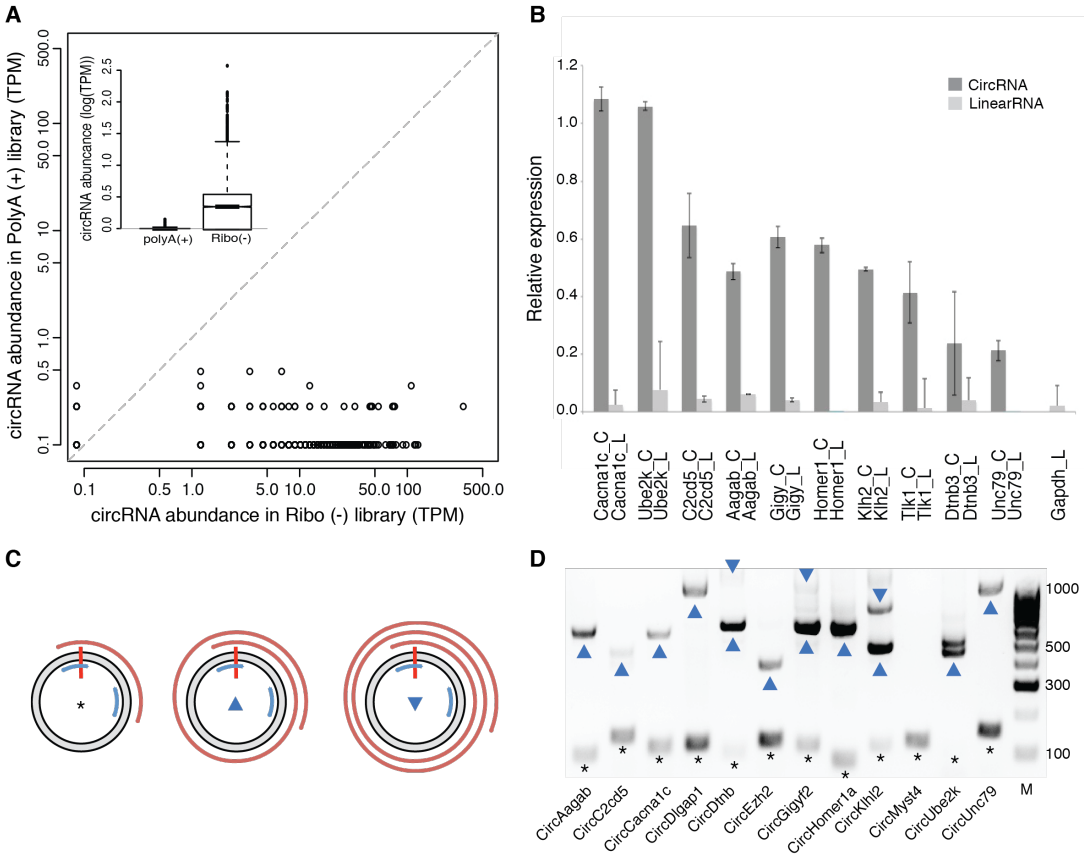

Figure 12. Successful validation of the authenticity of detected circRNAs.
A. Comparison of circRNA expression between an rRNA depleted library (x-axis) and a poly(A)-enriched library (y-axis). Each circle represents a circRNA. Compared to the rRNA depleted library, circRNA abundance is depleted in the poly(A)-enriched library. Inset shows that circRNAs, as a group, are strongly depleted in poly(A)-enriched library. Whiskers show extreme data points that are no more than 1.5 times the interquartile range from the box. **B.** qRT-PCR validation of 10 candidate circRNA and their host mRNAs after RNase R treatment. All tested circRNAs show greater RNase R resistance than their linear host transcript. Light grey bars show circRNA expression and dark grey bar linear mRNA expression, respectively. **C.** The rolling circle products from circRNAs. CircRNAs are depicted as grey circles, the head-to-tail junction as red vertical bar and the PCR primers as two blue arcs, respectively. The PCR product is shown as red spiral and obtained by deep sequencing using the PacBio technology. The asterisk, upward triangle and downward triangle symbols denote the 0 cycle, 1st cycle and 2nd cycle PCR products, respectively. **D.** DNA gel shows the rolling cycle PCR products of 12 tested candidate circRNAs. With the exception of *circMyst4*, all tested circRNAs generated rolling circle products (upward and downward triangle). DNA size marker is shown in lane M.
Modified from You et al. (2015).

synaptic functions, such as synapse, synapse part, presynaptic active zone, presynaptic membrane and postsynaptic density, were overrepresented. To test if circRNAs are not only derived from synaptic genes, but are also enriched in

synaptic sub-compartments, RNA-sequencing of two types of tissue samples from mouse brain was performed: i) synaptosomes, a biochemically purified preparation that is enriched in synapses and ii) microdissected synaptic neuropil from the hippocampus. Indeed, we found that most circRNAs were enriched in one or both of the synaptic fractions, with the circRNAs detected in the two synaptic fractions highly overlapping with each other. Fluorescence *in situ* hybridization of two candidate circRNAs, *circHomer1* and *circDscam*, validated their expression in the soma and dendrites of primary hippocampal neurons. Taken together, our results show that neuronal circRNAs are often derived from synaptic genes and enriched in synaptic tissue (Figure 13).

Dynamic expression of neuronal circRNAs during development and homeostatic plasticity

To understand how neuronal circRNAs expression is regulated during development, we profiled the circRNA population in the hippocampus over several developmental stages: embryonic (E18), early postnatal (P1), postnatal at the beginning of synapse formation (P10) and late postnatal hippocampus following the establishment of mature neuronal circuits (P30). Interestingly, a shift in circRNA expression was observed at P10, the time of synaptogenesis. Overall, 181 circRNAs were up-regulated and 43 circRNAs down-regulated throughout development, respectively. While up-regulated circRNAs derived from genes encoding proteins enriched for synapse-related functions, genes encoding down-regulated circRNAs were not enriched for any functional categories. When we compared the expression of linear host transcript and circRNA expression at the earliest (E18) and latest (P30) time points, we found that many circRNAs altered their expression independent of their host transcripts during synaptogenesis. While circRNAs, as a group, were up-regulated through development, the expression of most host mRNAs did not change much in abundance compared to all genes (Figure 14).

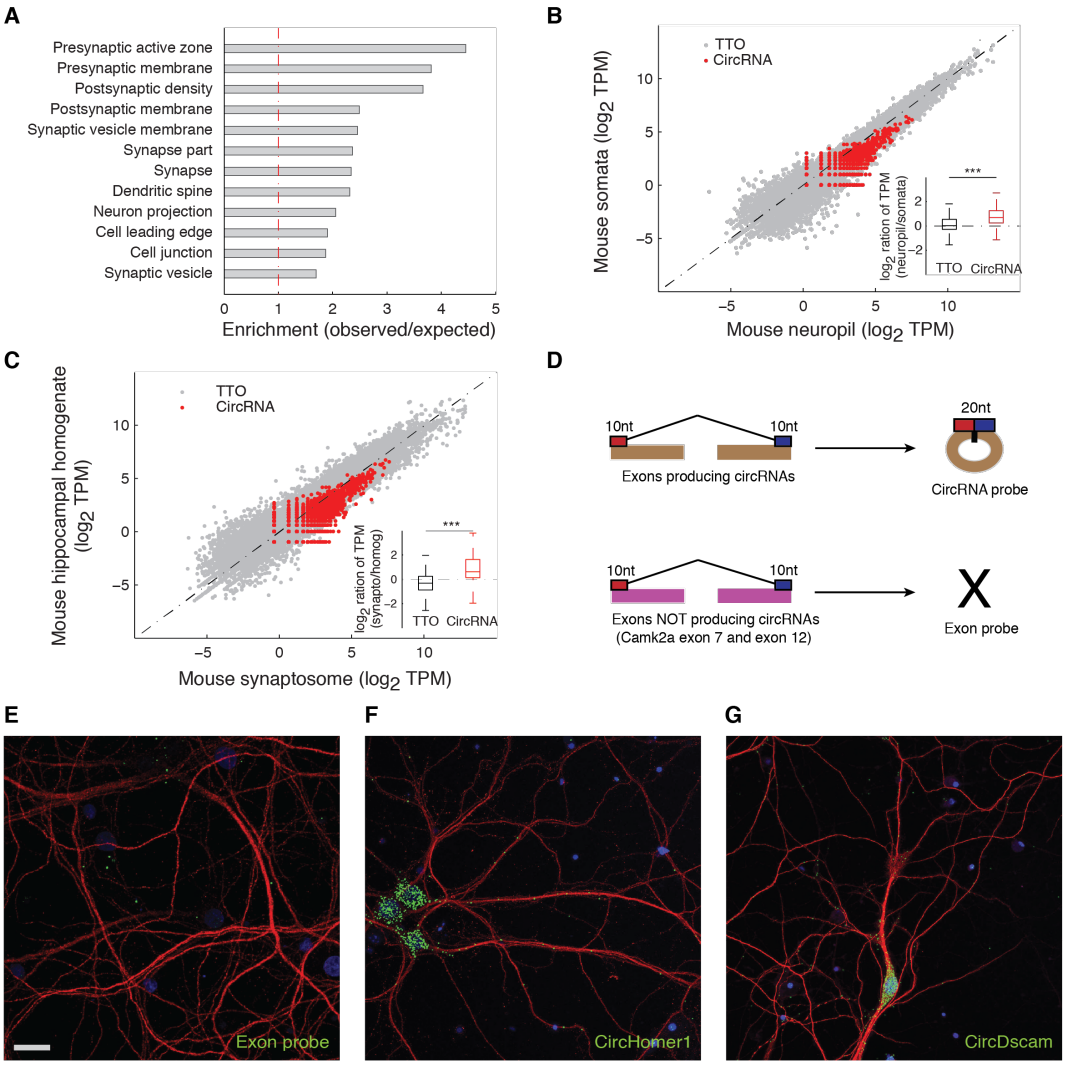

Figure 13. Neuronal circRNAs are derived from synaptic genes and enriched in synaptic tissues.

A. Gene Ontology enrichment analysis of genes that produce neuronal circRNAs. Genes of functional groups related to synaptic function are overrepresented to produce circRNAs. **B.** Comparison of circRNA and TTO (total transcript output) between mouse neuropil (x-axis) and somata (y-axis). Grey dots represent protein coding loci, while red dots represent circRNAs. Inset shows an enrichment of neuronal circRNAs but not TTO in the neuropil (***$p < 2.2 \times 10^{-16}$, two-sided, unpaired t-test). **C.** Comparison of circRNA and TTO abundance between mouse synaptosome (x-axis) and homogenate (y-axis). Grey dots represent protein coding loci, while red dots represent circRNAs. Inset shows an enrichment of neuronal circRNAs but not TTO in synaptosome fraction (***$p < 2.2 \times 10^{-16}$, two-sided, unpaired t-test). **D.** Schematic of circRNA probes for fluorescence *in situ* hybridization. Top: A circRNA probe was designed to span 20 nt of the head-to-tail junction (red and blue rectangle). Bottom: A control probe was targeting the junction of exon 7 and exon 12 of the *Camk2a* transcript, which do not circularize. **E-G.** Fluorescence *in situ* hybridization of candidate circRNAs or exon control probe is shown in cultured hippocampal neurons. Fluorescence *in situ* signal is shown in green. Dendrites were visualized using MAP2-staining (red) and nucleus using DAPI staining (blue), respectively. Scale bar = 20 μm**. E.** Little signal was observed using the exon control probe. **F.** *CircHomer1* was

detected in soma and dendrites of hippocampal neurons. **G.** *CircDscam* was detected in soma and dendrites of hippocampal neurons. Scale bar = 20 μm.
Modified from You et al. (2015).

To investigate modulations of circRNA expression after alterations of neuronal activity, we induced homeostatic plasticity in primary hippocampal neurons using a treatment with 40 μM bicuculline, an antagonist of $GABA_A$ receptors. Induction of homeostatic plasticity caused dynamic changes in circRNA population where 37 circRNA showed enhanced and five circRNAs reduced expression levels, respectively. In contrast, most linear host transcripts didn't exhibit prominent changes in their expression. qRT-PCR was used to validated the expressional changes of four circRNAs and their linear parent mRNA. Furthermore, fluorescence *in situ* hybridization was applied to visualize the increase in *circHomer1* expression upon bicuculline treatment in cultured hippocampal neurons. Taken together, our data show that circRNA expression is dynamically regulated by neural plasticity (Figure 15).

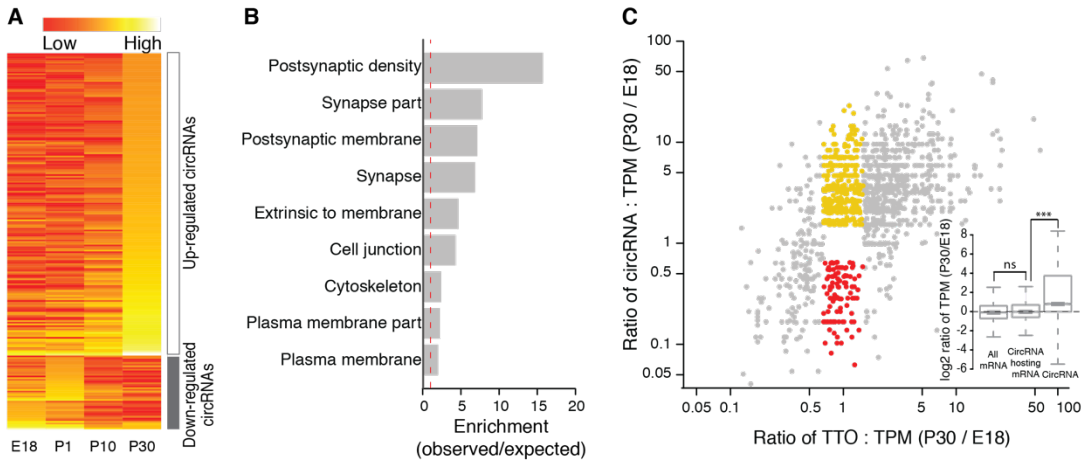

Figure 14. Regulated expression of neuronal circRNAs during development.
A. Heatmap of circRNA expression across four developmental stages. A total of 181 circRNAs were up-regulated throughout development, with a peak around postnatal day 10 (P10). A smaller group of 43 circRNAs showed consistent down-regulation through development. Scale bar show low expression of circRNAs in red and high expression of circRNAs in yellow, respectively. **B.** Gene Ontology enrichment analysis of functional groups of genes that give rise to circRNAs. Neuronal circRNAs were enriched for several synaptic functions. **C.** Scatterplot showing the expressional changes of circRNA (y-axis) and TTO of host gene loci (x-axis) between embryonic stage (E18) to postnatal day 30 (P30). Each dot represents a circRNA. CircRNAs that were up-regulated but whose host transcript was not substantially changed in expression are shown in

yellow. In red are shown circRNAs that were down-regulated through development and whose host transcripts remain unchanged. Inset shows that, as a group, circRNAs were significantly increased through development compared to host gene transcript (ns p = 0.09709, ***p < 2.2 x 10^{-16}, two-sided unpaired t-test)
Modified from You et al. (2015).

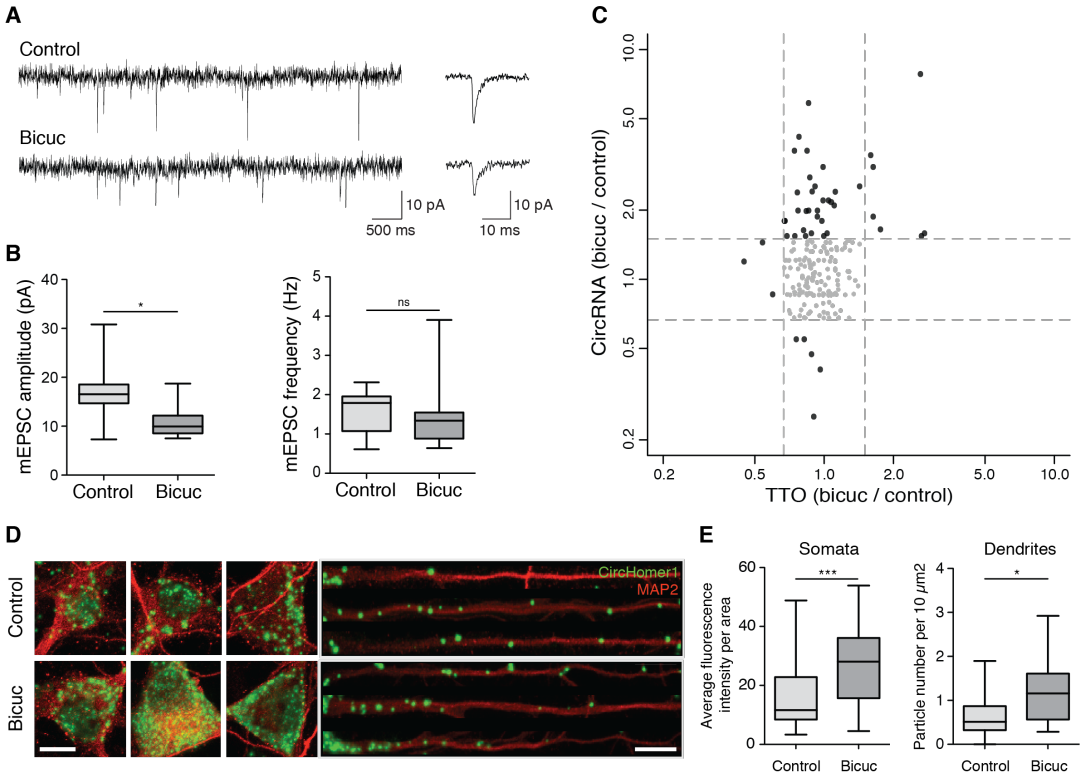

Figure 15. Regulation of circRNA expression upon induction of homeostatic plasticity.
A. Electrophysiology traces of mEPSCs from control neurons (top row) and neurons treated with bicuculline for 12 h (bottom row). Representative recordings (left) and average mEPSC (right) waveform are shown. **B.** Quantification of the mEPSC amplitude and frequency. Significant difference in mEPSC amplitude but not frequency was measured after bicuculline treatment (*p < 0.0499, ns p = 0.3717, Mann Whitney U test, n = 4). **C.** Expression changes of circRNA (y-axis) and TTO of host gene loci (x-axis) between bicuculline and control condition. Each dot represents a circRNA. CircRNAs and host gene loci that did not show substantial changes (less than 30%) in expression are represented in grey. **D.** Visualization of *circHomer1* changes in soma and dendrites after homeostatic plasticity using fluorescence *in situ* hybridization. *CircHomer1* signal is shown in green. Dendrites were visualized using MAP2-staining (red). Scale bar = 10 μm. **E.** Quantification of *circHomer1* FISH between bicuculline and control treatment. Both in soma and dendrites a significant increase in *circHomer1* expression was observed (soma: ***p < 0.0005, Mann Whitney U test, n = 34 and 43; dendrites: *p < 0.0208, Mann Whitney U test, n = 12 and 13).
Modified from You et al. (2015).

Visualization of circRNAs in rat hippocampal slices

Using fluorescence *in situ* hybridization we visualized circRNAs in cultured hippocampal neurons under baseline activity and after homeostatic plasticity. As the RNA-seq data of our study was obtained from murine hippocampus, we also aimed to visualize circRNA expression in hippocampal slices. Moreover, brain slices offer the advantage over culture systems that they are closer to the *in vivo* context, including the largely preserved tissue architecture of the brain regions that they originated from and the maintenance of neuronal activities with intact functional local synaptic circuitry. Hence, I established a FISH protocol for the detection of RNAs in tissue slices. I successfully visualized *circHomer1* in vibratome sections of the rat hippocampus. Similar to the observations we made in cultured hippocampal neurons, I detected an increase in *circHomer1* expression in somata and neuropil layer following homeostatic plasticity (Figure 16).

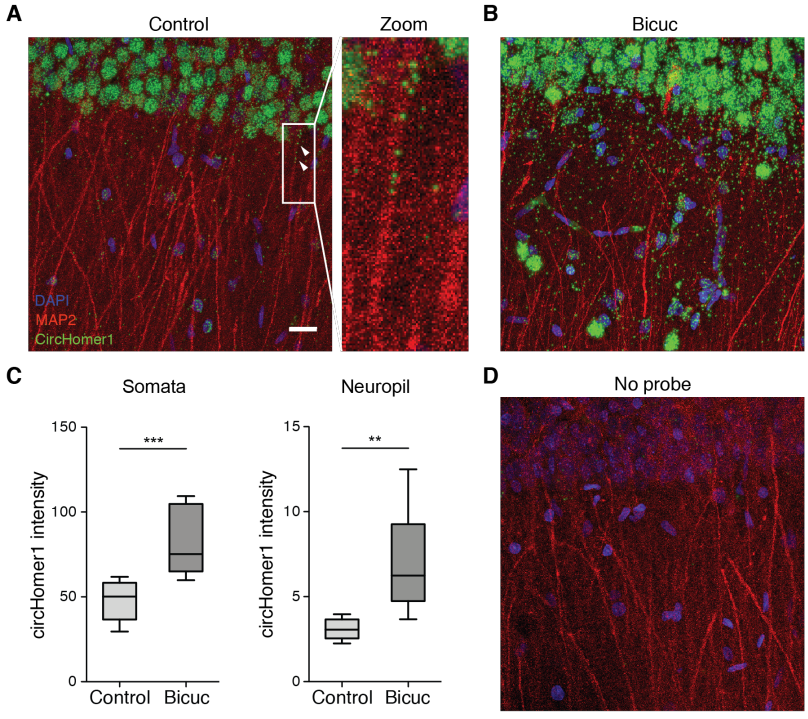

Figure 16. *CircHomer1* expression in hippocampal slices following homeostatic plasticity. **A.** Detection of *circHomer1* (green) in somata and neuropil under baseline conditions. The white box and its zoom-in (right) shows a stretch of dendrite along which *circHomer1* signal was detected (arrows). Cell body and dendrites are visualized using MAP2 (red). Scale bar = 75 μm.

B. *CircHomer1* expression after bicuculline treatment. An increase in both somatic and dendritic *circHomer1* was observed. **C.** Quantification of *circHomer1* intensity in the somata and the neuropil layer. A significant increase in *circHomer1* expression was observed after bicuculline treatment (***$p < 0.0005$, **$p < 0.01$, Mann Whitney U test, $n = 9$). **D.** No *circHomer1* puncta were detected in no probe control. *circHomer1* is shown in green and MAP2 immuno-staining in red.

Evolutionary conservation of splice sites of neuronal circRNA producing genes

So far, our data suggest an important role of circRNAs in neuronal development and synaptic function. However, it is still unknown how the generation of circRNAs is regulated in the brain. We found a first hint that the spliceosome might be a key player in neuronal circRNA biogenesis when we investigated the splice sites of circRNA producing genes. Interestingly, splice sites around exons that form a head-to-tail junctions were more conserved than splice sites from the same host gene that were not involved in circularization. Moreover, splice sites around the head-to-tail junction of circRNAs that are common in both mouse and rat were even more evolutionarily conserved, showing the highest PhastCons score. This result points towards a functional relevance of splice sites for neuronal circRNA formation (Figure 17).

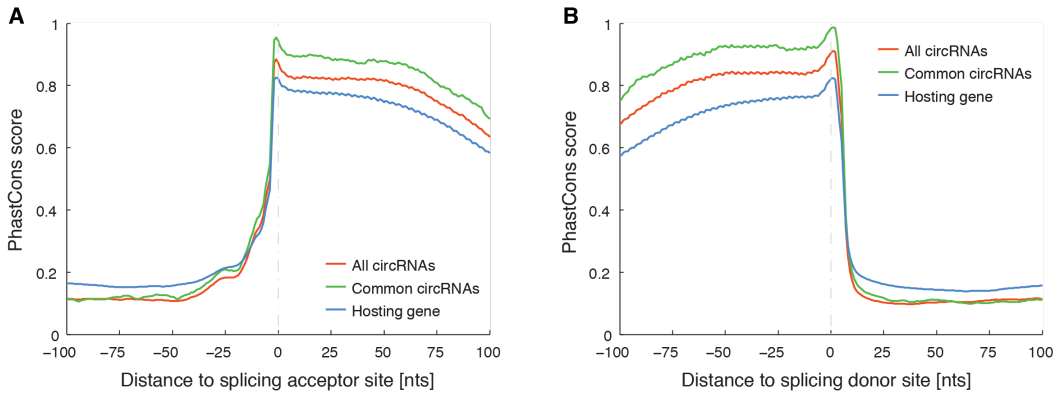

Figure 17. Evolutionary conservation of circRNA splice sites.
A. The exonic sequences around splice acceptor sites involved in the formation of mouse circRNAs (red) are more conserved than those of the same gene loci that are not involved in head-to-tail junction formation (blue). Splice acceptor sites common between mouse and rat were even more conserved, reaching nearly the maximal PhastCons score (green). **B.** Similar observations were made for the exonic sequences around the splice donor sites.
Modified from You et al. (2015).

Inhibition of spliceosome activity in primary hippocampal neurons using isoginkgetin

As our previous data suggests a spliceosome-mediated regulation of neuronal circRNA biogenesis, I next investigated how pharmacological inhibition of spliceosome activity affects the circRNA landscape in cultured hippocampal neurons. One reported chemical splicing inhibitor is the biflavonoid isoginkgetin that was first isolated from the leaf extract of *Ginkgo biliba*. Recent *in vitro* studies have shown that isoginkgetin prevents the stable recruitment of the U4/U5/U6 tri-small nuclear ribonucleoproteins at micromolar concentrations, resulting in the accumulation of the pre-spliceosomal complex and un-spliced endogenous pre-mRNA (O'Brien, Matlin, Lowell, & Moore, 2008). I treated cultured hippocampal neurons with 33 μM, 50 μM or 66 μM isoginkgetin for 12 h or 24 h, and validated the efficiency of spliceosome inhibition by quantifying the expression of *beta actin (ActB)* pre-mRNA using qRT-PCR. I found that an application of 33 μM isoginkgetin for 24 h inhibited spliceosomal activity most effectively (Figure 18).

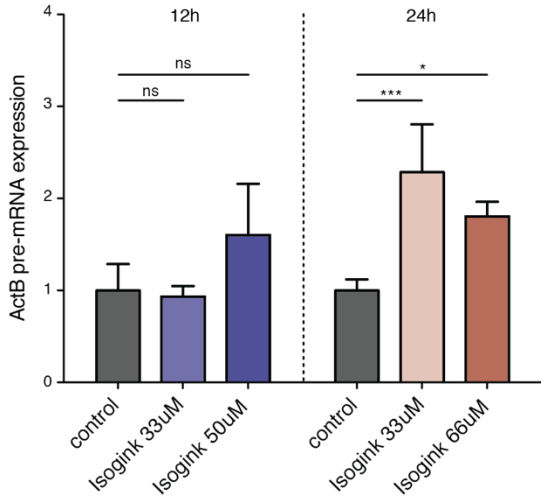

Figure 18. Optimizing the condition of isoginkgetin treatment in cultured hippocampal neurons.
Treatment of neurons with 33 μM, 50 μM or 66 μM isoginkgetin or DMSO for either 12 h or 24 h. The efficiency of spliceosome inhibition was determined by measuring the *actin-beta (ActB)* pre-mRNA content using qRT-PCR. The strongest increase of *ActB* pre-mRNAs was observed after 33 μM isoginkgetin for 24 h. (***$p < 0.0001$, *$p < 0.05$, one-way ANOVA followed by Bonferroni multiple comparison test, n = 3). Wang et al. (2019).

Profiling the circRNA and mRNA landscape after spliceosome inhibition

Hence, I incubated primary hippocampal neurons with 33 μM isoginkgetin or DMSO for 24 h and deep sequenced rRNA-depleted total RNA to examine the effect on circRNA biogenesis. From three biological replicates for each condition I obtained between 22 x 10^6 to 79 x 10^6 reads. Replicates of the same conditions correlated well with one another. To quantify mRNA and circRNA expression, I developed the following analysis pipeline: first, all reads were mapped to the rat genome using STAR, a high-performance aligner for RNA-seq data. STAR provides two distinct outputs files. The "classic" output file contains all reads that mapped to the genome in canonical order. These reads were used to determine the abundance of linear mRNA variants. Reads that span exon-intron junctions were used to measure the abundance of pre-mRNAs (un-spliced) and exon-exon junction reads to quantify mature (spliced) mRNAs. Reads that map to the body of an intron were used to quantify intron expression. Since reads that map to the body of exons cannot be clearly assigned to either pre- or mature mRNA, they were not considered for further analysis.

To profile circRNA expression, I quantified reads that map specifically to the head-to-tail junction and switched to the detection of "chimeric" aligments in STAR. A chimeric alignment consists of two segments which map to the genome in a non-canonical order. To identify head-to-tail junction reads the following criteria were set: i) both segments must originate from the same gene, ii) the 5' segment must align downstream of the 3' segment, iii) the segments must possess splice junctions and iv) each segment must be at least 20 bp long. Only circRNAs that were identified with at least one unique head-to-tail junction read and were consistently found in all replicates and conditions were retained for further analyses (Table 4).

Table 4. Details on RNA-sequencing samples.

	DMSO			**Isoginkgetin [33 μM]**		
	Repl 1	*Repl 2*	*Repl 3*	*Repl 1*	*Repl 2*	*Repl 3*
total number of reads	48775167	45505590	79203700	46558089	45724427	21831475
number of mapped reads	46902334	42075498	75172588	42708588	42337404	20194243
number of uniquely mapped reads	38566396	30894509	48283505	25809414	29450692	14387638
exon-body reads	17912355	14989485	22172891	9818742	11423787	5255304
exon-exon junction reads	7656382	6343313	9500829	4012615	4492982	2194226
intron body reads	3968750	2614698	4949182	3145322	3505727	2217062
exon-intron junction reads	547044	481658	867525	563174	572267	319903
back-splice junction reads	24155	18060	25692	23244	27633	15986
number of circRNAs detected	14382	11066	14984	14520	16603	11946
number of circRNA host genes	6284	5384	6426	6014	6481	5238

I validated the efficiency of the spliceosome inhibition of the RNA-seq samples by assessing the fraction of un-spliced pre-mRNA in total mRNA population (sum of pre- and mature mRNA). On a global level, I observed a 73.5% increase in pre-mRNA expression after spliceosome inhibition. Using qRT-PCR, I validated the pre-mRNA changes for individual transcripts and detected for *beta actin (ActB)* and *ATP synthetase membrane subunit E (ATP5I)* a 2.3-fold and 1.8-fold increase in pre-mRNA levels, respectively (Figure 19). Together, our results show that the spliceosome was successfully inhibited in cultured hippocampal neurons.

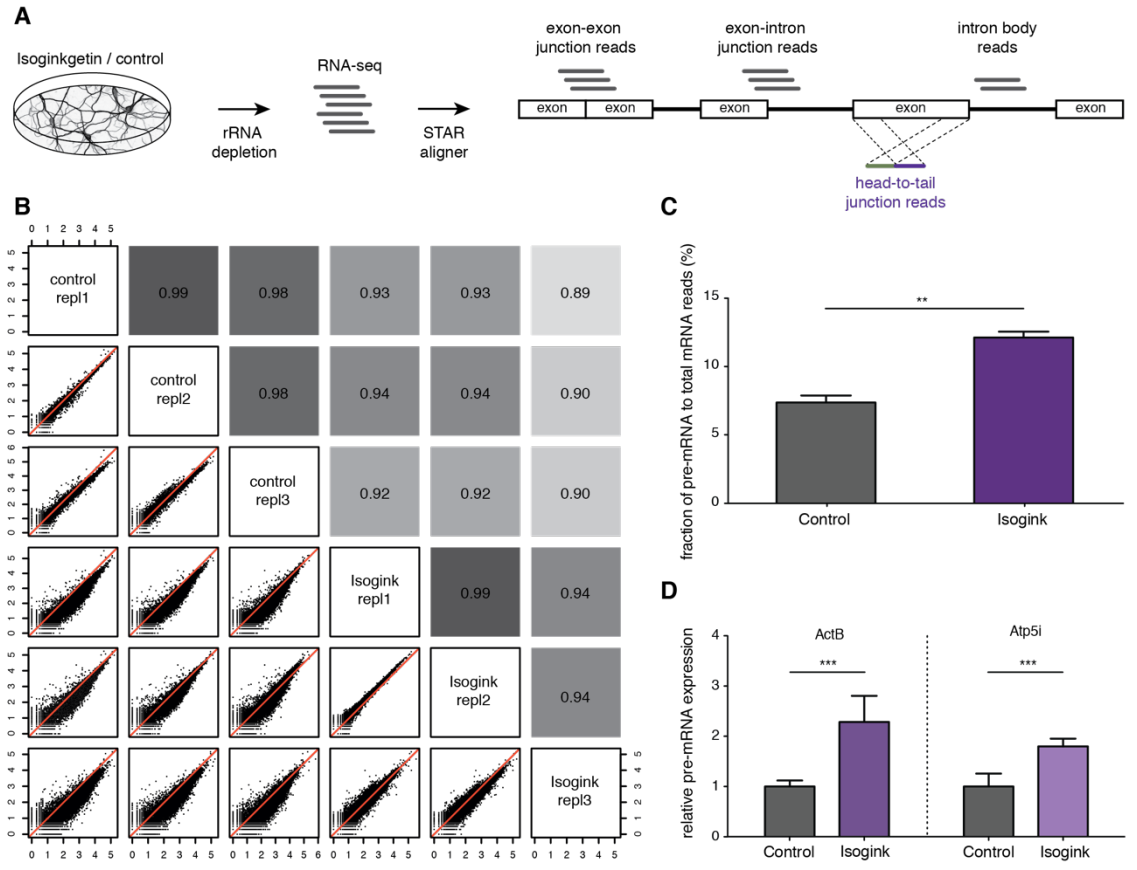

Figure 19. Application of isoginkgetin to inhibit spliceosome activity in cultured hippocampal neurons.
A. Experimental and analysis pipeline. Cultured neurons were treated with 33 μM isoginkgetin or DMSO for 24 h. rRNA-depleted total RNA was deep sequenced and aligned using STAR to the rat genome. Reads were grouped according to the gene features that they map to, such as exon-exon, exon-intron, head-to-tail junctions or intron body, and used to quantify mature mRNA, pre-mRNA, circRNA or intron expression, respectively. **B.** Correlation of RNA-seq between replicates and conditions. Values on x- and y-axis show the log10 transformed raw mRNA counts. A very good correlation was observed between the conditions (Pearson's correlation of 0.99 - 0.98). Only the third replicate of the isoginkgetin sample showed a correlation of 0.94 to the other treatment samples. **C.** The abundance of pre-mRNA to total mRNA was quantified in RNA-seq samples. We observed a significant increase of pre-mRNA expression after isoginkgetin treatment (purple) compared to the control (grey) (**$p < 0.01$, unpaired t-test, two-tailed, n = 3). **D.** Relative pre-mRNA expression of *ActB* and *Atp5i* was measured using qRT-PCR. For both candidates, we detected a significant increase in pre-mRNA expression after spliceosome inhibition (***$p < 0.001$, unpaired t-test, two-tailed, n = 3). Wang et al. (2019).

Isoginkgetin affects splicing rather than transcription

In a recent study, isoginkgetin has been reported as a transcription elongation inhibitor (Boswell et al., 2017). To examine whether spliceosome inhibition is the predominant effect of our treatment condition, I performed

differential analysis on total mRNA, pre-mRNA, mature mRNA and intron reads. I identified 11,052 isoginkgetin-enriched and 10,166 control-enriched transcript variants. While the total mRNA levels showed nearly no difference between isoginkgetin and control (median log FC of -0.16), I observed a larger reduction in mature mRNA levels (median log FC of -0.33) and a strong increase in both pre-mRNA and intron levels (median log FC of 0.62 and 0.92) after spliceosome inhibition. This result suggests that isoginkgetin primarily affects splicing rather than transcription under our treatment conditions (Figure 20).

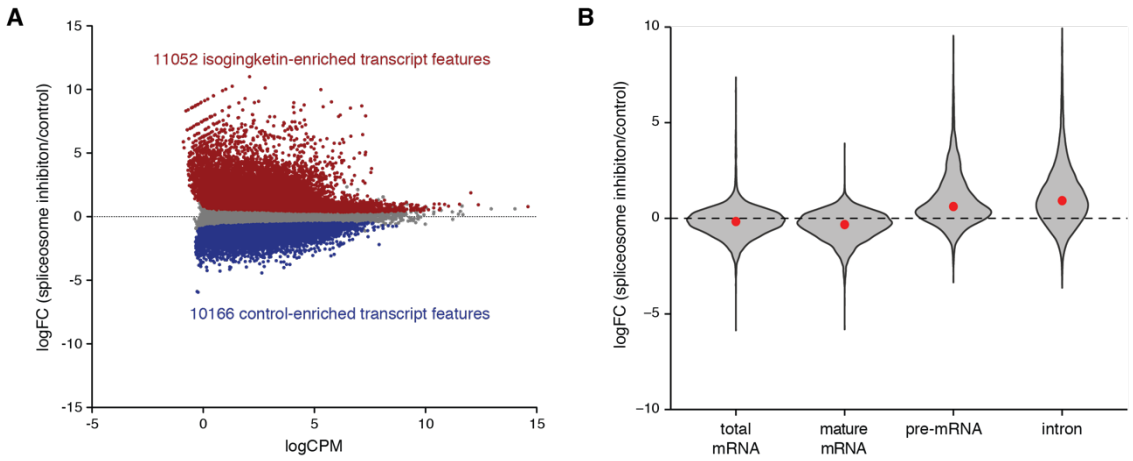

Figure 20. Isoginkgetin enhances pre-mRNA and intron expression.
A. Differential expression of transcript types in isoginkgetin vs control condition. We detected 11,082 transcript types that were significantly up-regulated (red dots) and 10,156 transcript types were significantly down-regulated (blue dots). Transcript types that were not significantly changed are shown as grey dots. **B.** Violin plot shows read distribution of all transcript types (total mRNA, mature mRNA, pre-mRNA and intron). Little change was observed in total mRNA reads between isoginkgetin and control condition, as reads are distributed closely around 0. An increase in pre-mRNA and intron reads was observed after isoginkgetin treatment, while mature mRNA reads were reduced in expression. Wang et al. (2019).

Detection of hundreds of neuronal circRNAs after spliceosome inhibition

Using this RNA-seq approach I identified on average 13,917 neuronal circRNAs per sample. Out of these, 1,659 and 1,911 circRNAs were detected in all isoginkgetin-treated and control samples, respectively. A group of 776 circRNAs were consistently expressed in all replicates and treatment conditions, and were used for further analysis. First, I tested the circularity of three candidate

circRNAs and their host mRNA using RNase R, an exoribonuclease that degrades linear but not circular transcripts. As expected, all tested circRNAs showed a significant enrichment after RNase R treatment while the linear mRNA was depleted. Next, I investigated the exon distribution of the detected circRNAs and found that the majority of them were generated by a single-exon. Moreover, the exon of single-exon circRNAs were significantly longer than exons of circRNAs that are formed by multiple-exons (Figure 21).

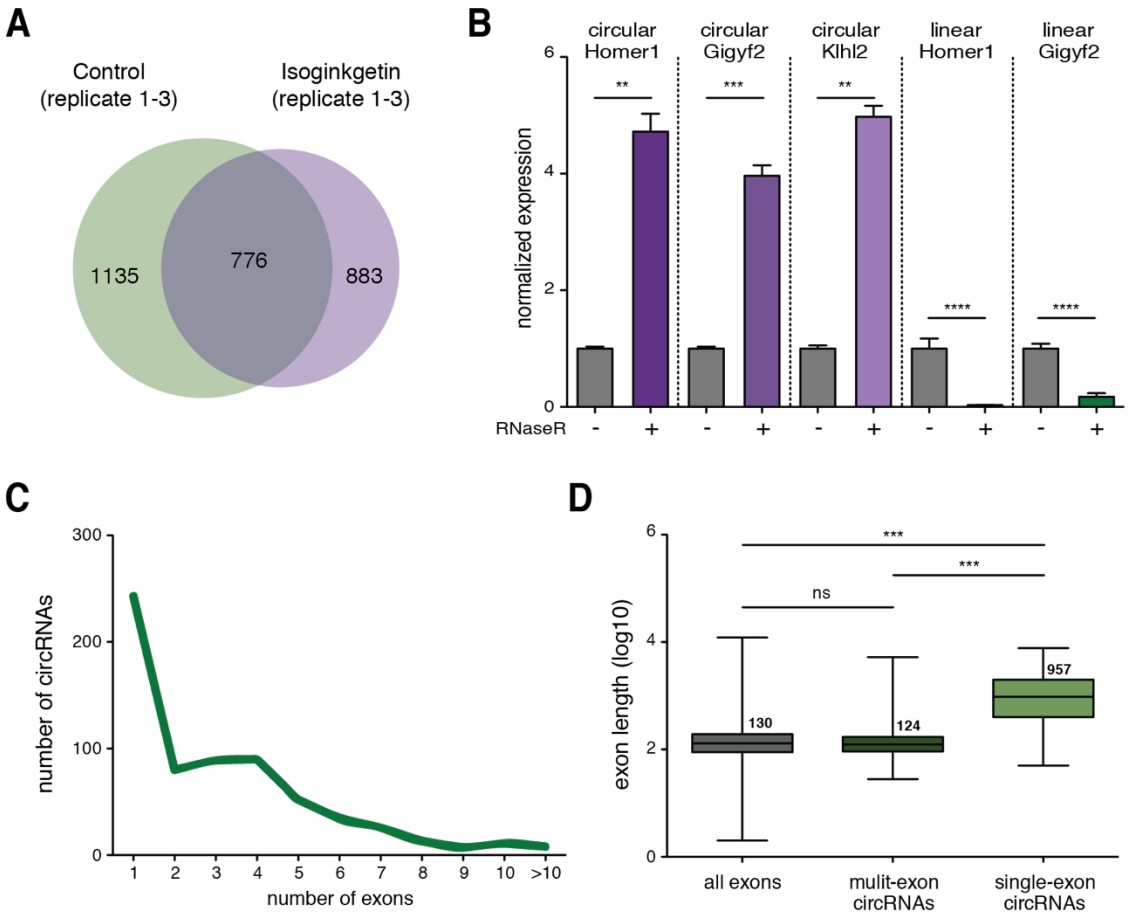

Figure 21. Characterization of neuronal circRNAs.
A. Venn diagram shows the number of circRNAs identified in all replicates in the isoginkgetin and control condition. 776 robustly expressed circRNAs were detected in all replicates and conditions, and used for down-stream analysis. **B.** Validation of the circularity of candidate circRNAs using RNase R treatment followed by qRT-PCR quantification. CircRNAs were strongly enriched and linear transcripts depleted after RNase R treatment (****p < 0.0001, ***p < 0.001, **p < 0.01, unpaired t-test, two tailed, n = 4). Error bars = s.d. **C.** Numbers of exons that the group of 776 circRNAs consists of. **D.** Distribution of the length (y-axis) of all rat exons and exons that form

circRNA head-to-tail junctions (x-axis). Exons forming single exon circRNAs were significantly longer than exons of multi-exon circRNAs or all rat exons (***p < 0.0001, Kruskal-Wallis test followed by Dunn's multiple comparison test). Error bars = s.d. Wang et al. (2019).

Reduced spliceosome activity causes dynamic changes of the neuronal circRNA landscape

To understand how spliceosome inhibition affects circRNA and mature host mRNA expression, I performed differential expression analysis in the isoginkgetin vs control conditions. Interestingly, I observed a general increase in circRNA expression compared to their host mRNA after spliceosome inhibition. Out of the 776 tested circRNAs, 142 circRNA were differentially expressed. While 134 circRNAs were up-regulated, a small fraction of 8 circRNAs were significantly down-regulated after spliceosome inhibition. For most up-regulated circRNAs the expression their host mRNAs were either un-changed or decreased. This indicates that enhanced circRNA biogenesis can but need not occur at the cost of processing the host mRNA. Intriguingly, for 11 up-regulated circRNAs the host mRNA levels were also increased (Figure 22).

I validated the circRNA expression changes using three independent methods. Consistent with our RNA-seq data, I observed with qRT-PCR the upregulation of *circHomer1* and *circGigyf2*, the down-regulation of *circHook3* and the un-changed expression of *circKlhl2* after spliceosome inhibition. All changes in host mRNA expression observed with qRT-PCR were in line with the RNA-seq data. Next, I directly visualized the changes in *circHomer1* expression using fluorescence *in situ* hybridization. In agreement with our RNA-seq and qRT-PCR data, we detected significantly higher numbers of *circHomer1* particles in the neuronal cell body with isoginkgetin treatment. Interestingly, when isoginkgetin and a cocktail of transcription inhibitors were simultaneously applied to cultured hippocampal neurons, *circHomer1* expression remained at levels of the control condition. This result suggests that spliceosome inhibition causes the generation of *circHomer1* from nascent transcripts (Figure 22).

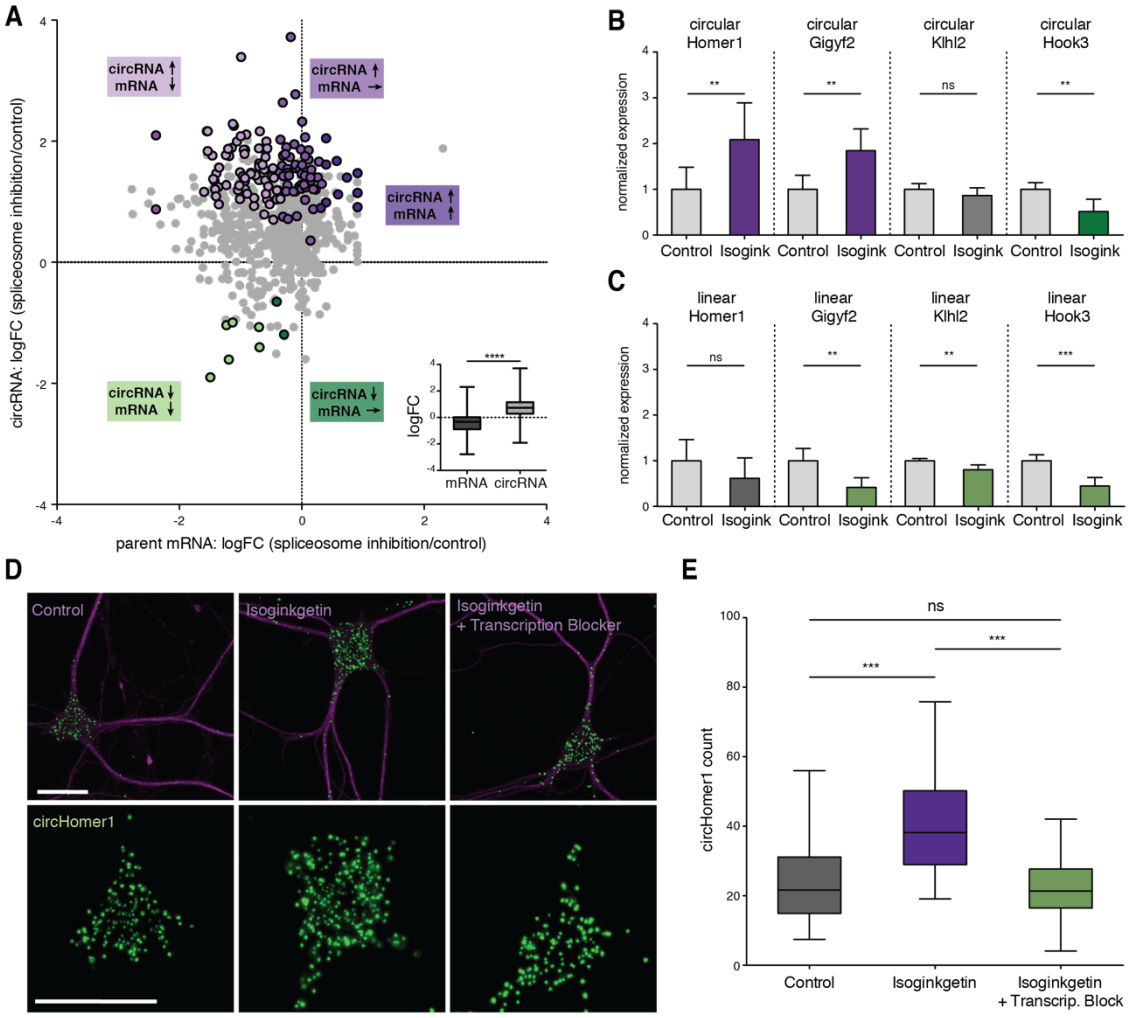

Figure 22. Differential expression of circRNA and host mRNA after spliceosome inhibition. **A.** Scatterplot displaying the log2 fold-change of the group of 776 robustly expressed circRNAs (y-axis) and their parent mRNAs (x-axis) between isoginkgetin and control condition. Each dot represents a circRNA. Magenta dots indicate circRNAs that were significantly up-regulated after isoginkgetin treatment. The shade of magenta (from light to dark) indicates whether the parent mRNA was down-regulated, un-changed or up-regulated, respectively. Green dots represent significantly down-regulated circRNAs, with the parent mRNA being also down-regulated (light green dots) or un-changed (dark-green dots). Grey dots indicate circRNAs that were un-changed. Inset shows that the general abundance of circRNAs was higher than the parent mRNA after isoginkgetin treatment (****$p < 0.0001$, unpaired t-test, two-tailed). **B.** qRT-PCR validated the expressional changes of 4 candidate circRNA upon isoginkgetin treatment (**$p < 0.01$, unpaired t-test, two-tailed, n = 3). Error bars = s.d. **C.** qRT-PCR validation of host transcript expression after isoginkgetin treatment (***$p < 0.001$, **$p < 0.01$, unpaired t-test, two-tailed, n = 3). Error bars = s.d. **D.** Visualizing *circHomer1* expression (green) using fluorescence *in situ* hybridization in control, isoginkgetin and isoginkgetin + transcription-inhibitor treated neurons. Neuron soma and dendrites were identified using anti-MAP2-immunostaining. Scale bar = 25 μm. **E.** Somatic *circHomer1* expression was significantly up-regulated in isoginkgetin-treated neurons compared to control. The inhibition of transcription prevented the isoginkgetin-induced up-regulation of *circHomer1*, indicating that the up-regulation is caused by nascent *circHomer1* (***$p < 0.0001$, Kruskal-Wallis test followed by Dunn's multiple comparison test, n = 73, 76 and 63). Error bars = s.d. Wang et al. (2019).

Depletion of core spliceosome components results in up-regulation of *circHomer1*

Next, I asked whether the depletion of core spliceosome components would have a similar effect on circRNA biogenesis as pharmacological inhibition of spliceosome activity. To test this question, I knocked down SF3B1 and SF3A2, two components of the U2 snRNP, in cultured hippocampal neurons. Similar to pharmacological inhibition using isoginkgetin, depletion of SF3B1 and SF3A2 caused a significant increase in *circHomer1* levels. Taken together, the multitude of validation experiments yielded results that are highly consistent with our RNA-seq data and strengthened the validity of our observations (Figure 23).

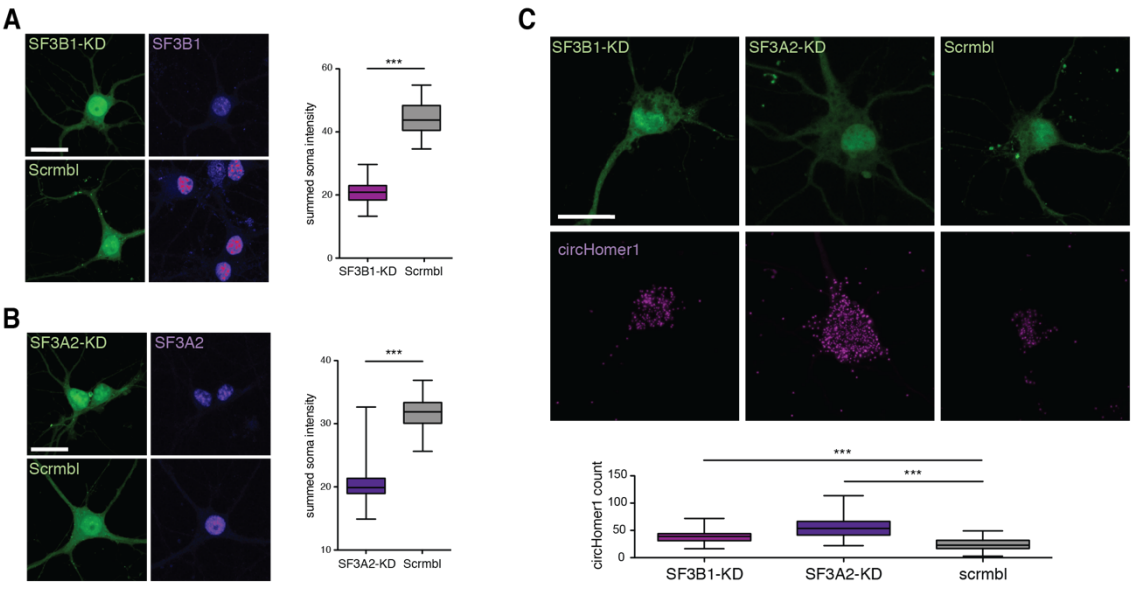

Figure 23. Depletion of SF2B1 and SF3A2 cause increased expression of *circHomer1*.
A, B. RNAi-mediated knock-down of SF3B1 **(A)** and SF3A2 **(B)** 4-days post transfection. The expression of SF3B1 or SF3A2 (magenta) in positively transfected cells (green) was validated (***p < 0.0001, Mann Whitney U test, n = 46, 39, 52 and 25). Scale bar = 25 μm. Error bar = s.d. **C.** Fluorescence *in situ* hybridization of *circHomer1* after SF3B1 or SF3A2 depletion. Somatic *circHomer1* was significantly up-regulated in SF3B1 and SF3A2 knock-down cells compared to scrambled control (***p < 0.0001, Mann Whitney U test, n = 37, 63 and 57) Scale bar = 25 μm. Error bars = s.d. Wang et al. (2019).

Up-regulated circRNAs are flanked by usually long introns

Interestingly, our data shows that spliceosome inhibition increased the biogenesis of some circRNAs but not others. I next asked which transcript features might have facilitated circRNA expression. Since introns have been described to influence circRNA generation, I focused on the characterization of introns flanking circularizing exons. Next, I compared the length of introns that flank circularizing exons to the introns that flank non-circularizing exons (henceforth referred to as “circRNA middle intron”) or to all introns in the rat genome. I found that introns flanking circularizing exons are significantly longer. Interestingly, up-regulated circRNAs possessed the longest flanking introns with the up- and down-stream flanking introns sharing a similar length. No difference in intron length between un-changed and down-regulated circRNAs could be observed. This result suggests that unusually long flanking introns favor circRNA formation under conditions of reduced spliceosome activity (Figure 24).

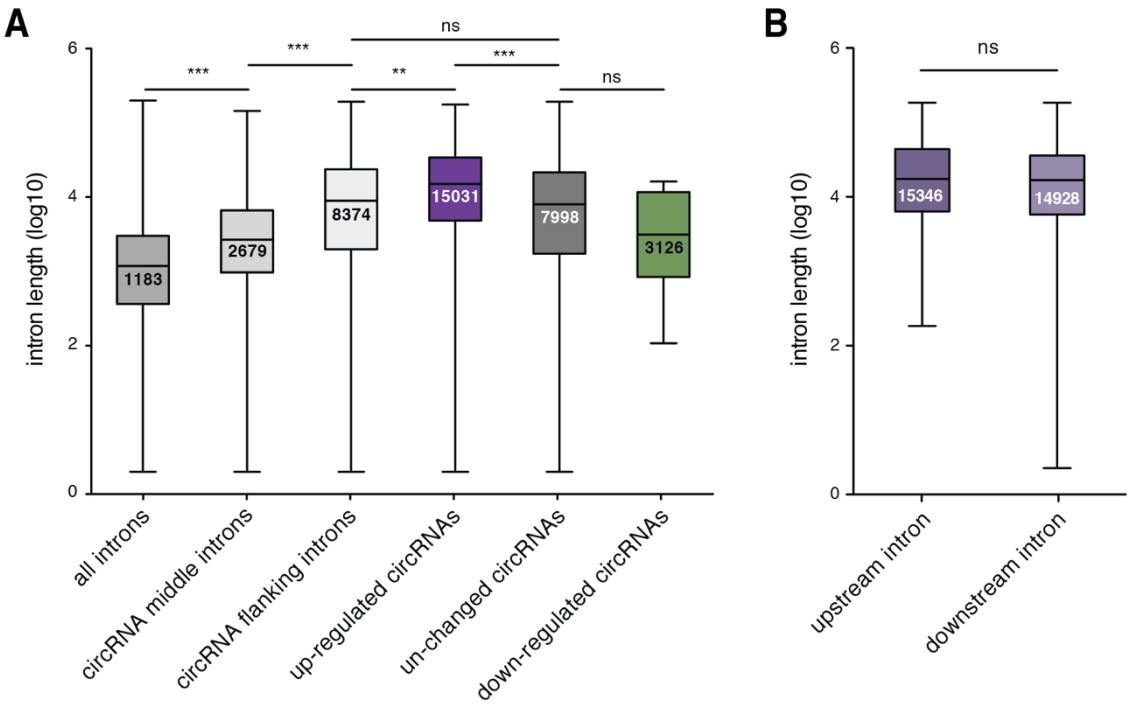

Figure 24. Up-regulated circRNAs are flanked by usually long introns.
A. Length distribution of introns. Introns flanking circularizing exons (light grey) were significantly longer than the median rat intron (steel grey) and circRNA middle introns (medium grey) (***p < 0.0001, Kruskal-Wallis test followed by Dunn’s multiple comparison test). Flanking introns of up-

regulated circRNAs (magenta) were significantly longer than flanking introns of un-changed circRNAs (dark grey) and all circRNAs (light grey) (*** $p < 0.0001$, **$p < 0.01$, Kruskal-Wallis test followed by Dunn's multiple comparison test). B. Similar length between up- and down-stream Intron length was detected (ns $p > 0.05$, Mann Whitney U test). Wang et al. (2019).

Strength of intron retention is unaffected by intron length

There are two potential explanations for why the biogenesis of circRNAs with very long flanking introns is favoured under conditions of reduced spliceosome activity. First, it could be that long introns are more effectively retained than short introns after isoginkgetin treatment. Their prolonged presence could facilitate circularization of distinct exons. To test this hypothesis, I performed differential analysis on introns. I detected 9,667 significantly up-regulated and 3,580 significantly downregulated introns after isoginkgetin treatment, with the up-regulated introns being shifted towards the first intron. This result indicates that introns become in general more retained after spliceosome inhibition. However, I found that intron length does not affect the strength of intron retention, indicating that longer introns are just as likely to be spliced out as shorter introns (Figure 25).

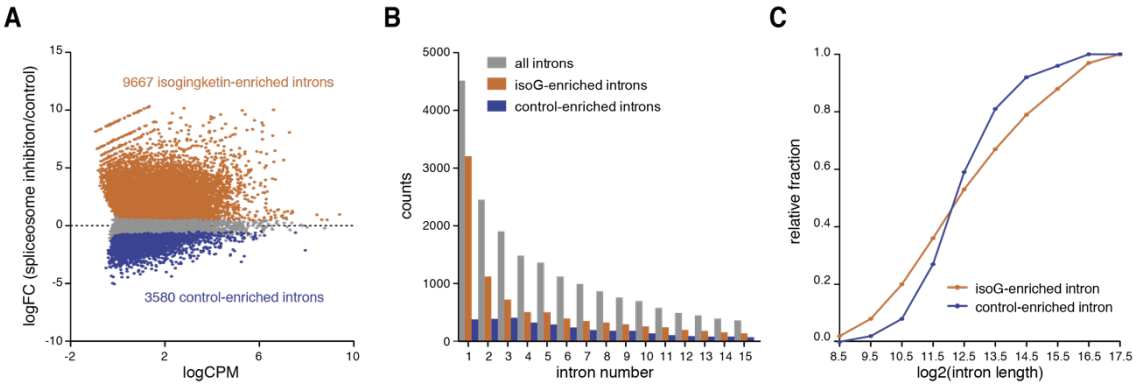

Figure 25. No correlation between intron length and strength of intron retention.
A. Differential expression analysis of individual introns between isoginkgetin and control condition. Orange dots indicate significantly up-regulated introns and blue dots significantly down-regulated introns, respectively. Grey dots show un-changed introns. **B.** Frequency of intron number occurrence of isoginkgetin- (orange bars) and control-enriched introns (blue bars). Frequency of intron occurrence of all detected introns is shown in grey. **C.** Cumulative frequency plot of binned intron length for isoginkgetin- and control-enriched introns. Wang et al. (2019).

Flanking introns of up-regulated circRNAs are enriched in repeat sequences

Another possible explanation for why circRNAs with very long flanking introns were up-regulated after isoginkgetin treatment is that long introns could

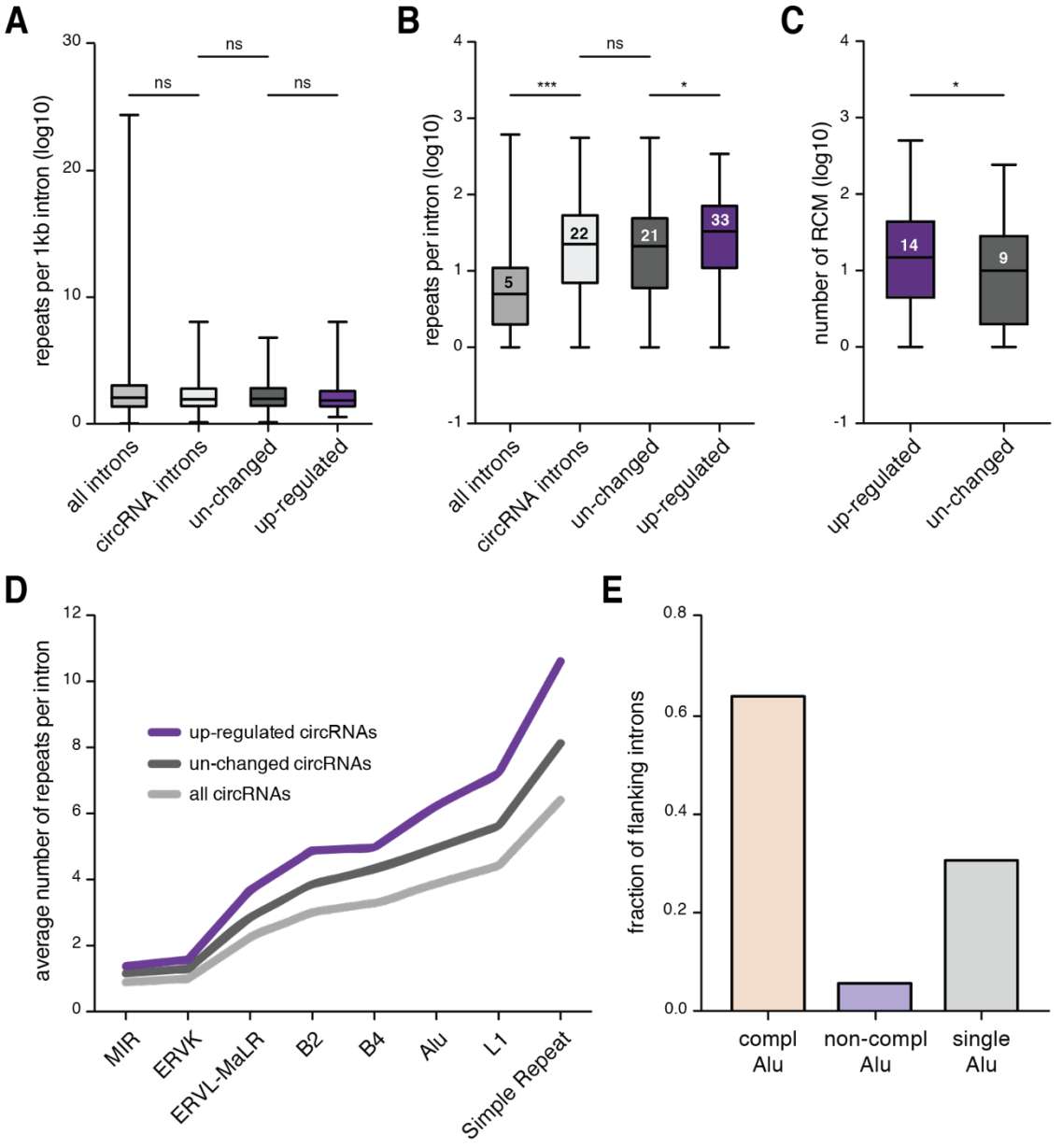

Figure 26. Flanking introns of up-regulated circRNAs harbor increased number and distinct quality of repeat sequences.
A. The frequency with which repeat sequence occur per one kilo base pair (kb) is shown. No difference in numbers of repeats per kb was observed between all introns (middle grey), all circRNA flanking introns (light grey), flanking introns of un-changed circRNAs (dark grey) and up-regulated circRNAs (magenta) (ns $p > 0.05$, Kruskal-Wallis test followed by Dunn's multiple comparison test). **B.** Number of repeat sequences detected per flanking intron. Flanking introns of circRNAs (light grey) harbored more repeats than the average rat intron (middle grey). Up-

regulated circRNAs (magenta) contained significantly more repeat sequences than the flanking introns of un-changed circRNAs (dark grey) (***p < 0.0001, *p < 0.05, Kruskal-Wallis test followed by Dunn's multiple comparison test). **C.** Number of RCM detected in flanking intron pairs. Flanking introns of up-regulated circRNAs (magenta) possessed significantly more RCMs define RCM compared to un-changed circRNAs (dark grey) (*p < 0.05, Mann Whitney U test). **D.** Comparison of the average number of repeats observed in the flanking intron. Distinct repeat families (x-axis) were more abundant in flanking introns of up-regulated circRNAs (magenta line) compared to un-changed circRNAs (dark grey line). A similar number of repeat families was observed between all circRNAs (light grey line) and the un-changed population. **E.** Fraction of flanking intron pairs that possessed complementary (orange bar), non-complementary (magenta bar) or single Alu repeats (grey bar). Wang et al. (2019).

harbor features in their sequence that promote circularization. For this reason, I examined factors that could facilitate the interaction between up- and downstream flanking introns, such as the presence and frequency of repeat sequences in the flanking introns, and their complementarity to each other. While a similar frequency of repeat sequences in flanking intron was observed between all circRNAs, un-changed and up-regulated circRNAs, flanking introns of up-regulated circRNAs possessed overall more repeat sequences due to their increased length. Moreover, intron pairs of up-regulated circRNAs harbored significantly higher numbers of reverse complementary motifs (RCMs) compared to the intron-pairs of un-changed circRNAs. Several repeat families were found to be enriched in the flanking introns of up-regulated circRNAs, such as Simple Repeats, L1 and Alu repeats. Among the Alu repeats, 63.8% were found to be arranged in complementing orientation in flanking intron pairs. Our data suggest that under conditions of reduced splicesome activity intron are less likely to be spliced out, enabling long and repeat-rich introns to interact with one-another and hence facilitating the formation of circRNAs (Figure 26).

Modulation of transcription rate increases *circHomer1* expression

An increase in transcription rate could potentially also elevate the number of introns retained and cause a similar effect on circRNA production as spliceosome inhibition. Therefore, I over-expressed human POLR2 in primary neurons and investigated the expression of *circHomer1*. I observed a significant increase in active RNA-Pol2 in the nucleus four days post transfection. In

agreement with our hypothesis, RNA-Pol2 overexpression lead to a significant increase in *circHomer1* expression compared to non-transfected control cells (Figure 27).

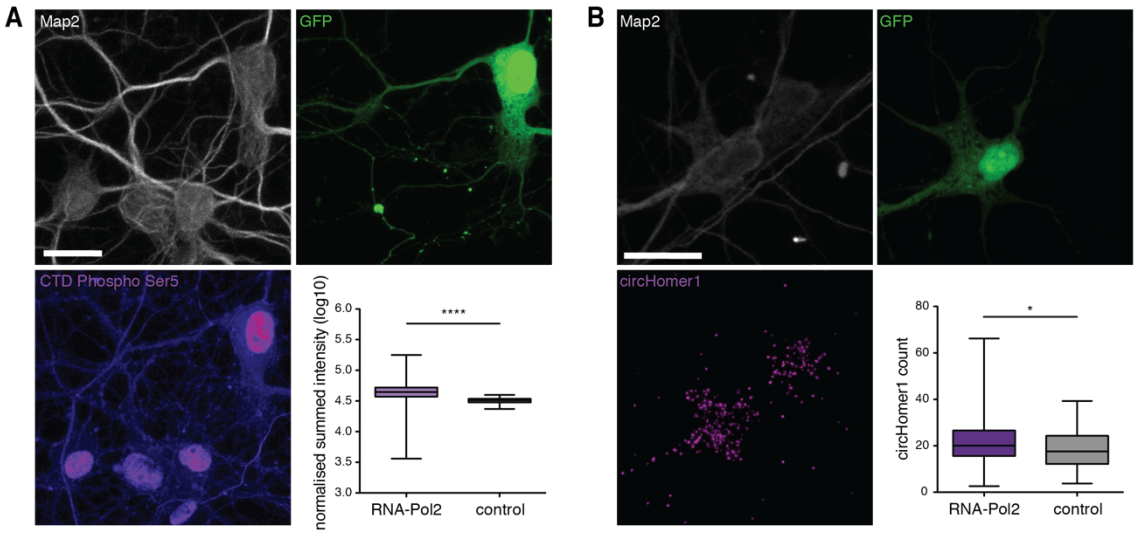

Figure 27. Increased *circHomer1* expression after modulation of transcription rate.
A. Modulation of transcription using POLR2 over-expression. Fraction of active RNA-Polymerase 2 (CTD Ser5-phospho antibody staining, magenta) was significantly increased in the nucleus of transfected neurons (green) after 4 days. Neuron soma and dendrites were identified using MAP2-immunostaining (***$p < 0.0001$, Mann Whitney U test, n = 98 and 98). Scale bar = 25 μm.
B. RNA-Pol2 over-expression caused a significant increase in *circHomer1* expression compared to mock transfected control neurons (*$p < 0.005$, Mann Whitney U test, n = 45 and 92). Scale bar = 25 μm. Wang et al. (2019).

DISCUSSION

CircRNAs have emerged as a new class of RNAs with great regulatory potential. As RNA-based gene regulation plays a key role in maintaining and modulating cellular processes in neurons, we aimed to characterize the neuronal circRNA landscape. Comparing circRNA expression across different mouse tissues, we identified the highest number of circRNAs in the brain where around 20% of all genes give rise to circRNAs. Our findings agree with other studies investigating circRNA expression in *Drosophila*, mouse and human brain (Kramer et al., 2015; Rybak-Wolf et al., 2015), indicating the evolutionary conserved role of circRNA-based regulation in the central nervous system (CNS). We validated our results using multiple independent methods, such as Pac-Bio deep sequencing to determine the full-length sequence of cDNA products derived from candidate circRNAs. Using this approach, we demonstrate, for the first time, not only their circular nature but also that circRNAs with the same head-to-tail junction can consist of different exon compositions. When we investigated the origin of neuronal circRNAs, we observed that circRNAs are both encoded by synaptic genes as well as enriched at synapses. As circRNAs were found to interact with RBPs and other RNAs (Abdelmohsen et al., 2017; Aktaş et al., 2017; Conn et al., 2015; Du et al., 2016; Errichelli et al., 2017; Holdt et al., 2016; Piwecka et al., 2017), the observations of us and others that neuronal circRNAs localize to subcellular compartments, such as axons, dendrites and synapses (Rybak-Wolf et al., 2015), is intriguing. Locally, circRNAs might serve as transporters or scaffolds, shuttling RBPs and/or RNA molecules to the periphery and releasing them upon demand. Further experiments are needed to test this hypothesis, such as investigating the local circRNA interactome in dendrites or spines using circRNA pull-down combined with omics tools.

Probing circRNA expression in the mouse hippocampus across different developmental stages, we observed of a strong increase in circRNA levels at the onset of synaptogenesis. This result further points to a potential role of circRNAs

in the regulation of synaptic function. Moreover, the increase in circRNA expression was mostly independent of the linear host transcript, suggesting a circRNA-specific regulation of biogenesis and/ or turnover. With this finding circRNAs join the list of RNA classes, such as miRNA or lncRNA, that have been shown to regulate developmental processes in neurons (Guttman et al., 2011; Mercer et al., 2010).

Activity-mediated changes of RNA expression is commonly observed in the brain and plays a crucial role in fine-tuning neuronal function (Flavell & Greenberg, 2008; Vo et al., 2005). When we treated primary hippocampal neurons with the $GABA_A$ antagonist bicuculline to induce homeostatic plasticity, we observed a dynamic shift in circRNA expression. Among the most up-regulated circRNAs was *circHomer1*. The Homer1 protein has a major role as scaffolding protein of the post-synaptic density. While the expression of Homer1a, an immediate-early gene variant of Homer1, increases upon neuronal stimulation, the expression of scaffolding protein Homer1 b/c remained unchanged (Bottai et al., 2002). Interestingly, the head-to-tail junction of *circHomer1* uses the splice site of intron 5, which is only required for the splicing of the *Homer1 b/c* variant but not of *Homer1a*. Hence, the generation of *circHomer1* may prevent an over-expression of Homer1 b/c during homeostatic downscaling.

The subcellular localization as well as the expressional changes of circRNAs upon plasticity were detected using fluorescence *in situ* hybridization probes that span the head-to-tail that is unique for circRNAs. Together with the development of methods for FISH labeling in tissues, we validated the expression of candidate circRNAs both in cultured neurons as well as in hippocampal slices.

Our comprehensive characterization of murine circRNAs showed that they are enriched in the brain, generated from synaptic genes, and display dynamic expression changes during development and plasticity. These findings suggest a

finely regulated generation and/ or turn-over of neuronal circRNAs. Hence, I set out to investigate the factors that circRNA biogenesis in the rat hippocampus. The spliceosome was a good candidate to start with as we observed a strong evolutionary conservation of splice sites between circRNAs of distinct species. Using pharmacological inhibition of the spliceosome and RNA-sequencing, I identified hundreds of robustly expressed circRNAs in both the control and isoginkgetin condition. Intriguingly, I found that circRNAs were either processed from one unusually long exon or consisted of several shorter exons. This result indicates the requirement of a minimal sequence length for successful circularization, which is in line with observations in human circRNAs (X. O. Zhang et al., 2014). Previous studies reported that an inhibition of the splicing complex resulted either in the decrease of all tested circRNAs (Starke et al., 2015) or an increased candidate circRNA expression (Kramer et al., 2015; Liang et al., 2017; Stegeman, Hall, Escobedo, Chang, & Weake, 2018). In our data, I observed three different groups of circRNAs. While some circRNAs became up-regulated, few circRNA were down-regulated, and others remained un-changed in their expression level. Multiple independent approaches were used to validate our results. There could be several explanations for why I observed a wider range of changes in circRNA expression after spliceosome inhibition than previous studies: i) the extent of spliceosome inhibition might differ between the studies or ii) the effect of reduced spliceosome activity on circRNA biogenesis may vary between different species. But another, more likely, reason may be our experimental approach: while most previous studies examined the expression of tens of candidate circRNAs, RNA-sequencing allowed us to follow the expression of hundreds of circRNAs simultaneously. Our approach enabled us to capture a broader view of the circRNA landscape after spliceosome inhibition. Another advantage of our unbiased approach is that we used the identity of the changed and un-changed circRNAs to investigate common gene features that determine the directionality of their regulation.

To do so, I decided to focus on the characterization of the introns flanking circularizing exons, as they can facilitate back-splicing (Ivanov et al., 2015; Jeck et al., 2013; Kim & Sheng, 2004; Liang & Wilusz, 2014; X. O. Zhang et al., 2014; Y. Zhang et al., 2016). Interestingly, up-regulated circRNAs possessed the longest but also most repeat-enriched flanking introns, compared to any other circRNA population. While I detected inversely oriented Alu repeats, which have been previously associated with facilitation of circRNA biogenesis (Jeck et al., 2013; Liang & Wilusz, 2014; X. O. Zhang et al., 2014), I also identified many new repeat elements that may benefit exon circularization, such as LINE (L1) and LTRs (ERVL_MALR, ERVK). I observed that spliceosome inhibition caused a general increase in intron retention independent of the intron length. Such conditions increase the opportunity for long and repeat-rich introns to interact with one another, facilitating the processing of their cognate circRNAs. Following our hypothesis, a modulation of transcription rate would also affect intron retention and therefore formation of circRNAs that are flanked by long and repeat-rich introns, such as *circHomer1*. Indeed, I observed a significant increase in *circHomer1* expression when RNA-polymerase 2 was over-expressed in primary neurons. Supporting our finding is a study in 293T cells that reported enhanced production of candidate circRNAs upon an increase of transcription speed (Y. Zhang et al., 2016). As modulation in transcription rate contributes to the maintenance of changes in synaptic efficacy (Bading, 2000), this may result in elevated expression of distinct circRNAs during modulation of neuronal-activity. Indeed, this might explain the elevated expression of *circHomer1* that we observed upon bicuculline treatment, as expression of Homer1a increases upon neuronal stimulation.

Based on these observations, I propose the following working model: The pre-mRNA transcript is spliced into mRNA or circRNA isoforms. Under conditions of normal spliceosome activity, introns are removed in a timely fashion thus reducing the opportunity for back-splicing to occur. Under these conditions, the production of circRNAs flanked by short and long introns is balanced.

Isoginkgetin interferes with the spliceosome assembly (O'Brien et al., 2008). As a consequence, introns are retained for longer. CircRNAs flanked by long and repeat-rich introns will benefit from these conditions, as the opportunity for their flanking introns to interact with one another increases – therefore enhancing the biogenesis of their cognate circRNAs. As the interaction with intron features can affect how the spliceosome processes the circRNA, our findings show that a delicate interplay between biogenesis factors determines the circRNA output of a given gene loci (Figure 28).

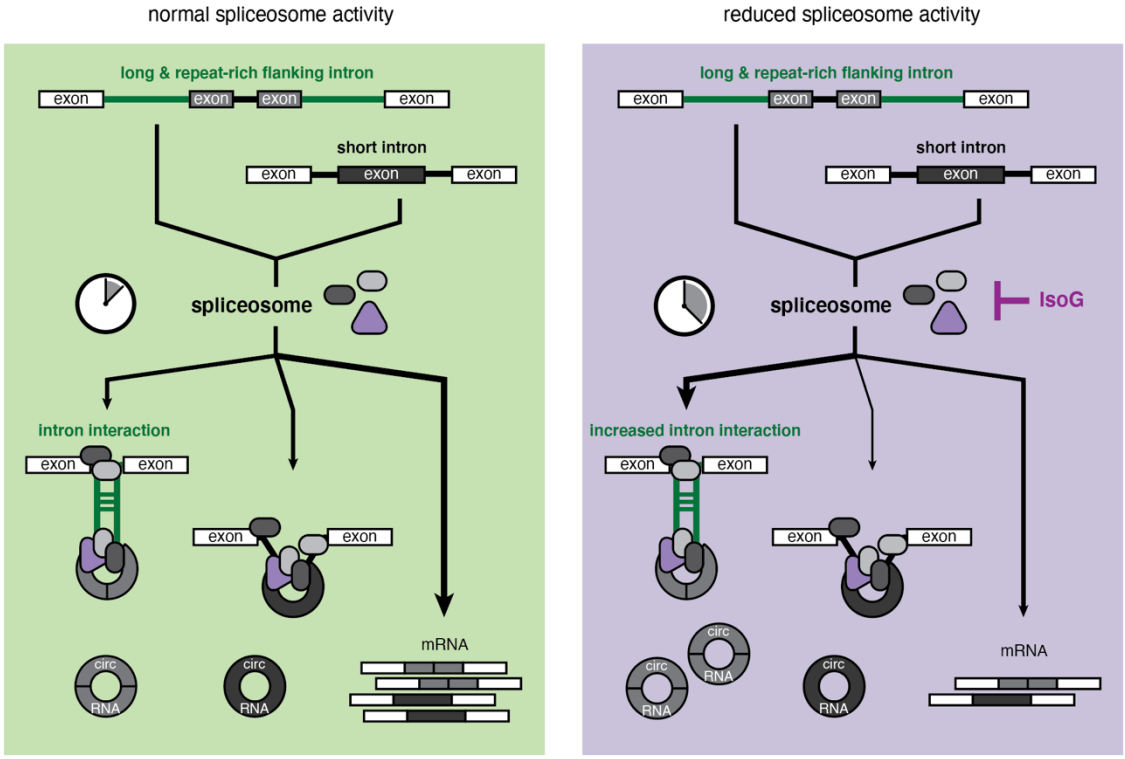

Figure 28. Proposed model for neuronal circRNA formation when spliceosome activity is reduced.
The pre-mRNA gives rise to a linear mRNA or circular circRNA isoform. Circularizing exons are flanked either by short introns (black line) or long introns (green line). Under normal spliceosome activity (left), introns are removed in a timely manner, providing little opportunity for flanking introns of circularizing exons to interact with another. Under conditions of reduced spliceosome activity (right), such as by treatment with isoginkgetin, introns are retained for longer periods of time. Long and repeat-rich introns benefit under such conditions, as their interaction and thus the processing of their cognate circRNA is facilitated.

Many human diseases are closely linked to a disruption of the basal splicing machinery, such as retinitis pigmentosa (RP) and spinal muscular atrophy (SMA) (Faustino & Cooper, 2003). It will be interesting to investigate the expression of circRNAs under these pathological conditions, as it may shed light on the role of circRNA abundance on disease states and their potential as targets for designing therapeutic approaches.

Chapter III

SPATIO-TEMPORAL DYNAMICS OF MICRO RNA-MEDIATED REGULATION OF LOCAL TRANSLATION

INTRODUCTION

Efficient neuronal function depends on the continued modification of the local protein pool in dendrites and axons (Sutton & Schuman, 2006; Sutton et al., 2007; Sutton et al., 2004). Neurons achieve this by distributing mRNAs into processes and using them for local translation (Huntzinger & Izaurralde, 2011; Kang & Schuman, 1996; Martin et al., 1997). Thousands of mRNAs have been identified in dendrites, encoding nearly an entire tool box needed to modify and maintain synapses (Biever et al., 2020; Cajigas et al., 2012). One dendritically-enriched mRNA encodes Ca^{2+}/calmodulin-dependent protein kinase 2 alpha (Camk2a) (Burgin et al., 1990; Cajigas et al., 2012), a key protein involved in learning, memory and synaptic plasticity (Coultrap & Bayer, 2012; Lisman, Schulman, & Cline, 2002; Lucchesi, Mizuno, & Giese, 2011). Disruption of the dendritic localization and local translation of Camk2a results in impaired stabilization of LTP and memory deficits (Miller et al., 2002). But how do neurons regulate when and which localized mRNAs are translated?

Micro RNAs are repressors of gene expression

One potential regulator of local translation are micro RNAs (miRNAs), small non-coding RNAs that act as post-transcriptional regulators of gene expression. miRNAs are transcribed as long primary transcripts, which are further processed in the nucleus and cytoplasm to yield the mature ~21 bp miRNA duplex (Fabian, Sonenberg, & Filipowicz, 2010). One strand of the duplex is loaded into the RNA-induced silencing complex (RISC) and the active miRISC is recruited to the 3'UTR of the target mRNA (Bartel, 2009; Moss, Lee, & Ambros, 1997; Reinhart et al., 2000; Wightman, Bürglin, Gatto, Arasu, & Ruvkun, 1991). In mammals, most miRNAs are partially complementary to their target sequence, in some cases only with the 6-8 nt long seed region at the 5´ end of the miRNA (Brennecke, Stark, Russell, & Cohen, 2005; S. Davis, Lollo, Freier, & Esau, 2006; Lewis, Burge, & Bartel, 2005; Lewis, Shih, Jones-Rhoades, Bartel, & Burge,

2003; Yekta, Shih, & Bartel, 2004). Hence a single miRNA can suppress the translation and/ or promote the degradation of up to a few hundred target genes (Eulalio, Huntzinger, & Izaurralde, 2008; Filipowicz, Bhattacharyya, & Sonenberg, 2008; Jackson & Standart, 2007).

The neuronal miRNA landscape

Consistent with the functional and cellular complexity of the nervous system, a disproportionally large number of tissue-specific and tissue-enriched miRNAs have been found in the brain (Krichevsky et al., 2003; Lagos-Quintana et al., 2002; Sempere et al., 2004). Similar to mRNAs, ribosomes and other non-coding RNAs, miRNAs are present in dendrites, axons and dendritic spines. Over the past years, the number of identified miRNAs that are localized has been steadily increasing. It began with the identification of the brain-specific miRNA, miR-134, and it's synapto-dendritic localization in rat hippocampal neurons (Schratt et al., 2006). A few more miRNAs were subsequently found to be enriched in laser-captured dendrites compared to cell bodies (Kye et al., 2007). This number rose further when tens of miRNAs were found to be enriched in synaptoneurosomes, a biochemical fraction highly enriched for synapses (Lugli, Torvik, Larson, & Smalheiser, 2008; Siegel et al., 2009). More recently, we detected hundreds of miRNAs residing in the neuropil layer of the rat hippocampus (Sambandan et al., 2017).

Moreover, miRNAs are subject to regulation by neuronal activity. On the transcriptional level, the expression of several miRNAs is regulated by activity-dependent transcription factors such as CREB and MEF2 (Fiore et al., 2009; Nudelman et al., 2010; Remenyi et al., 2013; Vo et al., 2005). Furthermore, it was shown that sensory input evokes significant changes in miRNA stability and turn-over rates in the visual system (Krol et al., 2010). Neuronal activity does not only affect miRNA expression but also modulates the activity of the miRNA machinery itself (Ashraf, McLoon, Sclarsic, & Kunes, 2006; Lugli, Larson, Martone, Jones,

& Smalheiser, 2005). A recent study added another aspect of activity-dependent regulation of miRNAs by showing that local glutamate uncaging at dendrites or individual synapses triggers the local maturation of miR-181a in cultured hippocampal neurons (Sambandan et al., 2017). The subcellular localization and activity dependent regulation of miRNAs place them in a key position to regulate synaptic plasticity and local translation.

The role of miRNAs in synaptic plasticity and local translation

Work by Schratt et al (2006) first hinted at the role of miRNAs in regulating synapse development and plasticity. Over-expression of miR-134, a dendritically localized miRNA, caused a reduction in dendritic spline size in cultured hippocampal neurons which was mediated by the translational repression of *LIMK1*, an activator of actin polymerization. Application of BDNF relieved the repression on *LIMK1* translation by miR-134, indicating the activity-dependent regulation of their interaction and the relevance for plasticity (Schratt et al., 2006). The role of miR-134 on the regulation of synaptic plasticity was later confirmed by an *in vivo* study (Gao et al., 2010). Overexpression of miR-134 and subsequent suppression of its target *SIRT1* in the CA1 region of the mouse hippocampus impaired LTP and long-term memory formation during contextual fear conditioning (Gao et al., 2010). Several other studies have shown that *in vivo* inhibition of several miRNAs in different brain regions causes disrupted learning and memory abilities (Ai et al., 2013; R. Y. Wang et al., 2013; Yang et al., 2012; Zovoilis et al., 2011). While we have increasingly gained an understanding of the role of individual miRNAs on synaptic function over the past years, the dissection of the local role of miRNAs in synaptic plasticity is still missing. This is largely due to the fact that in almost all studies miRNA expression was perturbed within the entire cell by plasmid over-expression or locked-nucleic-acid (LNA) mediated knock-down (Ai et al., 2013; Gao et al., 2010; Schratt et al., 2006; Yang et al., 2012; Zovoilis et al., 2011). An exception was the recent work by Sambandan et al. (2017), where the maturation of miR-181a was controlled by local glutamate-

uncaging in cultured hippocampal neurons using a novel probe encoding the immature pre-miR-181a. Maturation of miR-181a resulted in a significant decrease of local translation of *Camk2a*, a miR-181a target. Hence, to elucidate the role of endogenous miRNAs on local gene expression the control of miRNA activity in specific subcellular regions such as dendrites and spines is crucial.

Using photo-caged oligonucleotides to study local miRNA regulation

The recent development of photo-caged oligonucleotides has created opportunities to control RNA activity with very high spatial and temporal resolution (Brieke, Rohrbach, Gottschalk, Mayer, & Heckel, 2012; Mayer & Heckel, 2006). In this approach, a photo-caged oligonucleotide strand that is complementary to the target RNA sequence (antisense strand) is used to sequester the target and inactivate it. To prevent the antisense strand from binding the target RNA before photo-activation, photo-cleavable linkers connect the antisense strand to a blocking strand (Griepenburg, Ruble, & Dmochowski, 2013; Zheng, Cochella, Liu, Hobert, & Li, 2011). Previous studies have shown that the length of the blocking strand, as well as the number and position of the photo-protective linkers are essential for specific binding and inactivation of target miRNAs (Griepenburg et al., 2013; Zheng et al., 2011). Alternatively, molecular beacons, which are widely used for the detection of nucleic acids sequences *in vitro,* can be used to regulate endogenous RNA activity (Tan, Wang, & Drake, 2004; Tyagi & Kramer, 1996). Joshi et al (2012) inserted photo-labile protective groups into the loop region of the molecular beacon, which successfully prevented the base pairing of the target RNA before photo-activation and allowed the specific visualization of the hybridization event between the molecular beacon and the target RNA (Joshi et al., 2012).

To investigate the role of miRNA-mediated regulation of local mRNA translation and plasticity in cultured hippocampal neurons, we set out together with the laboratory of Prof. Alexander Heckel (Goethe University Frankfurt) to

develop an anti-miRNA (antimiR) which enables us to perturb miRNA activity, using light, in subcellular domains such as dendrites and spines. Moreover, the desired probe shall give us a readout of successful miRNA sequestration and enable its visualization in real-time. Furthermore, we will use the antimiR to dissect the spatiotemporal dynamics of miRNA regulation on local translation at both baseline conditions and upon synaptic plasticity.

RESULTS

Development of a photo-activatable antimiR against miR-181a

The development and testing of the antimiR requires a robustly expressed endogenous target miRNA. For this purpose, we chose miR-181a as Nanostring measurements of the miRNA population in the neuropil layer of the rat hippocampus showed that miR-181a is one of the most abundant miRNAs. The expression of miR-181a in dendrites of primary hippocampal neurons and hippocampal slices was validated using fluorescence *in situ* hybridization (Figure 29). Moreover, previous data demonstrated that miR-181a targets *Camk2a* mRNA (Sambandan et al., 2017), a protein that is crucial for the regulation of glutamatergic synapses and whose local protein synthesis is necessary to induce changes in synaptic efficacy (Lisman et al., 2002).

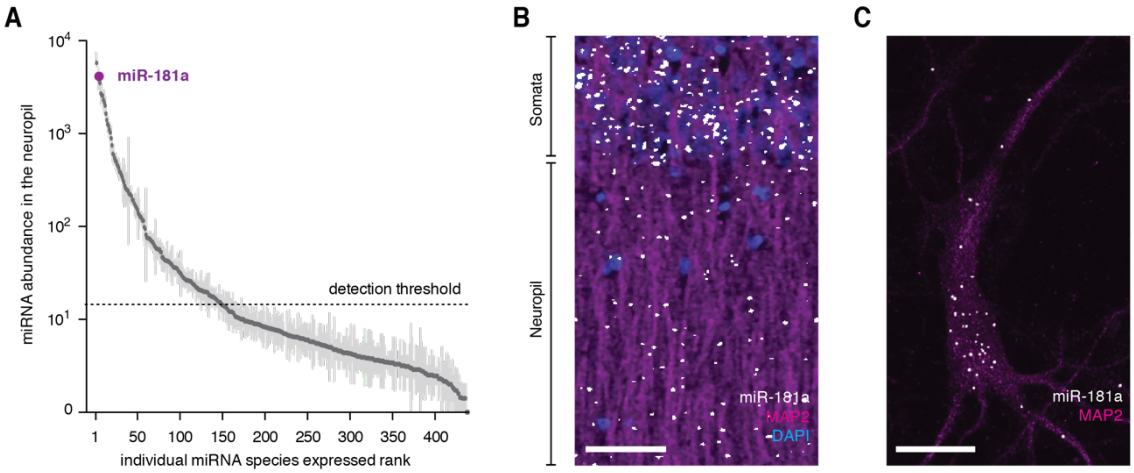

Figure 29. Distribution of miR-181a in the neuropil layer of the rat hippocampus.
A. Nanostring quantification of miRNA expression in the hippocampal neuropil. Individual miRNAs were ranked (x-axis) according to their abundance in the neuropil layer (y-axis). Each dot represents a miRNA. The detection threshold is shown as dotted line. Among all detected miRNAs, miR-181a (purple) was the third highest expressed. Modified from Sambandan et al. (2017). **B.** Detection of miR-181a in both somata and neuropil layer of the rat hippocampus using fluorescence *in situ* hybridization. miR-181a is shown in white. Soma and dendrites were visualized using MAP2-staining (magenta). Nuclei were labelled using DAPI (blue). Scale bar = 50 μm. Modified from Sambandan et al. (2017). **C.** Fluorescence *in situ* hybridization of miR-181a (white) in cultured hippocampal neurons. miR-181a signal was detected in soma and dendrites. Neurons were visualized using MAP2-staining (magenta). Nuclei were labelled using DAPI (blue). Scale bar = 25 μm.

A desirable feature to endow the antimiR with is the ability to control its activity with light in specific cellular locations. That way, we can control miR-181a function in dendrites or spines upon photo-activation. To visualize the interaction of the antimiR with miR-181a there should also be a fluorescent read-out. Hence, we incorporated a hybridization sensing fluorophore. Note that in the absence of the target miRNA as well as before photo-activation, the hybridization sensing fluorophore is quenched. Finally, we added a tracking fluorophore to continuously visualize the antimiR in real time, enabling us to determine the intracellular distribution and motion of the antimiR (Figure 30).

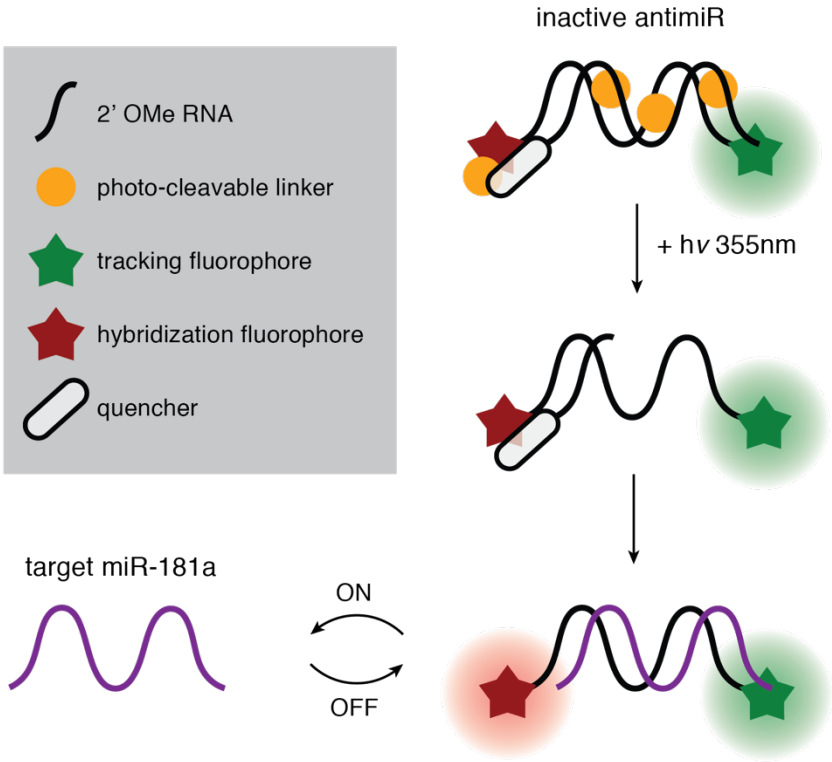

Figure 30. Hypothesized mode of action of the photo-activatable antimiR.
The antimiR is formed by a 2' OMe RNA oligonucleotide strand (black line) that is complementary to the sequence of miR-181a. A tracking fluorophore (green star) is incorporated into the antimiR to enable real-time visualization of the probe. A quencher (white ellipse) blocks the hybridization fluorophore (dark red star). The attachment of photo-cleavable linkers (orange circles) prevents the binding of the antimiR to miR-181a before photo-activation. Photo-activation with 355nm wavelength removes the photo-cleavable linkers, hence allowing the antimiR to bind to miR-181a. Consequently, the quencher is released and the hybridization sensing fluorophore lights up, enabling the detection of controlled inactivation of miR-181a activity.

We developed two distinct antimiR designs and each of them will be discussed in detail in the next sections. The syntheses of the all antimiR probes mentioned in this thesis were performed by Thomas Goldau.

A photo-activatable molecular beacon

First, we synthesized a dual-labelled photo-activatable molecular beacon, in which the loop region is complementary to the sequence of miR-181a. To prevent the base pairing of the molecular beacon to miR-181a before light induction, 8 photo-labile protective groups were placed into the loop region. Furthermore, each end of the molecular beacon was increased by 3 cytosine or guanine nucleobases. At the 5' end of the molecular beacon the hybridization sensing fluorophore Cy5.5 was attached, while at the 3' end two BBQ-650 were positioned. Before photo-activation, a stem is formed by the C-G base pairings, resulting in the quenching of the Cy5.5 fluorescence by BBQ-650. As a tracking fluorophore, 6-FAM was added to a tyrosine residue in the loop region, far away from the stem to avoid spurious quenching of the tracking fluorophore. To test the behavior of the molecular beacon before and after photo-activation, Thomas Goldau performed fluorescence studies in cuvettes under PBS conditions. No Cy5.5 intensity was measured before photo-activation. Upon photo-activation and with the addition of miR-181a, an increase in Cy5.5 intensity was observed. To test the effect of photo-bleaching on the Cy5.5 and 6-FAM dyes, samples were imaged repeatedly. While no change in Cy5.5 intensity was observed, 6-FAM was less photo-stable and bleached with each measurement (Figure 31).

A photo-activatable hairpin probe

Alternatively, we developed a photo-activatable hairpin probe, which consists of a strand complementary to miR-181a, the antimiR strand. To prevent the binding of miR-181a before photo-activation, a blocking strand is connected to antimiR strand via a single photo-cleavable linker (PC-linker), while two

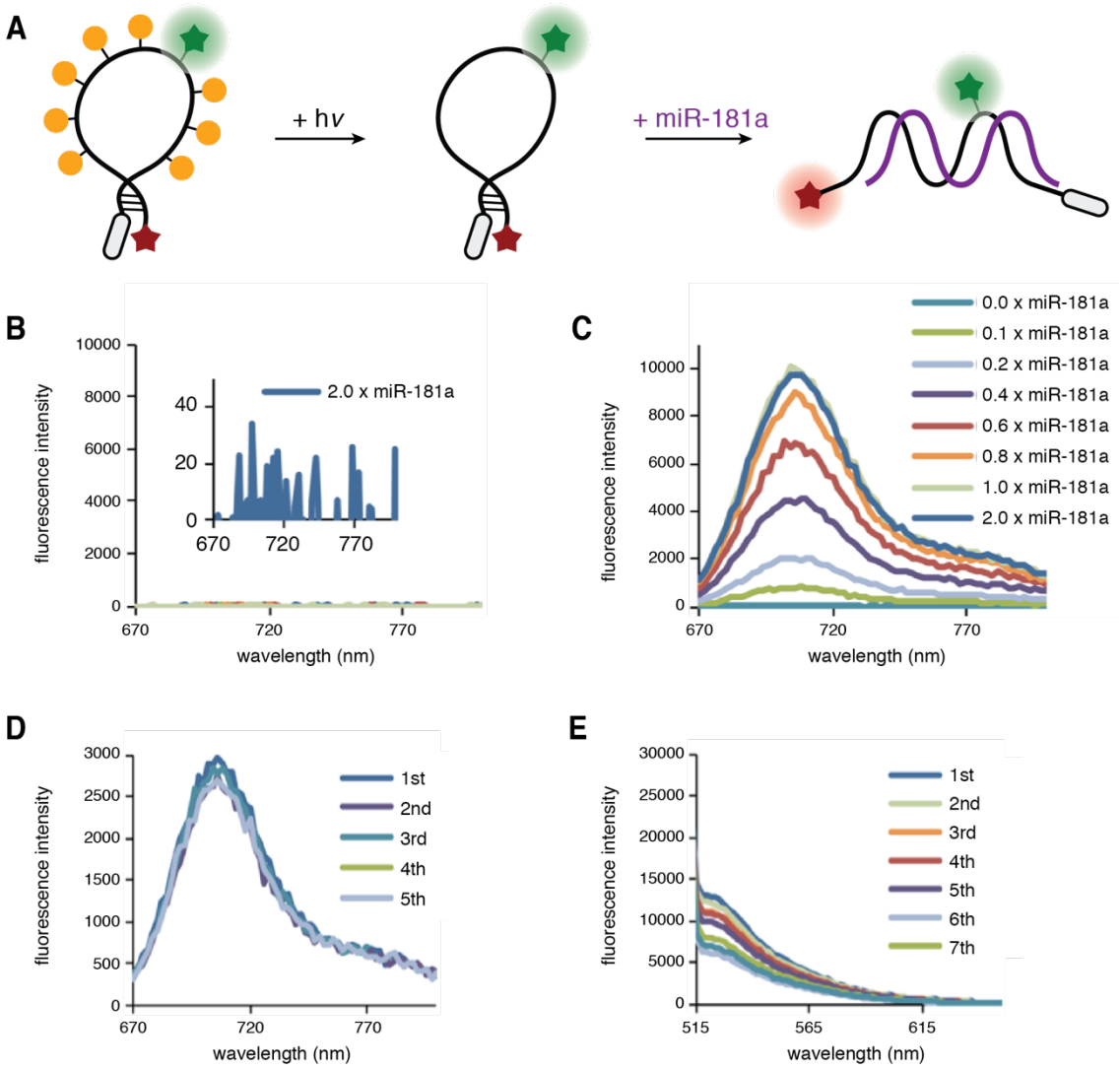

Figure 31. Design of the dual-labelled and photo-activatable molecular beacon.
A. Hypothesized mode of action of the photo-activatable molecular beacon. The loop region of the molecular beacon is complementary to the sequence of miR-181a. The stem carries the hybridization fluorophore Cy5.5 (red star) and two BBQ-650 quenchers (white ellipse). Before photo-activation, photo-labile protective groups (orange circles) block the nucleotide pairing of the loop region to miR-181a (purple line). Upon photo-activation and removal of the photo-labile protective groups, miR-181a binds to the molecular beacon and cause the release of the quenchers. This results in the appearance of the hybridization sensing fluorophore (dark red star). The tracking fluorophore 6-FAM is represented as green star. **B.** Molecular beacon (1 μM) was incubated in PBS with different concentrations of miR-181a RNA oligonucleotides. No Cy5.5 intensity was detected at any tested condition before photo-activation. The inset shows a zoom-in of the y-axis. Even at the highest concentration of miR-181a RNA oligos (2 μM) only background levels of Cy5.5 intensity was measured. Coloured lines show the different concentrations of miR-181a RNA oligos added to the molecular beacon (0 μM – 2 μM). **C)** Cy5.5 fluorescence intensity measurements after photo-activation. A strong increase in Cy5.5 fluorescence was observed after light-induction. The increase in Cy5.5 signal was dependent on the concentration of miR-181a RNA oligos added (coloured lines). **D.** Photo-bleaching

experiments to determine the photo-stability of Cy5.5. A sample containing molecular beacon and miR-181a RNA oligos in PBS was repeatedly imaged. No photo-bleaching of the Cy5.5 fluorophore was observed. Coloured lines show the number of the imaging cycle, from the first until the 5th measurement. **E.** Photo-bleaching experiments to determine the photo-stability of 6-FAM. When molecular beacon and miR-181a RNA oligos were repeatedly imaged in PBS, photo-bleaching of the 6-FAM fluorophore was observed and increased with each measurement. Coloured lines show the number of the imaging cycle.
Modified from dissertation of Thomas Goldau.

additional PC-linkers were placed within the blocking strand. One Cy5.5 fluorophore and two BBQ-650 were placed at the 5' end of the antimiR and 3' end of the blocking strand, respectively. As the tracking fluorophore, 6-FAM was attached to the 3' end of the antimiR strand. In addition, we developed an alternative, longer hairpin probe, which contained an additional 3 C-G base pairs after the tracking fluorophore, with the aim of increasing the stability of the probe before photo-activation. Light-induced cleavage of all PC-linkers converts the stable intra-molecular duplex of the hairpin probe into an unstable inter-molecular duplex. This destabilization between the antimiR strand and blocking strand enables the binding of miR-181a, resulting in the displacement of the quencher-carrying blocking strand and the appearance of the hybridization signal. The hairpin probes were tested under PBS conditions and with the addition of miR-181a RNA oligos by Thomas Goldau. No Cy5.5 fluorescence was measured in the presence of miR-181a before photo-activation. Upon photo-activation an increase in Cy5.5 intensity was observed, which was proportional to the amount of miR-181a oligos added. The short and long hairpin probes behaved similar to each other (Figure 32).

Global miR-181a sequestration increases Camk2a mRNA and protein expression

Before moving to *in vitro* experiments with the photo-activatable antimiR, I first performed pilot experiments with Cy5 labelled and non-caged anti-miR-181a oligonucleotides to find an effective method of probe delivery into primary neurons and determine the global effect of miR-181a inhibition on Camk2a expression. Comparing the performance of three transfection reagents side by

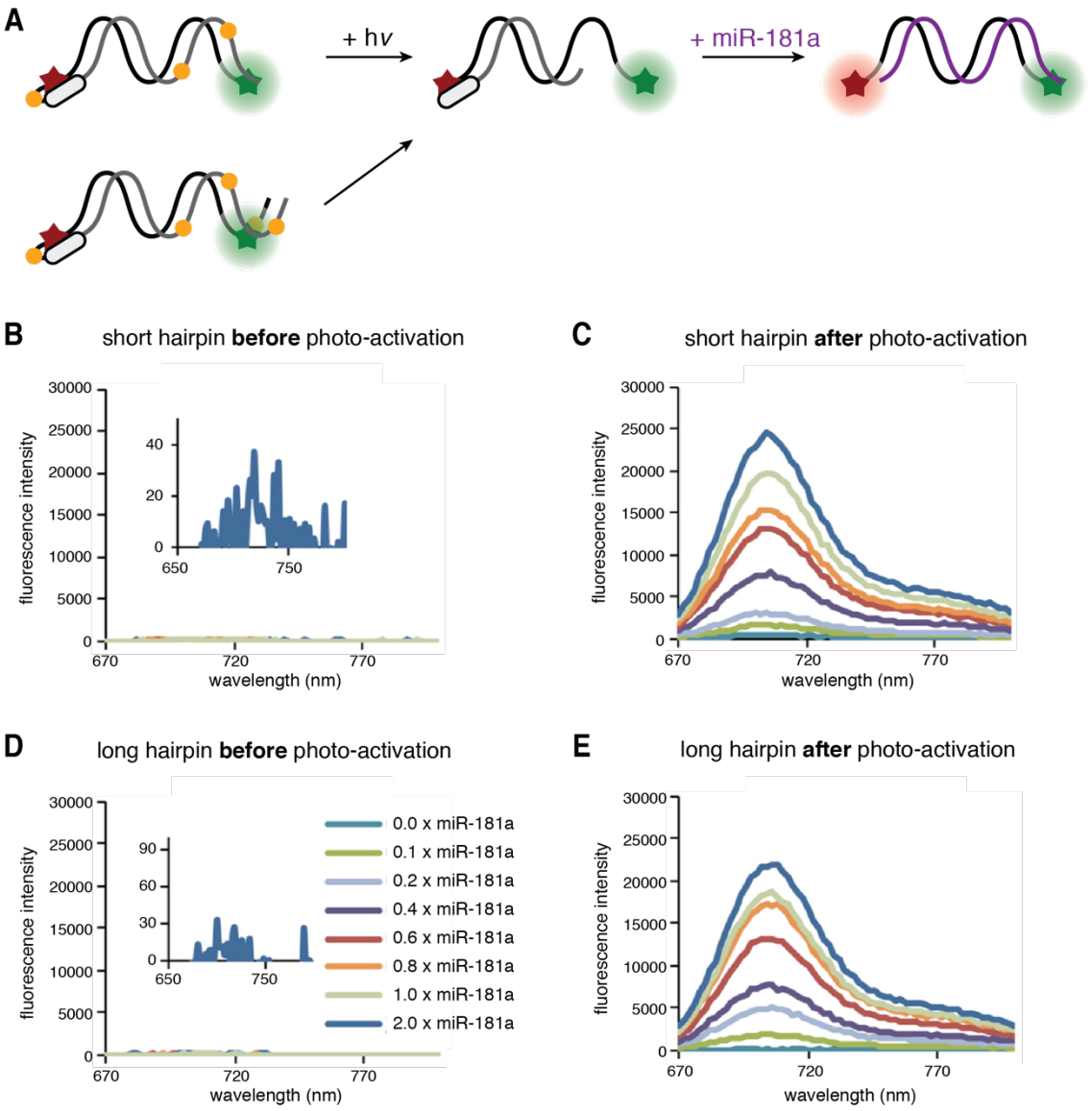

Figure 32. Design of the dual-labelled and photo-activatable hairpin probe.
A. Mode of action of the hairpin probe. The antimiR strand (black line) is complementary to miR-181a. The blocking strand (grey line) prevents the binding of miR-181a before photo-activation. The antimiR and blocking strand were connected to each other via several photo-cleavable linkers (orange circles). While 3 PC-linkers were incorporated into the short hairpin probe (top probe), 4 PC-linkers were placed within the long hairpin probe (bottom probe). The tracking fluorophore 6-FAM (green star) was attached to the 3' end of the antimiR strand, while the hybridization fluorophore Cy5.5 (red star) was linked to the 5' end. Before photo-activation the presence of the two BBQ-650 (white ellipse) quench the Cy5.5 fluorescence. Upon photo-activation, the photo-cleavable linkers were removed and the hairpin is converted into an intra-molecular duplex. This in combination with the fragmentation of the blocking strand enables the binding of miR-181a (purple line) to the hairpin probe and the release of the quencher. **B.** Cy5.5 fluorescence intensity of the short hairpin probe (1 μM) incubated with different concentrations of miR-181a RNA oligos (coloured lines) in PBS was measured. Before photo-activation, no Cy5.5 intensity was detected at either condition. The inset shows a zoom-in of the y-axis. Even with the highest concentration

of miR-181a RNA oligos (2 μM) tested, only background levels of Cy5.5 fluorescence were measured. Tested miR-181a RNA oligo concentrations ranged between 0 μM – 2 μM. **C.** Upon photo-activation an increase in Cy5.5 intensity was observed that scaled with the amount of miR-181a RNA oligos added. Coloured lines show the different concentrations of miR-181a RNA oligos added to the molecular beacon, ranging from 0 μM to 2 μM. **D.** Cy5.5 fluorescence intensity of the long hairpin probe (1 μM) was measured before photo-activation. No increase in Cy5.5 fluorescence was observed before photo-activation when the long hairpin probe (1 μM) was incubated with any tested concentration of miR-181a RNA oligos in PBS buffer. Coloured lines show the different concentrations of miR-181a RNA oligos added to the molecular beacon, ranging from 0 μM to 2 μM. **E.** Upon photo-activation, an miR-181a concentration-dependent increase of Cy5.5 intensity was observed for the long hairpin probe. Coloured lines show the different amounts of miR-181a RNA oligos added to the molecular beacon, ranging from 0 μM to 2 μM.
Modified from dissertation of Thomas Goldau.

side, I observed the lowest background signal and highest Cy5 intensity in transfected neurons when Lipofectamine Messenger Max, a newly developed reagent for mRNA delivery, was used. Interestingly, the Cy5 labelled oligonucleotides appeared in punctate structures rather than an even cytoplasmic distribution throughout the neuron (Figure 33).

As the Cy5 labelled oligonucleotides inhibited miR-181a activity throughout the entire cell, I validated the global Camk2a mRNA and protein expression 48 h after transfection. Quantitative real-time PCR showed a significant increase in *Camk2a* mRNA levels post-transfection. Newly synthesized Camk2a protein were labelled using the Puro-PLA technique (tom Dieck et al., 2015), see methods). A significant increase in newly synthesized Camk2a protein was observed after global miR-181a sequestration. These results strengthen previous data indicating that miR-181a regulates *Camk2a* translation (Sambandan 2017) (Figure 33).

<u>The antimiR appears in clusters and co-localizes with stress granule marker</u>

To investigate the behavior of the photo-activatable molecular beacon and hairpin probes in primary hippocampal neurons, I performed live-cell imaging experiments. Similar to the Cy5 labelled oligonucleotides, all photo-activatable

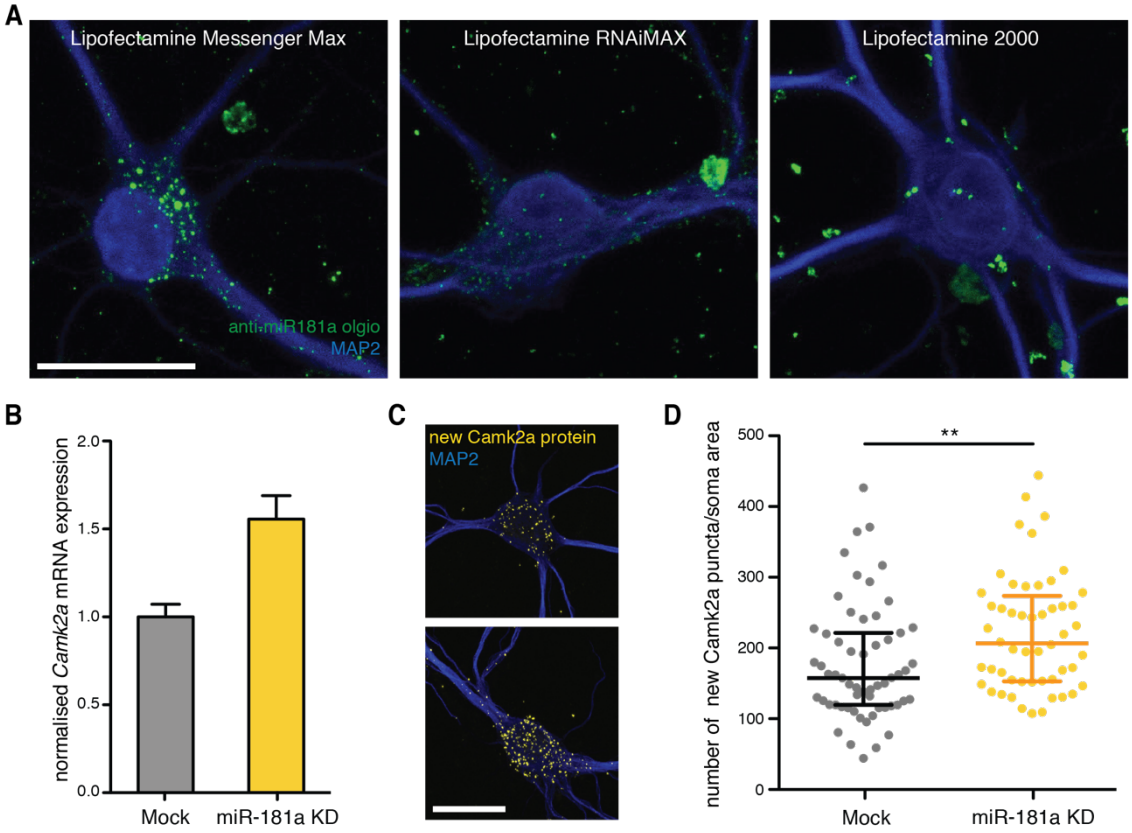

Figure 33. Depletion of miR-181a results in a global increase in Camk2a mRNA and protein expression.
A. Comparison of 3 transfection reagents to deliver Cy5 labelled and non-caged anti-miR-181a oligonucleotides (green) into primary hippocampal neurons: Lipofectamine Messenger Max, Lipofectamine RNAiMAX, Lipofectamine 2000 (from left to right). Neurons were visualized using immuno-staining against MAP2 (blue). Anti-miR-181a oligos were distributed in punctae in the cytoplasm of transfected neurons. The best Cy5 signal was obtained using Lipofectamine Messenger Max, followed by Lipofectamine RNAiMAX. Barely any cytoplasmic Cy5 signal was detected with Lipofectamine 2000. Scale bar = 25 μm. **B.** Cultured neurons were treated for 48 h with the Cy5 labelled and non-caged anti-miR-181a oligonucleotides and *Camk2a* mRNA level was quantified using qRT-PCR. Compared to the mock-transfected control neurons (grey bar), an increase in *Camk2a* mRNA expression was observed when miR-181a was knocked down (yellow bar). Y-axis represents the *Camk2a* expression levels normalized to *beta-actin* mRNA and *18S* rRNA expression. **C.** Puro-PLA was performed to visualize newly synthesized Camk2a protein after mock-treatment (top) or miR-181a knock down (bottom). Representative neurons of either treatment condition are shown. Newly synthesized Camk2a protein is shown in yellow. MAP2 staining was used to visualize the soma and dendrite (blue). Scale bar = 25 μm. **D.** Quantification of the newly synthesized Camk2a protein signal in the soma of transfected neurons or controls. Significantly more newly synthesized Camk2a puncta were detected after miR-181a inhibition compared to control (** $p < 0.01$, Mann Whitney U test, n = 53 & 59).

antimiR probes displayed a punctate distribution throughout the transfected neuron. Since each antimiR carried a single 6-FAM molecule as tracking fluorophore, the puncta most likely represented a cluster of multiple antimiR

molecules. To investigate the nature of these antimiR clusters, I performed immunostaining against marker proteins of membrane-bound organelles such as endosomes or lysosomes. Furthermore, I stained against three classes of neuronal RNA granules: transport messenger ribonucleoproteins (mRNPs), stress granules and processing-bodies (P-bodies). Out of all tested antibodies, robust immunostaining was obtained for only three of them (Table 5). No co-localization of antimiR clusters with early endosome antigen 1 (EEA1) or lysosomal-associated membrane protein 1 (LAMP1) was observed. However, many antimiR clusters co-localized with poly(A)-binding protein 1 (PABP1). This result indicates that some antimiRs were taken up into stress granules and therefore located in close proximity to mRNAs (Figure 34).

Table 5. List of marker proteins used for immuno-staining to identify distinct cellular organelles.

ORAGNELLE	MARKER PROTEIN	ANTIBODY	DILUTION	QUALITY OF STAINING
ENDOSOME	EEA1	Abcam ab2900	1:1000	good
LYSOSOME	LAMP1	Sigma L1418	1:200	good
TRANSPORT MRNPS	Staufen 1	Abcam ab50914	1:500, 1:1000	weak
	hnRNP-A2/B1	Sigma R4653	1:500, 1:1000	weak
STRESS GRANULE	PABP	Abcam ab21060	1:500	good
P-BODIES	GW182	Abcam ab84403	1:100	weak
	Dcp1A	Sigma HPA013202	1:200, 1:500	weak

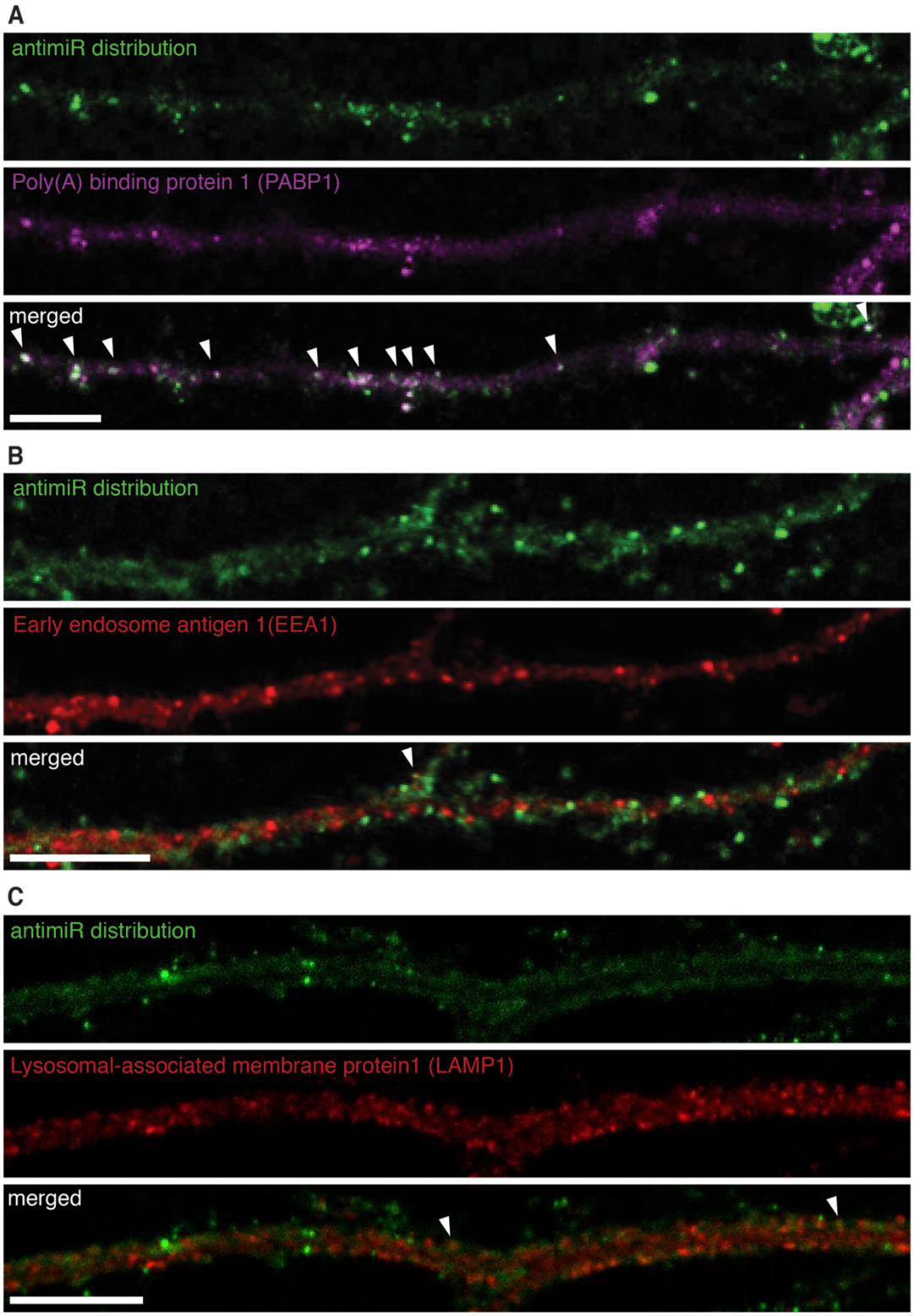

Figure 34. AntimiR clusters overlap with stress granules and not with endosomes or lysosomes.
A. Distribution of the short hairpin probe and Poly(A) binding protein 1 is shown in dendrites. Co-localisation between several antimiR clusters (green) and PABP1 staining (purple) was observed and marked by arrows. Images are shown as single z-plane images. Scale bar = 10 μm. **B.**

Distribution of the short hairpin probe and early endosome antigen 1 is shown in dendrites. Hardly any overlap between antimiR clusters (green) and EEA1 staining (red) was detected. A single overlapping event was detected and marked with an arrow. Images are shown as single z-plane images. Scale bar = 10 μm. **C**. Distribution of the short hairpin probe and lysosomal-associated membrane protein 1 is shown in dendrites. A few overlaps between antimiR clusters (green) and lysosomal marker (red) were observed and marked with arrows. Images are shown as single z-plane images. Scale bars = 10 μm.

The molecular beacon displays hybridization signal in the soma before photo-activation

Next, I examined the intensity of the hybridization sensing fluorophore of the antimiRs in the soma of transfected neurons before photo-activation. In contrast to the fluorometric measurements under buffer conditions described above, I detected Cy5.5 fluorescence before photo-activation with all three antimiRs *in vitro*. Among all antimiR variants, the molecular beacon displayed the strongest Cy5.5 signal before photo-activation, indicating either partial quencher release or insufficient quenching by the BBQ-650 *in vitro*. This result suggests that further optimization is required, especially with the molecular beacon. We nevertheless explored the properties of the antimiR probes further to test if the hybridization signal increases upon photo-activation (Figure 35).

Rapid appearance of hybridization signal upon photo-activation in soma and dendrites

How does each antimiR variant perform *in vitro* after photo-activation? To answer this question, I performed the following live-cell imaging experiment: The soma or dendrite of transfected hippocampal neurons was imaged for a total duration of 300 sec (acquisition speed of 5 sec / frame). No photo-activation was performed during the first 50 sec to determine the baseline intensity of the Cy5.5 and 6-FAM fluorophores. After the 50th second, I photo-activated the entire soma or dendrite using a 365nm laser, at either 1.487 mW, 2.174 mW or 3.588 mW power. After a single photo-activation event, I observed a rapid increase of Cy5.5

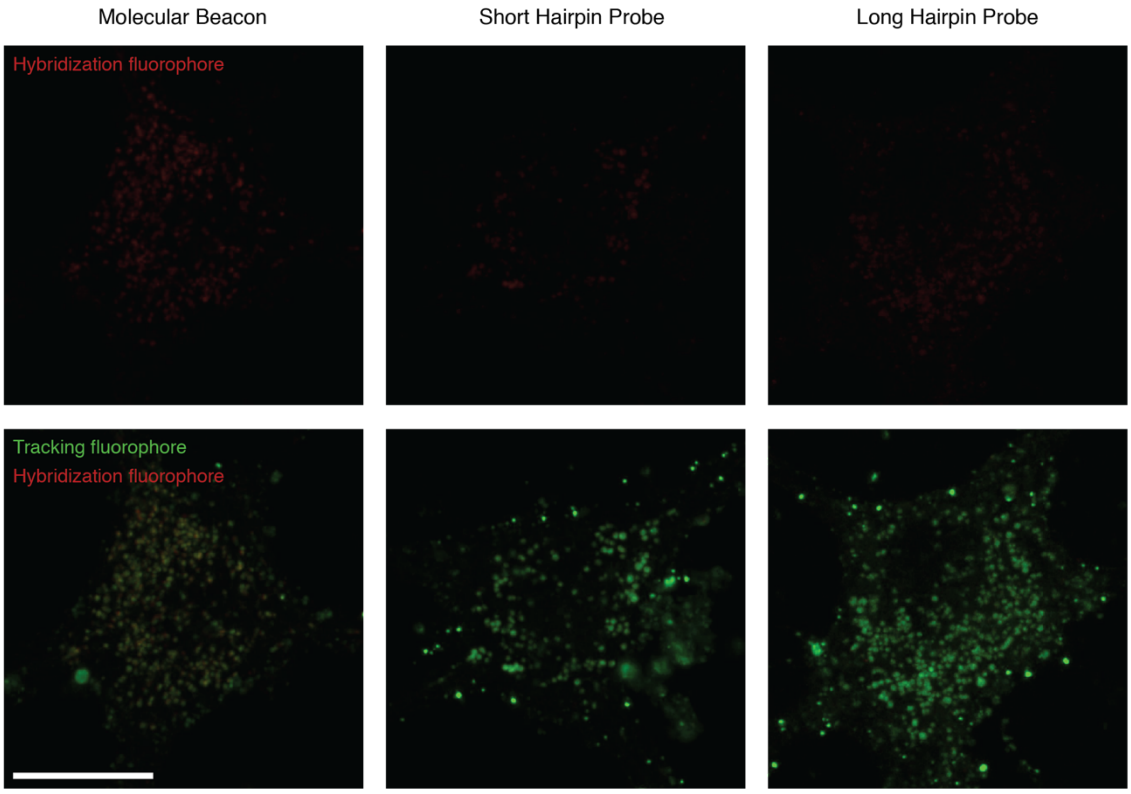

Figure 35. The molecular beacon showed the strongest hybridization signal before photo-activation.
Side-by-side comparison of the soma of neurons that were transfected with the molecular beacon, the short hairpin probe or the long hairpin probe (from left to right) before photo-activation. Compared to the hairpin probes, the molecular beacon yielded the strongest Cy5.5 fluorescence before photo-activation (red, upper panels). The tracking fluorophore signal in the soma is shown in green. Scale bar = 10 μm.

fluorescence in both cell soma and dendrites, suggesting fast sequestration of miR-181a by all antimiR variants. While a 10% increase of cy5.5 fluorescence was measured after photo-activation at 1.487 mW laser power, an up to 30% elevation of the Cy5.5 intensity was observed with a light-induction at 3.588mW laser power. No further increase of Cy5.5 intensity was measured over the remaining imaging time, which suggests that the sequestration of miR-181a saturated rapidly. While little to no bleaching of the Cy5.5 fluorophore was observed, the 6-FAM intensity decreased upon photo-activation and steadily declined further with imaging time (Figure 36).

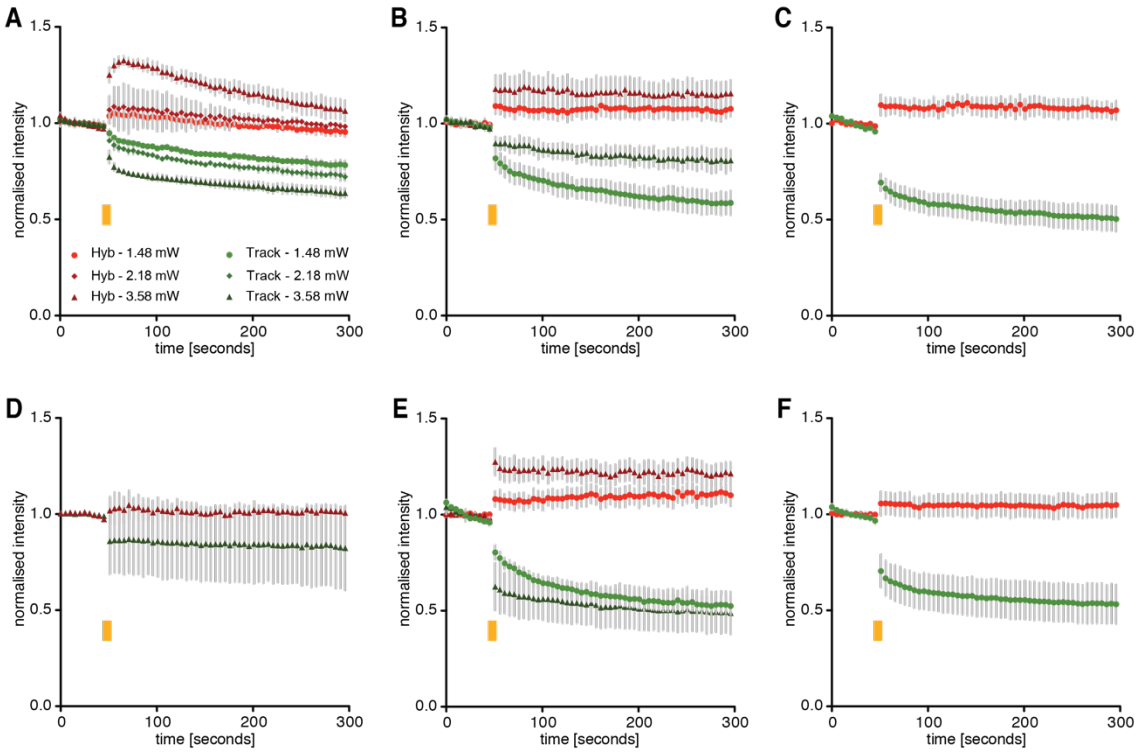

Figure 36. Rapid appearance of hybridization signal after a single light pulse in soma and dendrites.

A – F. Graphs show the changes of tracking and hybridization fluorophore intensity measured in the soma and dendrites of transfected neurons before and after photo-activation. **A, B, C.** Intensity of the Cy5.5 (red) and 6-FAM (green) fluorophores (y-axis) was measured in the soma. Values were normalized to the average Cy5.5 or 6-FAM intensity before photo-activation and plotted over time (x-axis). Photo-activation (orange rectangle) was performed once at either 1.48 mW (circle), 2.18 mW (diamond) or 3.58 mW (triangle) laser power. **A.** A single photo-activation event led to an immediate increase of Cy5.5 fluorescence in a laser power dependent manner in soma of neurons transfected with the molecular beacon. Bleaching of the 6-FAM signal was observed upon photo-activation and with increased imaging time. Plot shows mean ± SEM, n = 4. **B.** Cy5.5 intensity increase was observed in the soma of neurons transfected with the long hairpin probe upon photo-activation and in a laser power dependent manner. Decrease in 6-FAM intensity was detected upon photo-activation and increased with imaging time. Plot shows mean ± SEM, n = 7. **C.** Soma of neurons transfected with the short hairpin probe were photo-activated with 1.48 mW laser power only. Increase in Cy5.5 intensity and decrease in 6-FAM intensity was detected upon photo-activation. Plot shows mean ± SEM, n = 6. **D, E, F.** Intensity of the Cy5.5 (red) and 6-FAM (green) fluorophores (y-axis) was measured in dendrites. Values were normalized to the average Cy5.5 or 6-FAM intensity before photo-activation and plotted over time (x-axis). Photo-activation (orange rectangle) was performed once at either 1.48 mW (circle) or 3.58 mW (triangle) laser power. **D.** Little increase in Cy5.5 intensity was observed in the dendrites of neurons that were transfected with the molecular beacon. Photo-activation was only performed at 3.58 mW laser power. Bleaching of 6-FAM was observed upon photo-activation. Plot shows mean ± SEM, n = 4. **E.** A stronger increase in Cy5.5 intensity was measure in the dendrites of neurons transfected with the long hairpin probe when 3.58 mW instead of 1.48 mW laser power was used for light-induction. However, 6-FAM also bleached stronger with 3.58 mW laser power

and continued with imaging. Plot shows mean ± SEM, n = 10. **F.** The short hairpin probe showed similar increase in Cy5.5 intensity as the long hairpin probe upon photo-activation at 1.48 mW laser power. 6-FAM intensity decreased upon photo-activation and with imaging time. Plot shows mean ± SEM, n = 20.

To test whether repeated light pulses could enhance the hybridization signal, I photo-activated dendrites 8-times and monitored the Cy5.5 and 6-FAM intensity over 250 sec. At 1.487 mW laser power, I observed with all antimiR probes an increase in cy5.5 fluorescence upon each photo-activation event. The rise of Cy5.5 intensity plateaued after the 5th light pulse with the hairpin probes and after the 7th light pulse with the molecular beacon, respectively. At 2.174 mW or 3.588 mW laser power, Cy5.5 florescence increased more rapidly, but also declined faster due to photo-bleaching effects. Here, maximal increase in Cy5.5 intensity was observed after the second light pulse for both the short and long hairpin, and after the 4th light pulse for the molecular beacon. Overall the molecular beacon displayed a higher variance of Cy5.5 intensity after photo-activation which was independent of the laser power applied. A decline of 6-FAM intensity was observed with all antimiR probes upon photo-activation and with imaging time. In summary, the short hairpin probe displayed the least Cy5.5 intensity before photo-activation and the most consistent increase of Cy5.5 signal upon repeated photo-activation (Figure 37).

Investigating the effect of local miR-181a sequestration on newly synthesized Camk2a protein in distal dendrites

To study the miR-181a-mediated regulation of local Camk2a protein synthesis in distal dendrites, I transfected the short hairpin probe into 3-weeks old cultured hippocampal neurons. I imaged a dendritic segment that is 100 μm long and between 80-100 μm away from the soma for 250 sec. The first 50 sec were used to determine the baseline intensity of the Cy5.5 and 6-FAM fluorophores, while photo-activation was performed starting with the 51st sec and repeated 7 times. In this. manner, 3-4 dendritic stretches were imaged

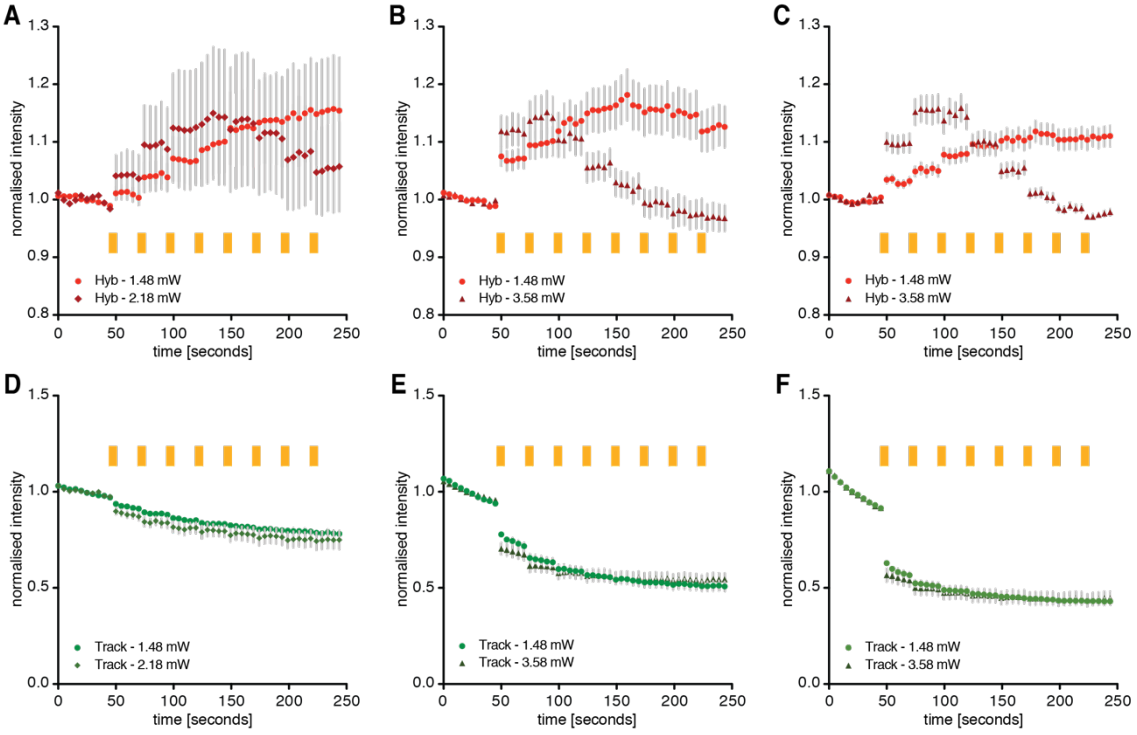

Figure 37. Increase in dendritic hybridization signal with repeated photo-activation events. **A – F.** Graphs show the changes of tracking and hybridization fluorophore intensity measured in the dendrites of transfected neurons before and after repeated photo-activation events. **A, B, C.** Quantification of the changes of Cy5.5 fluorescence intensity (y-axis) when dendrites were photo-activated for 8-times (orange rectangle) using either 1.48 mW (circle), 2.18 mW (diamond) or 3.58 mW (triangle) laser power. Values were normalized to the average Cy5.5 intensity before photo-activation and plotted over time (x-axis). **A.** Increased Cy5.5 intensity was measured in dendrites of neurons that were transfected with the molecular beacon. A steady increase of Cy5.5 signal was observed until the 8th photo-activation event when 1.48 mW laser power was applied. Although, the rise in Cy5.5 intensity was faster at 2.18 mW laser power, bleaching of the Cy5.5 fluorophore was observed starting from the 5th photo-activation event. Intensity increase varied strongly between dendrites and was independent of the laser power used for photo-activation. Plot shows mean ± SEM, n = 26. **B.** Dendrites of neurons transfected with the long hairpin probe displayed a rapid increase in Cy5.5 intensity upon the first photo-activation at 3.58 mW laser power, followed by a strong decline of the Cy5.5 signal starting with the 3rd photo-activation event. A more steadily increase in Cy5.5 intensity was observed at 1.48 mW laser power, where the Cy5.5 signal plateaued with the 5th light pulse. Plot shows mean ± SEM, n = 24. **C.** In dendrites of neurons transfected with the short hairpin probe, an increase of Cy5.5 intensity was detected until the 3rd photo-activation event, followed by a complete decline of the signal back to baseline levels by the 8th photo-activation event at 3.58 mW laser power. A more steady increase in Cy5.5 intensity was observed at 1.48 mW laser power, where the Cy5.5 signal plateaued with the 6th light pulse. Plot shows mean ± SEM, n = 38. **D, E, F.** Quantification of the changes of 6-FAM intensity (y-axis) when dendrites were photo-activated for 8-times (orange rectangle) using either 1.48 mW (circle), 2.18 mW (diamond) or 3.58 mW (triangle) laser power. Values were normalized to the average 6-FAM intensity before photo-activation and plotted over time (x-axis). **D.** Dendrites of neurons transfected with the molecular beacon showed a decrease in 6-FAM intensity upon photo-activation and with imaging time. A comparable decline of 6-FAM intensity was measured

at any laser power used for photo-activation. Plot shows mean ± SEM, n = 26. **E.** A decrease in 6-FAM intensity was measured in dendrites of neurons transfected with the long hairpin probe. This effect was observed both upon photo-activation and with imaging time. A comparable decline of 6-FAM intensity was measured at any laser power used for photo-activation. Plot shows mean ± SEM, n = 24. **F.** Dendrites of neurons transfected with the short hairpin probe showed a decrease in 6-FAM intensity upon photo-activation and with imaging time. A comparable decline of 6-FAM intensity was measured at any laser power used for photo-activation. Plot shows mean ± SEM, n = 38.

per culture dish. Immediately after the last dendrite, 1 μM puromycin was added to medium for 10 min to label newly synthesized protein. Neurons were fixed and Puro-PLA was performed to visualized newly synthesized Camk2a protein. Images of the dendrites that were photo-activated before were acquired and used for analysis (Figure 38).

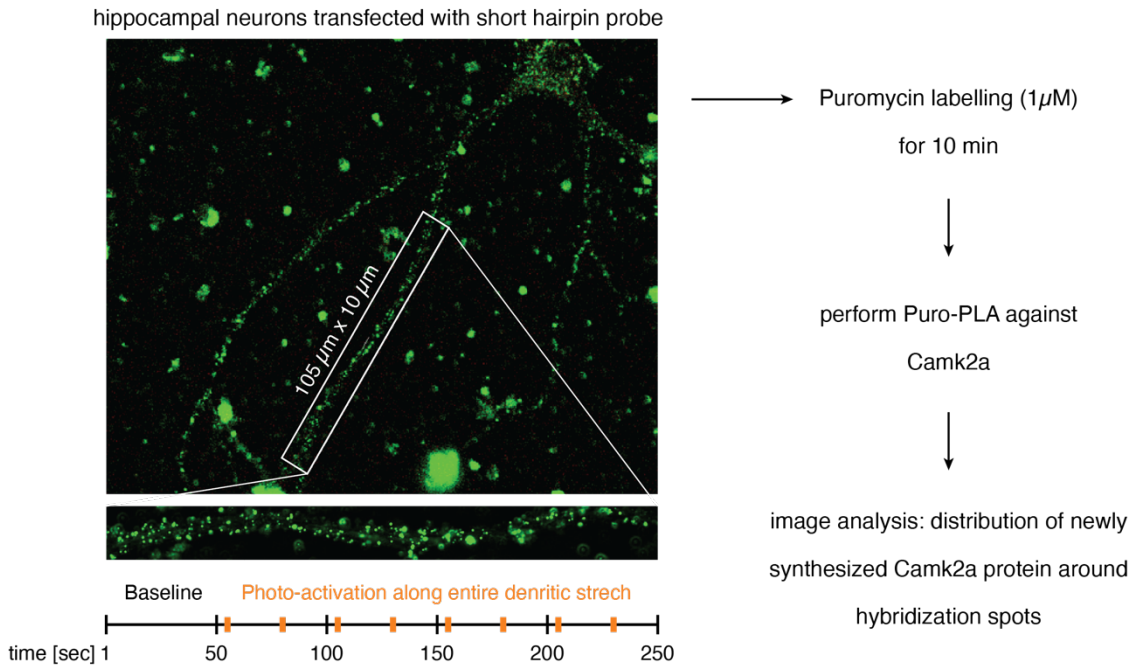

Figure 38. Experimental procedure to investigate the influence of miR-181a on local Camk2a translation.
Cultured hippocampal neurons of 3-weeks age were transfected with the short hairpin probe. Distal dendritic segments (105 μm x 10 μm) of 3-4 different neurons were each sequentially live-imaged for a duration of 250 sec. During the first 50 sec no photo-activation was performed. Beginning with the 51st sec, each dendritic stretch was photo-activated 8-times (orange rectangles). Immediately after the acquisition of the last time-series, neurons were incubated with 1 μM puromycin for 10 min. The Puro-PLA technique was then applied to visualize newly synthesized Camk2a protein. Live-cell images and Puro-PLA staining were then analyzed to determine the distribution of newly synthesized Camk2a protein around each hybridization spot.

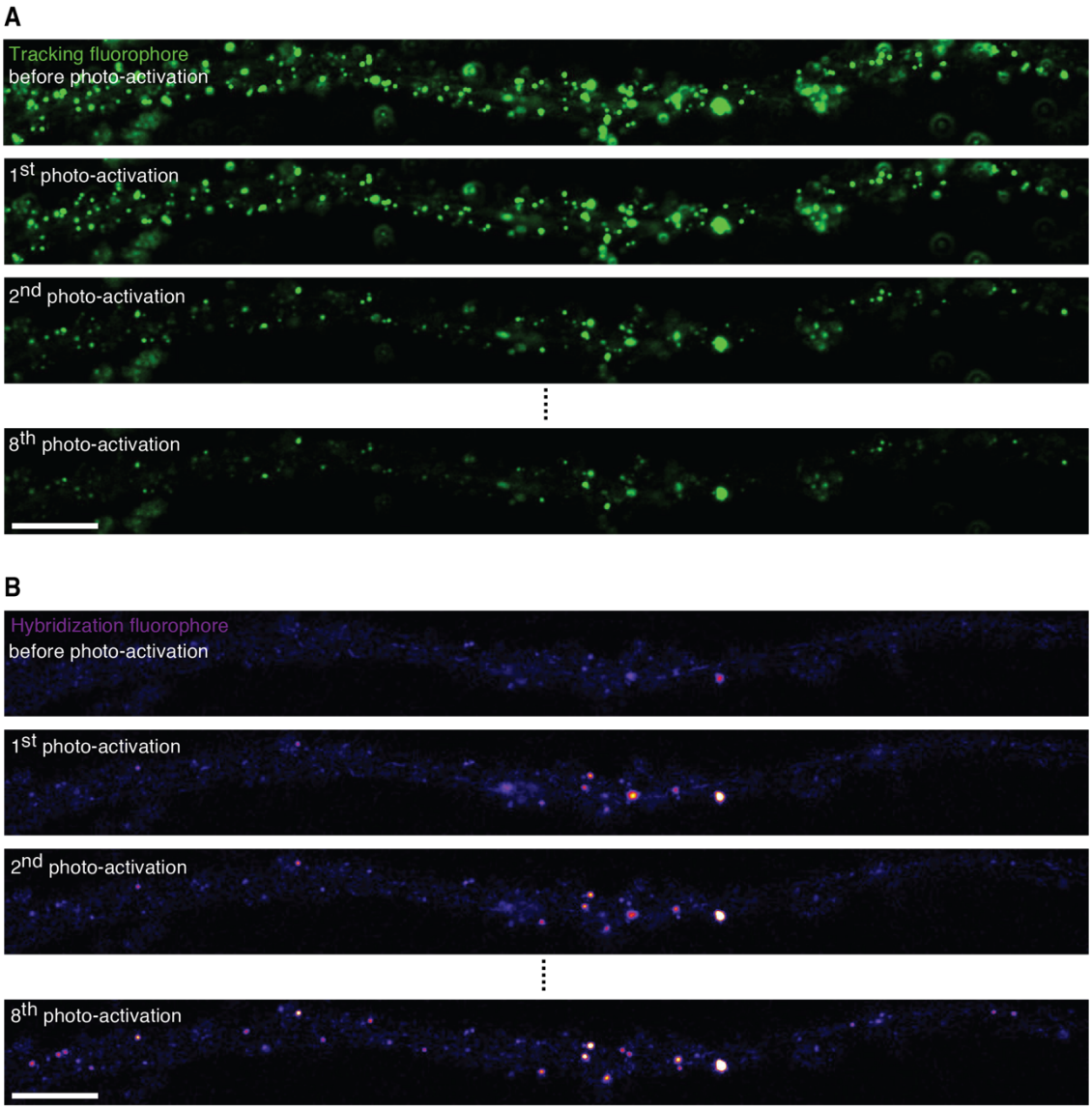

Figure 39. In distal dendrites approximately 20% of all antimiR clusters display hybridization signal after photo-activation.
A. Tracking fluorophore signal of the short hairpin probe (green) is shown in distal dendrite before and after photo-activation. A steady decline of 6-FAM intensity was observed over the course of 8 photo-activation cycles. Scale bar = 10 μm. **B.** Hybridization fluorophore signal of the short hairpin probe (magenta) is shown in distal dendrite shown before and after photo-activation. Hybridization signal appeared upon first photo-activation event and increased in intensity until the 8th and last photo-activation. Approximately 20% of all antimiR clusters displayed Cy5.5 fluorescence signal. Scale bars = 10 μm.

Along the distal dendrites I observed a dense but even distribution of the short hairpin clusters, with little Cy5.5 signal detected before light induction. Upon photo-activation, hybridization signal appeared rapidly in around 20% of all antimiR spots upon the first light pulse and the Cy5.5 intensity increased steadily

over the 8 photo-activation cycles. The 6-FAM intensity, however, decreased strongly and was barely visible at the end of the time series. While most antimiR spots were stationary, I observed the movement of few antimiR clusters along the dendrite (Figure 39).

Quantifying the spatial dynamics of miR-181a regulation on local Camk2a synthesis

As miR-181a suppresses *Camk2a* translation, the sequestration of miR-181a by the short hairpin probe should result in the local increase of newly synthesized Camk2a protein. But how local is "local"? What is the radius within which miR-181a can suppress *Camk2a* translation in distal dendrites? To address this question, we quantified the distribution of newly synthesized Camk2a protein within different distances around each hybridization spot. To identify the hybridization spots, I wrote an ImageJ macro. In brief, an average intensity projection of the hybridization channel was generated before photo-activation (1 – 50 sec, "baseline") and after photo-activation (51 – 250 sec, "photo-activation"). After subtracting the "baseline" from the "photo-activation" image, a common threshold was set to create a binary image of the hybridization spots detected in each dendrite. To count the number of newly synthesized Camk2a protein punctae within a defined radius around each hybridization spot, I used a customized MATLAB script. The analysis script took as input files the binary image of the hybridization spots, an image with all tracking spots, and an image of the newly synthesized Camk2a protein signal. First, all hybridization spots that overlapped with tracking spots were identified. The same number of randomly selected tracking spots that did not overlap with hybridization spots were used as controls. Within a user defined radius (μm) around each the hybridization and control spot, the number of newly synthesized Camk2a protein puncta were counted and reported (Figure 40).

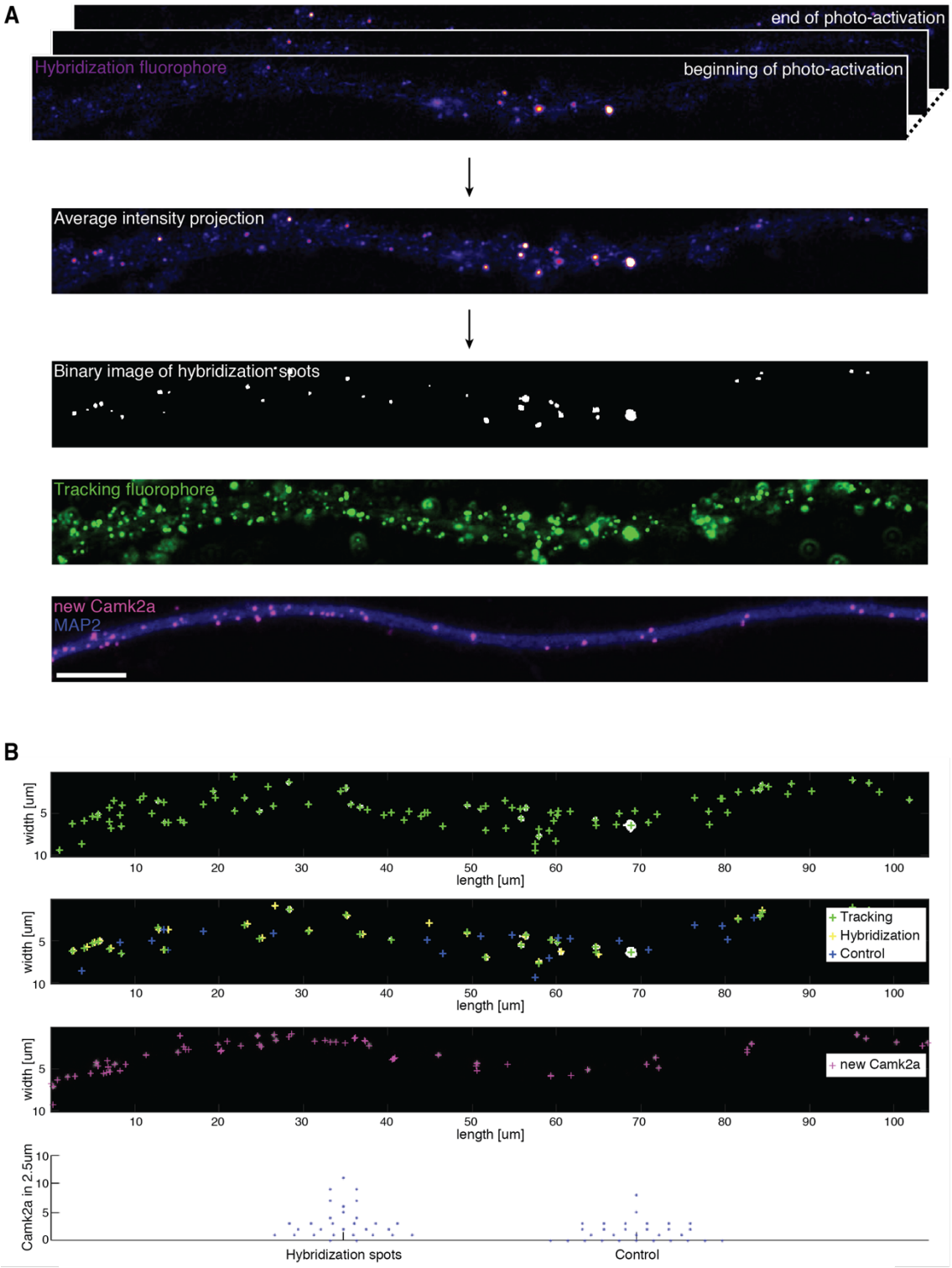

Figure 40. Quantifying the spatial dynamics of miR-181a regulation on local Camk2a synthesis.

A. Process of image analysis is shown. First, a binary image of the hybridization spots was generated by subtracting the average intensity project of the Cy5.5 images before photo-activation from the average intensity projection of the Cy5.5 images after photo-activation. A custom MATLAB script was applied to count the number of newly synthesized Camk2a protein

spots around each hybridization spot. As additional input files an image of the tracking fluorophore channel (green) as well as the Puro-PLA channel (pink) was required. Neuron were visualized using MAP2-staining (blue). Scale bar = 10 μm. **B.** Image analysis of an example dendritic stretch. All hybridization spots (yellow cross) that overlap with tracking spots (green cross) were determined. The same number of randomly selected tracking spots that did not overlap with any hybridization spots were used as control spots (blue cross). The number of newly synthesized Camk2a puncta (pink cross) in a user defined radius (μm) was quantified for the hybridization and control spots. Scatter dot plot shows the number of newly synthesized Camk2a protein (y-axis) detected around hybridization or control spots (x-axis) of the example dendrite in the radius of 2.5 μm.

Increased newly synthesized Camk2a protein puncta detected within 2.5 μm radius around hybridization spots

First, I investigated the distribution of newly synthesized Camk2a signal and found an uneven distribution of the Puro-PLA puncta along distal dendrites. Overlaying the Puro-PLA signal with the hybridization signal, I observed that newly synthesized Camk2a puncta were often found in close proximity to hybridization spots. When I quantified the newly synthesized Camk2a puncta in a radius of 1 μm - 6 μm around hybridization and control spots, significantly more Camk2a puncta was detected in a radius of 2.5 μm around hybridization spots compared to control spots. No difference in newly synthesized Camk2a protein distribution was measured within a smaller (1 μm - 2 μm) or larger (3 μm - 6 μm) radius. As a control, I performed Puro-PLA against beta-actin. As the *beta-actin* mRNA is not targeted by miR-181a, no differences in the distribution of newly synthesized beta-actin protein around hybridization and control spots is expected. Indeed, I found no significant difference in the number of newly synthesized beta-actin puncta between the hybridization spots and the control spots at any radius tested. These results suggest that within a radius of 2.5 μm miR-181a affects the local translation of *Camk2a* in distal dendrites (Figure 41).

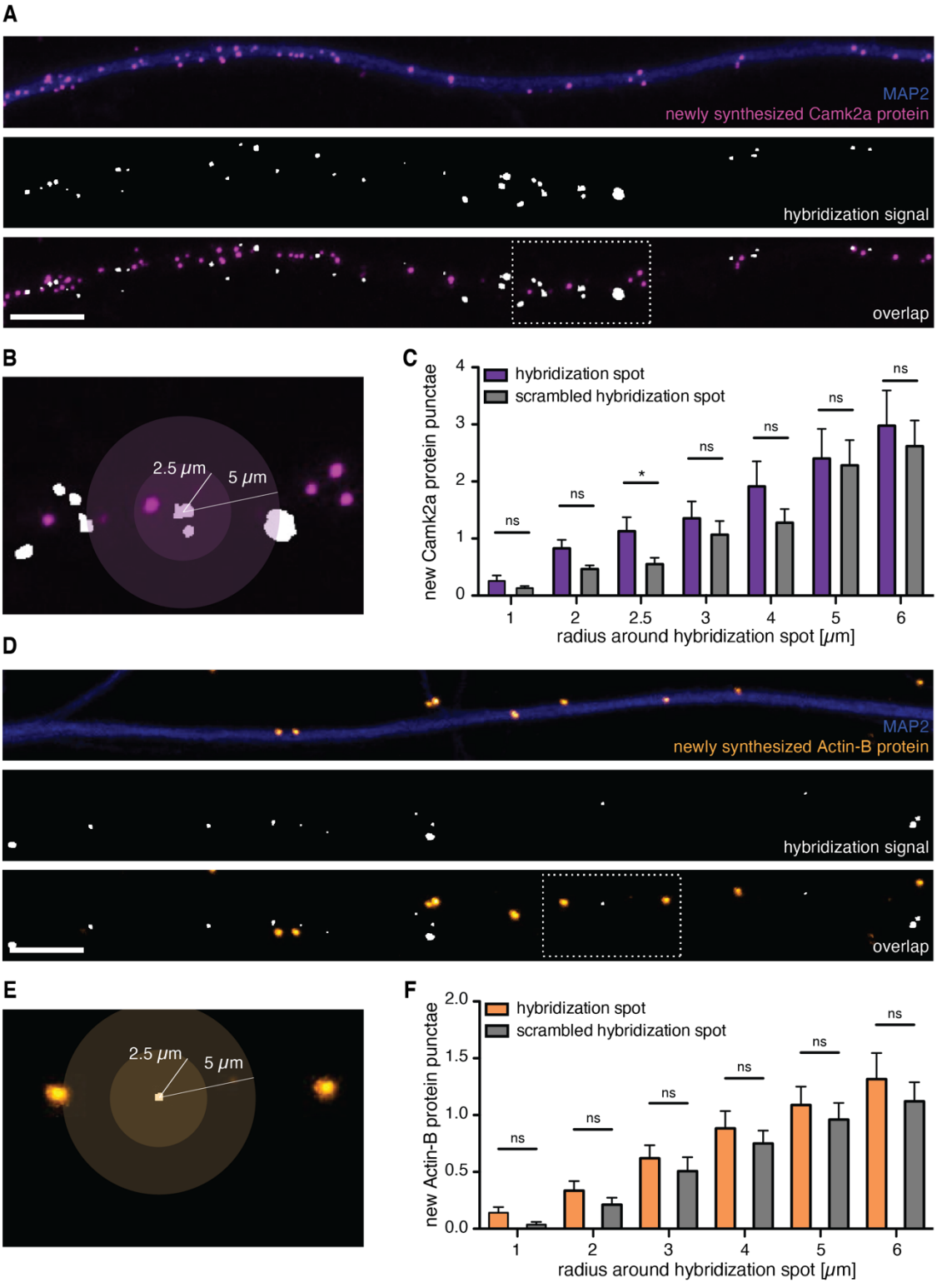

Figure 41. Increased number of newly synthesized Camk2a protein detected within a radius of 2.5 µm around hybridization spots.
A. Distribution of newly synthesized Camk2a protein (pink) and hybridization spots (white) are shown in a distal dendrite. The neuron was visualized with MAP2 staining (blue). Dotted box shows zoom-in region in **B.** Scale bar = 10 µm. **B.** Zoom-in of newly synthesized Camk2a protein (pink) and hybridization spot (white) in a distal dendrite. Circles indicate radius of 2.5 µm and 5

μm around a hybridization spot. **C.** Quantification of the number of newly synthesized Camk2a puncta (y-axis) observed around hybridization spots (purple bar) and control spots (grey bar) within tested radii (x-axis). Significantly more newly synthesized Camk2a puncta were detected around hybridization spots compared to the control in a radius of 2.5 μm (* $p < 0.05$, Mann Whitney U test, n = 6). Plot shows mean $\pm$ SEM. **D.** Distribution of newly synthesized beta-actin protein (orange) and hybridization spots (white) in distal dendrites. Neuron was visualized using MAP2 staining (blue). Dotted box shows zoom-in region in **E.** Scale bar = 10 μm. **E.** Zoom-in of newly synthesized beta-actin protein (orange) and hybridization spots (white) in distal dendrite. Circles indicate radius of 2.5 μm and 5 μm around a hybridization spot. **F.** Quantification of the number of newly synthesized beta-actin puncta (y-axis) observed around hybridization spots (purple bar) and control spots (grey bar) within tested radii (x-axis). No significant difference in the number of newly synthesized beta-actin protein was detected between hybridization spots and control spots at any tested radius (ns $p \geq 0.05$, Mann Whitney U test, n = 5). Plot shows mean $\pm$ SEM.

DISCUSSION

The spatial and temporal control of biochemical processes is essential for cellular homeostasis. This is especially important for neurons which, due to their unique morphology, translocate mRNA to specific cellular compartments such as axons and dendrites where the mRNAs are locally translated into protein (Sutton & Schuman, 2006). To study the spatio-temporal dynamics of endogenous miRNA-regulation of local *Camk2a* translation, we developed dual-labelled and photo-activatable antimiR probes to control miR-181a activity in specific subcellular regions such as dendrites and spines using light.

To identify an effective and easy delivery system for the antimiR probes, I tested three transfection reagents. I found Lipofectamine Messenger Max to be the most efficient for the delivery of the antimiR into primary neurons. Interestingly, I observed a punctate distribution of the antimiR throughout the cytoplasm. Using antibody staining against cellular organelle markers, I investigated the origin of these clusters. No overlap of the antimiR with endosome or lysosome marker was observed, suggesting that antimiR clusters were neither artefacts of our transfection method nor the result of antimiR degradation. To test if antimiR clusters co-localized with mRNAs or miRNAs, I performed immunostaining against three types of RNA granules in neurons: transport messenger ribonuleoproteins (mRNPs), stress granules and processing-bodies (P-bodies). Dendritically localized mRNAs are found in mRNPs that are transported to distal dendrites (Besse & Ephrussi, 2008; Costa-Mattioli et al., 2009). To protect mRNAs from harmful conditions, such as stress, mRNAs are translocated transport mRNPs into stress granules (Anderson & Kedersha, 2006; Nover, Scharf, & Neumann, 1989; Vessey et al., 2006). mRNAs within stress granules can either re-enter translation or further be translocated into P-Bodies, the site of translational repression and/ or mRNA degradation (Buchan & Parker, 2009). As such, P-bodies contain components, among others, of RISC machinery including miRNAs (Anderson & Kedersha, 2006; Schratt et al., 2006; Vessey et

al., 2006). Out of all tested RNA granule markers, robust immunostaining was only obtained for PABP1, a stress granule marker, with which many antimiR clusters overlapped. Co-localisation with stress granules suggests the close proximity of some antimiRs to non-translating mRNAs. Limited by reliable antibodies, we currently cannot entirely rule out the overlap of antimiR clusters with transport mRNPs and P-bodies. Specifically, it would be important to determine if antimiRs are also positioned in close proximity to P-bodies, hence miRNAs. Moreover, to exclude the possibility that stress granule formation was triggered by our transfection method, other delivery methods would need to be evaluated.

Before photo-activation, I observed with the hairpin probes some hybridization signal in the soma of transfected neurons, while the strongest Cy5.5 fluorescence was detected with the molecular beacon. This result suggests that a molecular beacon with a stem consisting of 3 C-G base pairs partially opens in the cytoplasm before photo-activation and miR-181a binding. Hence, further optimization of the stem length is needed. Interestingly, my *in vitro* observations contrast fluorometric measurements of the antimiR probes under PBS buffer conditions in which no Cy5.5 signal was found before photo-activation with any antimiR variants. While buffer solutions mimic the intracellular ion concentrations, they cannot account for the molecular complexity of the cytoplasm. Hence, fluorometric measurements should be optimized and performed with neuronal cell lysate and combined with *in vitro* experiments.

Upon photo-activation, I detected a rapid increase in hybridization fluorophore intensity with all antimiR probes in both soma and dendrites, which remained stable over the imaging session. However, I observed bleaching of the 6-FAM intensity both upon photo-activation and with imaging time. For the selection of green tracking and far-red hybridization sensing fluorophores the photo-stability and the feasibility of their incorporation during solid-phase synthesis were considered. Cy5.5 and 6-FAM were chosen, as they were

commercially available as phorphoramidites which simplified the chemical synthesis and also fulfilled the spectral requirements. To improve the antimiR design, ATTO dyes represent good alternatives in terms of brightness and photo-stability. As such, Atto647N and ATTO488 would be a substantial improvement to the currently used Cy5.5 and 6-FAM dyes, respectively. Moreover, brighter and more photo-stable tracking and hybridization sensing fluorophores would enable us to tackle remaining open questions, such as how many antimiRs form a cluster and what is the number of miRNAs that are sequestered upon photo-activation.

While I observed no increase in Cy5.5 intensity after a single photo-activation event over time, repeated photo-activation resulted in a steady increase of Cy5.5 intensity with each photo-activation cycles. This was observed both at lower (1.48 mW) and the maximum (3.58 mW) laser power. This result suggests that not all PC-linkers or photo-protective groups were removed with a single photo-activation event. While the hairpin probes possess either 2 or 4 PC-linkers, 8 photo-labile protective groups prevent the binding of miR-181a to the molecular beacon before photo-activation. This suggests that, compared to the hairpin probes, a higher number of photo-activation events are required to completely remove all photo-labile protective groups of the molecular beacon. This could also explain the higher variance of the hybridization signal observed after photo-activation with the molecular beacon. Another explanation for the variance of Cy5.5 fluorescence after photo-activation is the secondary structure of the molecular beacon. In comparison to previously reported molecular beacons (Joshi et al., 2012), the loop region of the molecular beacon against miR-181a forms a stem consisting of 5 base-pairings. The photo-labile protective groups along the loop region may prevent the secondary structure before photo-activation. However, upon light induction and removal of the photo-labile groups the formation of this additional stem could further stabilize the molecular beacon and therefore prevent the binding of miR-181a. One way to test this hypothesis is by performing hybridization experiments with RNA oligos consisting of different fragments of the miR-181a sequence.

To determine the spatial dynamics of miR-181a regulation on local *Camk2a* translation, we quantified the number of newly synthesized Camk2a protein within 1-6 μm radius around each hybridization spot. Our results suggest that within a 2.5 μm radius miR-181a suppresses the local translation of its target mRNA in distal dendrites. No significant difference in newly synthesized beta-actin protein, a non-target of miR-181a, was measured at any tested radius between hybridization and control spots, further strengthening our findings.

We noted, however, that a dissociation of the blocking strand in the absence of the mi-R181a binding would also result in the appearance of Cy5.5 fluorescence. To rule out the detection of such a false positive hybridization signal, a negative control probe is needed. Ideally, the negative control antimiR should target an RNA sequence that is not expressed in rat hippocampal neurons. Another alternative explanation for the increased levels of newly synthesized Camk2a protein around hybridization spots could be that antimiR clusters are localized in close proximity to *Camk2a* mRNA, but not to *ActB* mRNA. A way to test this is by visualizing *Camk2a* and *ActB* mRNA using FISH after photo-activation and analyze their distribution around antimiR clusters.

Despite the need for further optimization, the development of the photo-activatable antimiR makes it possible, for the first time, to perturb miRNA activity with spatio-temporal precision. This enables an assessment of the range and speed of miRNA-mediated inhibition on local target mRNA translation, which was not possible before due to the lack of tools. In our experiments, we investigated the spatial regulation of miR-181a on local *Camk2a* translation under baseline condition in distal dendrites. As demands in local protein synthesis changes upon plasticity, we will next explore the dynamics of miRNA regulation upon stimulating or suppressing neuronal activity. Furthermore, we will investigate the temporal aspects of miRNA regulation. In previous studies, when miRNA expression was perturbed within the whole cell by over-expression or depletion, changes in the target protein level were measured only after hours to days (Béthune, Artus-

Revel, & Filipowicz, 2012; Djuranovic, Nahvi, & Green, 2012). However, the speed of miRNA-mediated inhibition may be faster than the currently estimated, as miRNAs are generally seen as rapid fine-tuners of translation (Sevignani, Calin, Siracusa, & Croce, 2006). This information could be especially important in dendrites and spines, where rapid changes in protein synthesis are required upon signal input. Combining the photo-activatable antimiR with the Puro-PLA approach we can, for the first time, get a precise measurement of the temporal dynamics of local miRNA regulation down to the scale of minutes. Thus, the photo-activatable antimiR can greatly impact our understanding on the spatiotemporal dynamics of miRNA regulation on local translation.

Chapter IV

CONCLUSION AND FUTURE PERSPECTIVES

CONCLUSION

Activity-dependent alterations in the composition, form and strength of synapses are termed synaptic plasticity and believed to underlie some forms of learning and memory formation. Now, it is well established that certain forms of neuronal plasticity rely on modifications of the local protein pool (Sutton & Schuman, 2006). Neurons achieve this by translocating thousands of the mRNAs, aka the local transcriptome, into dendrites and spines and use them for local protein synthesis (Biever et al., 2020; Cajigas et al., 2012; Tushev et al., 2018). Besides protein coding mRNAs, many non-protein coding RNA species have been identified in neuronal sub-compartments as key regulators of neuronal function and synaptic plasticity (Gao et al., 2010; Kye et al., 2007; Lugli et al., 2008; Sambandan et al., 2017; Schratt et al., 2006; Tiedge et al., 1991; Tripathi et al., 2010). Recently, covalently closed circular RNAs were added as a new family member to the rich and heterogenous repertoire of the non-coding RNA world. As we yet had limited knowledge about the expression and biogenesis of circRNAs in the CNS, we set out to characterize the circRNA landscape in the murine hippocampus and investigate the mechanisms regulating circRNA synthesis using RNA-sequencing and fluorescence *in situ* hybridization. We found that the brain expresses the highest number of circRNAs compared to other tissues, mostly due to the fact that many circRNAs are generated from gene loci encoding for synaptic proteins (You et al., 2015). Moreover, circRNAs are enriched in synaptic compartments, such as the neuropil and synaptoneurosomes (You et al., 2015). We also observed dynamic changes in circRNA expression across different developmental stages and upon induction of homeostatic plasticity in the hippocampus. Developmental and homeostatic plasticity caused an up- and down-regulation of certain circRNAs that was often independent of their cognate linear transcripts (You et al., 2015; Zheng et al., 2011). These findings point towards an important regulatory role of circRNAs during neuronal development and function. Furthermore, the enrichment of

circRNAs specifically in brain tissue and their dynamic expression suggest a tight regulation of the biogenesis of neuronal circRNAs.

As we observed a high conservation of splice sites around circularizing exons (You et al., 2015), we next investigated the role of the splicesosome on neuronal circRNA generation. We used isoginkgetin to pharmacologically inhibit spliceosome activity and RNA-sequencing to profile changes of the circRNA landscape. If the spliceosome is crucial for circRNA formation, one would hypothesize that reduced spliceosome activity would result in a down-regulation of circRNA expression. Surprisingly, we detected for many circRNAs, such as *circHomer1*, an up-regulation of their expression and for only a few circRNAs decreased expression upon reduced spliceosome activity (M. Wang et al., 2019). The increase in circHomer1 expression, for example, was also observed after RNAi-mediated knock-down of splicing factors (M. Wang et al., 2019). We asked if information in the circRNA producing gene loci facilitated circRNA expression. Analyzing the sequence features of introns flanking circularizing exons, we found that upregulated circRNAs are flanked by unusually long introns. Moreover, these long introns harbored a significantly higher number of repeat sequences that have the potential to base-pair with another. The interaction of such intronic repeat sequences may have facilitated the expression of their cognate circRNAs under conditions of reduced spliceosome activity. Moreover, our findings suggest that biogenesis factors work in synchrony to regulate neuronal circRNA production (M. Wang et al., 2019).

Another family of non-coding RNAs are miRNAs that mediate post-transcriptional gene silencing by the recognition of specific sequences in target mRNAs. miRNAs are highly expressed in the brain, often enriched in neuronal processes, and they play regulatory roles in synaptic function and plasticity (Gao et al., 2010; Krichevsky et al., 2003; Kye et al., 2007; Lagos-Quintana et al., 2002; Lugli et al., 2008; Sambandan et al., 2017; Schratt et al., 2006; Yang et al., 2012; Zovoilis et al., 2011). Although miRNAs were proposed as fine-tuners of local

protein synthesis (Holt & Schuman, 2013; Sevignani et al., 2006), due to the lack of suitable tools the spatio-temporal dynamics of miRNA-mediated regulation on local translation could not yet be studied. To tackle this question, we developed in collaboration with the research group of Prof. Alexander Heckel a probe – the antimiR – to inactivate miR1-81a in dendrites and spines using light. The antimiR consists of an antisense strand that is complementary to the miR-181a sequence and a blocking strand which prevents sequestration of miR-181a before light-induction. Furthermore, we incorporated two fluorophores into the antimiR: a tracking fluorophore that enables the visualization of the probe live and a hybridization sensing fluorophore to detect the successful sequestration of miR-181a. In hippocampal neurons, the transfected antimiR appeared in clusters and co-localized with an RNA granule marker PABP1 which suggests a close proximity of antimiRs to untranslated mRNA and miRNAs (Leung, 2015). Upon local photo-activation, we detected a rapid sequestration of miR-181a by the antimiR in distal dendrites. To determine the spatio-temporal dynamics of miR-181a sequestration on local protein synthesis of one of its targets, we quantified the newly synthesized population of Camk2a around the hybridization spots. We detected a significant increase in newly synthesized Camk2a protein in a radius of 2.5 μm around each hybridization spot within 15-20 min post-photoactivation. Previous studies reported a translational repression by miRNAs in the time frame of hours (Béthune et al., 2012; Djuranovic et al., 2012). However, in dendrites and at spines, rapid regulation of the local protein pool may be needed upon signal input. Our findings suggest that local protein synthesis at distal dendrites increases as early as tens of minutes after local miRNA sequestration.

FUTURE PERSPECTIVES

Regulation of sub-cellular localization of neuronal circRNAs

In neurons circRNAs are often localized to axons, dendrites and synapses (Rybak-Wolf et al., 2015; You et al., 2015). Moreover, there seems to be a regulated switch in the nucleocytoplasmic localization of circRNAs during embryonic brain development (Venø et al., 2015). A recent study suggested that the nuclear export of circRNAs is promoted by two different proteins, *Drosophila* Hel25E and *human* UAP49/56, in a circRNA size-dependent but sequence-independent manner (C. Huang, Liang, Tatomer, & Wilusz, 2018). While some information has been gained on how circRNAs may enter the cytoplasm, it still remains unclear how circRNAs accumulate in neuronal processes. How are circRNAs transported within the cytoplasm? Are neuronal circRNAs, like other RNA species, carried via motor proteins in a complex with RBPs and other RNAs to their destined location? Or do circRNAs diffuse throughout the cytoplasm? Are there specific mechanisms to retain circRNAs in distal neuronal compartments once they have localized there? A good way to study these mechanisms is to fluorescently label circRNAs and follow their journey through the cell using live-cell imaging approaches.

Function of neuronal circRNAs

CircRNAs are a heterogeneous class of RNAs which is reflected in their diversity of functions. While miRNA binding sites have been predicted in the sequence of few circRNAs (Hansen et al., 2013)(*SRY*, *ciRS-7*), (Memczak et al., 2013) (*CDR1as*), (Y. Li et al., 2017) (*circHIPK3*), (Du et al., 2016) (*circFOXO*), (G. Huang et al., 2015) (*circITCH*), (Yu et al., 2017) (*circBIRC6*)), the physiological importance of circRNAs to act as miRNA sponges has so far only been shown for *CDR1as* (Kleaveland et al., 2018; Piwecka et al., 2017). Other circRNAs seem to act as RBP decoys or transport platforms for proteins

(Abdelmohsen et al., 2017; Du et al., 2016; Holdt et al., 2016). More recently, a subset of circRNAs were suggested to produce protein in fly brain and in murine and human cells (Legnini et al., 2017; Pamudurti et al., 2017; Yang et al., 2017). Although, we have yet to understand the function of these translated peptides from circRNAs, they add to the rich repertoire of mechanisms of circRNA function. We investigated these potential functions for neuronal circRNAs of the murine hippocampus. However, we did not find any evidence that would suggest that neuronal circRNAs are more likely bound by miRNAs than linear RNA (You et al., 2015). Our findings rather suggest that circRNAs, as a class, might not act as miRNA sponges in brain tissue. Moreover, we found neuronal circRNAs are unlikely to be translated into protein and to bind RBPs when compared to the coding sequence or the 3'UTR of protein-coding genes (You et al., 2015). Although not enriched in miRNA and RBP binding sites, circRNA interaction with these factors can be rendered meaningful in sub-cellular compartments where miRNAs and RBPs are present in limiting amounts. Moreover, the potential interaction of circRNAs with other RNA species remain yet to be addressed. These questions are especially interesting in synaptic compartments where neuronal circRNAs are enriched (You et al., 2015). One potential approach to address these questions is to use a biotinylated circRNA to pull-down local interaction partners.

CircRNAs as biomarkers for human diseases

Biomarkers are a routine approach for diagnosis and prognosis of various diseases and several circRNAs have been associated with human disorders such as cancer, myotonic dystrophy and atherosclerotic vascular disease (Bachmayr-Heyda et al., 2015; Burd et al., 2010; Lukiw, 2013; Qin et al., 2016; Qu et al., 2015). Especially in the brain, where circRNAs are enriched, circRNAs were shown to play crucial roles in the development of neurological diseases, such as Alzheimer's disease (Bingol & Sheng, 2011; Lonskaya et al., 2013; Lukiw, 2013), Parkinson's Disease (Ghosal, Das, Sen, Basak, & Chakrabarti, 2013; Memczak

et al., 2013) and ischemic brain injury (Bai et al., 2018; Han et al., 2018). Various characteristics of circRNA make them good candidates for use as biomarkers. CircRNAs are highly stable molecules due to their closed loop structure lacking of free 5' and 3' ends. The average half-life of circRNAs in plasma exceeds 48 h and is therefore much longer than the average half-life of mRNAs (Jeck & Sharpless, 2014). Furthermore, the high conservation of circRNAs between species suggest that circRNAs are universal molecules distributed in various cell types (Salzman et al., 2012). Many circRNAs display tissue and development-specific expression. In particular, distinctive expression of circRNAs was found between cancerous and non-cancerous tissues (Memczak et al., 2013). Moreover, an age-dependent accumulation of circRNAs in *Drosophila* suggests circRNAs as promising markers for aging (Westholm et al., 2014). The simple detection of circRNAs in various body fluids such as plasma and blood (Memczak, Papavasileiou, Peters, & Rajewsky, 2015) further facilitates the usage of circRNAs as diagnostic biomarkers for human diseases.

Assessment of off-target effects of the antimiR

One potential source for a false positive appearance of hybridization signal is the binding of the antimiR to RNAs other than the target miRNA. Thus, it is important to understand the interaction of an antimiR with endogenous RNA and test our current design for any off-target effects. To do so, we plan as a next step to develop a negative control antimiR to determine the specificity of our hairpin probe. One challenge in the development of the negative control antimiR is that kinetics for the release of the quencher strand from the antimiR strand is dependent on the nucleotide sequence. Hence a comparable nucleotide composition between the miR-181a antimiR and the control antimiR should be achieved. The target sequence of the control antimiR could be either a miRNA that is not expressed in the target tissue or a scrambled sequence of miR-181a. As our Nanostring data suggest that miR-159a from *Arabidopsis* is not detected in the rat neuropil (Sambandan et al., 2017), we will use it as the target sequence.

Furthermore, we will test whether interactions between the antimiR strand and the target miRNA likely occur though imperfect base pairings. To address this question, we will perform a series of hybridization experiments using oligo nucleotides with different numbers and positions of mismatches compared to the miR-181a and miR-159a sequences. These experiments will give us valuable insight into the stringency of target miRNA binding using our antimiR.

Optimization of the antimiR design

Light-activated oligonucleotides are an important tool to study biological process with high spatial and temporal control (Ruble, Yeldell, & Dmochowski, 2015). A major goal is to achieve specific and efficient activation of the "caged" oligonucleotide with little light-induced damage to the cell. A potential downside of the current design of the hairpin probe is the number of photo-cleavable linkers that were incorporated to achieve efficient miR-181a binding upon light-induction. As a result, we were forced to use high laser powers and several photo-activation cycles to ensure complete removal of all photo-linkers. As a future optimization step, we plan to reduce the number of photo-cleavable linkers to ideally a single one. This would allow us to use minimal laser power to achieve complete photo-activation of the antimiR. However, to do so, we need to switch the antimiR design to that of a molecular beacon, where a cyclization of the molecular beacon can be achieved using photo-tethers (Müller, Seyfried, Frühauf, & Heckel, 2019; Seyfried, Eiden, Grebenovsky, Mayer, & Heckel, 2017).

Determine the sub-cellular localization of the antimiR

Endogenous miRNAs localize to multiple subcellular locations in the cytoplasm, such as P bodies, stress granules (SGs), endo-membranes and mitochondria (Leung, 2015). While P-bodies contain various proteins associated with mRNA decay, translational control and RNA interference (Liu, Valencia-Sanchez, Hannon, & Parker, 2005; Sheth & Parker, 2003), stress granules

include mRNAs stalled at translation initiation or disassembling from polysomes and characterized by the presence of translation initiation factors, RBPs and 40S ribosomal subunit (Anderson & Kedersha, 2008; Protter & Parker, 2016). Stress granules are hypothesized to contain mRNAs that are translationally blocked by miRNAs (Leung, 2015). Indeed, we found many, but not all, antimiR clusters colocalized with RNA granules throughout neurons. Hence, it is crucial to understand mechanism of antimiR uptake and localization within the cell to determine the fraction of transfected antimiR that can physically interact with its target miRNA. Future co-localization studies with P-body and RISC markers will give insight in the cellular nature of antimiR uptake.

Role of miRNA-mediated regulation of local translation in synaptic plasticity

Long-term memory is established via modifications of neural circuits which include alterations in the patterning and strength of synaptic connections as well as the integration of new synapses in existing circuits. These modifications are in part achieved by dynamic changes in the local proteome as a response to synaptic input (Sutton & Schuman, 2006). One of the best-studied examples is Camk2a, whose local translation rapidly increases after LTP induction (Miller et al., 2002). Synaptic stimulation also changes the local miRNA pool and miRNAs are increasingly considered as central players in synaptic plasticity (Aksoy-Aksel, Zampa, & Schratt, 2014). Chemical LTP in hippocampal slices, for example, causes an up-regulation of nearly all detectable miRNAs within 15min (Park & Tang, 2009), while rapid maturation of miRNAs is observed at synapses upon local glutamate uncaging (Sambandan et al., 2017). Yet it remains unknown whether miRNAs regulate specific aspects of LTP induction or maintenance, or specific stages in learning and memory. One way to address these questions is to deplete the local miRNA pool (using the antimiR) after different time points after local stimulation. Future experiments will shed light on the effect of local miRNA depletion on synaptic plasticity, such as number and morphology of spines. Moreover, it has been hypothesized that due to their long stability in the

range of days to weeks, loaded RISCs associated with synaptic mRNAs could act as a persistent local regulator of long-term synaptic efficacy within previously activated synapses (Omi, Tokunaga, & Hohjoh, 2004; Smalheiser & Lugli, 2009). Furthermore, locally loaded RISC at synapses may serve as a “trap” to mRNAs that are transported to dendrites (Smalheiser & Lugli, 2009). Using the antimiR we will investigate the potential role of miRNAs in synaptic tagging and capture, by local glutamate uncaging and determine the effect of local miRNA sequestration in activated and neighboring control spines.

Chapter V

MATERIAL AND METHODS

Disclaimer

The “material and methods” section is in part taken from the publications associated with the work described in this dissertation:

You, X.*, Vlatkovic, I.*, Babic, A.*, Will, T.*, Epstein, I.*, Tushev, G.*, Akbalik, G.*, **Wang, M**., Glock, C., Quedenau, C., et al. (2015). Neural circular RNAs are derived from synaptic genes and regulated by development and plasticity. Nat Neurosci 18, 603-610

- = Authors contribulted equally

Wang, M., Hou J., Müller-McNicoll M., Chen W., Schuman EM. (2019). Long and repeat-rich intronic sequences favor circular RNA formation under conditions of reduced spliceosome activity. iScience 20, 237-247

Animal tissue and cell culture work

Preparation of tissue samples

Tissue collection were performed by Irena Vlatkovic and Irina Epstein as described You et al. (2015). In brief, wild-type C57B6 or C57BL/6J-Etv1-ARRAy TS88 (male and female) mice and Sprague Dawley (male) rats were housed in standard cages and fed standard low chow and water *ad libitum*. All animal work was performed following regulations of German animal welfare law. Animals were anesthetized with CO_2 for a few minutes and decapitated using a guillotine. Brains were removed and place in ice cold ACSF. To profile circRNA expression across different tissues two wild-type C57B6 male mice (20 weeks old) were used to dissect brain, heart, liver, lung and testes. To compare circRNA expression across different developmental stages, hippocampi of mice at the age of E18, P1, P10 and P30 were isolated. To profile circRNA expression in neuropil and somata, C57BL/6J-Etv1-ARRAy TS88 mouse and Sprague Dawley rat hippocampal slices of 500 μm were prepared. After 1 h recovery, the slices were used for tissue microdissection as described in Cajigas et al. (2012). To probe circRNA expression after induction of homeostatic plasticity, rat hippocampal slices were treated with bicuculline (40 μM, Tocris) or water for 12 h and micro-dissected. All tissues that were used for RNA isolation were collected in RNA-later (Ambion).

Preparation of synaptosomes

Synaptosomes of adult mice were prepared by Ana Babic and described in You et al. (2015). In brief, hippocampi were homogenized in sucrose-buffer (320 mM sucrose, 5 mM HEPES, pH 7.4) with a 15 ml Teflon-glass tissue grinder with eight even strokes. The homogenate was loaded onto a percoll gradient (3%, 10%, 15% and 23% PercollPlus (GE Healthecare) in sucrose buffer) and centrifuged at 31,000 g for 5 min for three times. The fraction at the interface between 15% and 23% Percoll was then isolated and used for RNA isolation.

Vibratome sections for fluorescence *in situ* hybridization

To visualize circRNA expression in hippocampal slices, rat hippocampi were prepared as described above and fixed overnight in 4% PFA/PBS at 4°C. Prior sectioning, hippocampi were embedded into 4% w/v low-melting agarose (Sigma) and carefully glued onto the sample holder of the vibratome (Leica). Hippocampi were then sliced into 30 – 50 μm thick sections and stored at 4°C in PBS or TBS until usage.

Primary hippocampal neurons

Hippocampi from postnatal day 0-1 rat pups of either sex were dissected and dissociated with papain (Sigma). For RNA isolation, neurons were plated at a density of 700K onto a 6 cm poly(D-lysine)-coated petri dish. For fluorescence *in situ* hybridization (FISH), 30K cells were plated onto a poly(D-lysine)-coated glass-bottom Petri dish (Mattek). Hippocampal neurons were maintained at 37°C and 5% CO_2 in growth medium consisting of Neurobasal-A (Gibco) supplemented with B27 (Gibco) and GlutaMax-I (Gibco).

Pharmacological treatments

To probe circRNA expression after induction of homeostatic plasticity, rat hippocampal slices were treated with bicuculline (40 μM, Tocris) or water for 12 h and micro-dissected. To determine how spliceosome inhibition affect neuronal circRNA expression, rat hippocampal neurons were treated at DIV 28-30 i) with 33 μM or 50 μM isoginkgetin (Merck, dissolved 0.1% v/v in DMSO) for 12 h or ii) with 33 μM or 66 μM Isoginkgetin for 24 h. Neurons treated with 0.1% v/v DMSO (VWR) for the matching duration of 12 h or 24 h were used as negative controls. To inhibit transcription and splicing, neurons were incubated with isoginkgetin and a cocktail of 40 μM Actinomycin D (Sigma), 1 μM Triptotide (Sigma) and 50 μM 5,6-Dichlorobenzimidazole (Sigma) for 24 h and used for fluorescence *in situ* hybridization.

FLAG-Pol2 over-expression analysis

Cultured hippocampal neurons were co-transfected using Magnetofectamine (OZ Biosciences) at DIV 9-12 with 0.5 μg of pAcGFP1-N1 (Clontech) and 1 μg of FLAG-Pol2-WT plasmid construct (a gift from Benjamin Blencowe, Addgene plasmid #35175, (Rosonina & Blencowe, 2004)). Immuno-staining against RNA-Polymerase II CTD (Abcam ab5131, 1:2000 dilution) and fluorescence *in situ* hybridization were performed 4 days post-transfection to quantify RNA-Polymerase II and circHomer1 expression, respectively.

SF3A2 and SF3B1 knock-down analysis

Cultured hippocampal neurons were transfected at DIV 9-12 with 1 μg of SF3A2, SF3B1 or scrambled control shRNA-plasmid constructs (OriGene) using Magnetofectamine (Oz Biosciences). Knock-down efficiency was quantified after 4 days by immunostaining against SF3A2 (Thermofisher PA5-61969, 1:500 dilution) or SF3B1 (Abcam ab172634, 1:500 dilution). To quantify circHomer1 expression fluorescence *in situ* hybridization was performed.

Fluorescence *in situ* hybridization

The following procedure was applied to visualize circRNAs in primary neurons. Cultured neurons were fixed for 25 min in 4% paraformaldehyde/PBS and *in situ* hybridization was performed using the ViewRNA miRNA ISH Cell Assay kit (Thermo Fisher Scientific) following the manufacturer's protocol, omitting the dehydration/rehydration step as well as the protease treatment. In brief, neurons were incubated with the FISH probes (dilution 1:100) for 3 h at 40°C and washed with washing buffer. To build up the FISH signal amplification tree, neurons were then incubated with pre-AMP, AMP and LP mixture for 1 h each. To adjust the manufacturer's protocol for the visualization of circRNAs in hippocampal slices, we increased the incubation of the FISH probes to over night at 40°C. Remaining steps were kept the same. Lastly, dendrites were stained with an anti-MAP2 antibody (Millipore AB5622, 1:1000 dilution). The following FISH probes were used:

Table 7. List of circRNA *in situ* hybridization probes.

circRNA	Probes
circHomer1	TTTCACATAGGGAACAACCT
circDscam	CTTGTCTCAGTTTTCAGTGA
scramble control	GTGTAACACGTCTATACGCCCA

Image acquisition and quantification of circRNA signal

Confocal microscopy was performed using a Zeiss LSM780 or LSM880 confocal laser fluorescence microscope system. Maximum intensity projections of image series of 20-32 confocal planes taken at 0.485 μm intervals using a 40x oil immersion objective were used for image analysis. The circRNA *in situ* signal in the cell body was quantified using a custom MATLAB script and normalized to cell body area.

Electrophysiology

Whole patch clamp recordings were made with an Axopatch 200B amplifier from cultured hippocampal neurons (DIV 28-29) bathed in HBS containing 119 mM NaCl, 5 mM KCl, 2 mM $CaCl_2$, 2 mM $MgCl_2$, 30 mM glucose, 10 mM HEPES [pH 7.4; ~310 mOsm] plus 1 μM TTX and 20 μM bicuculline. Whole-cell pipette internal solution contained 120 mM potassium gluconate, 20 mM KCl, 0.1 mM EGTA, 2 mM $MgCl_2$, 2 mM ATP, 0.4 mM guanosine triphosphate, 10 mM HEPES (pH 7.2; ~300 mOsm) and the pipette resistances ranged from 4–6 MΩ. Bicuculline was added in conditioned media for 12 h and the media was replaced with the HBS 15 min before recording. Neurons were voltage clamped at –70 mV while the series resistance was left uncompensated during the recordings. mEPSCs were analyzed offline using Stimfit39 software by employing a template-matching algorithm. Recordings were started 5 min after patching and the recording duration usually ranged from 5–10 min. Statistical differences between experimental conditions were determined by Mann-Whitney *U* test.

RNA sequencing work

RNA isolation and RNA-sequencing

Total RNA was isolated from animal tissue and primary neurons using Trizol (Invitrogen) following the manufacturer's protocol. RNA clean up and on-column DNase I digest was performed using the RNeasy Mini kit (QIAGEN). The following steps of the RNA seq library preparation were performed in the laboratory of Wei Chen (Max-Delbrück-Center for Molecular Medicine, Berlin). In brief, ribosomal RNA was depleted using the RiboZero Gold kit (Epicentre Biotechnologies). Poly(A) RNA was enriched using oligo-dT beads (Invitrogen). RNA-seq library was then generated from rRNA depleted RNA or poly(A) enriched RNA using Illumina stranded RNA Sample Prep kit according to the manufacturer's instructions and sequenced for 150 nt from single end on an Illumina HiSeq2000.

PacBio sequencing of RT-PCR products

The following experiment was performed in the laboratory of Wei Chen (Max-Delbrück-Center for Molecular Medicine, Berlin). RT-PCR products obtained from mouse brain and rat brain samples were directly sequenced using PacBio RS system as previously described (Sun et al., 2013).

TTO estimation

Quantification of total transcriptional output was performed by Xintian You and described in detail in You et al. (2015). In brief, reads were aligned after removing of the Illumina sequencing adaptors to the mouse (mm9) or rat (rn5.0) genome reference using Tophat2 (up to 6 mismatches). Cufflinks (v2.21) was used to estimate the total transcriptional output based on Ensembl gene annotation for mouse (mm9, version67) or rat (rno5.0, version 72). Only circRNAs derived from protein coding genes and lincRNAs were retained for further analysis. Furthermore, FRKM (Fragments per kilobase million) were converted into TPM

(Transcript per million) using the following formula: TPM = FPKM * 1,000,000 / (sum of FPKM) to compare the expression between two samples.

CircRNA identification and quantification

To identify circRNAs in different tissue samples, across developmental stages and after homeostatic plasticity, the following pipeline was developed by Xintian You as described in You et al. (2015). Unmapped reads were aligned to their respective genome reference sequences by BWA (H. Li & Durbin, 2009) in local mode. Reads for which partial alignments were mapped to i) regions of the same chromosome and no more than 1 Mb away from each other ii) on the same strand iii) but in reversed order were kept as potential head-to-tail junction reads. The splicing site strength of these reads were estimated using MaxEntScan (Yeo & Burge, 2004). Candidate circRNA were reported if the head-to-tail junction was supported by at least two reads and the splicing score was greater than or equal to 10. All un-mapped reads were realigned to the circRNA candidate to determine the expression of circRNAs. TPM was calculated for each circRNA candidate, where the effective length was calculated as (sequencing length – 2 * 6).

Transcript feature identification and differential expression

To assess the expression of pre-mRNA, mature mRNA and intron expression, we quantified the expression of reads that map to exon and/or introns as described in M. Wang et al. (2019). In brief, after removing the Illumina sequencing adaptor, the reads were aligned to the rat (rn5.0) genome reference sequences using STAR aligner (Dobin et al., 2013). We used the BEDTool software suit (Quinlan & Hall, 2010) to annotate each read by intersecting its genomic coordinates with the Ensembl gene annotation for rat (rno5.0). To identify and count the reads that mapped to the exon- and intron-body, as well as exon-exon and exon-intron junction, we applied a custom script. To evaluate the differential expression of total mRNA, pre-mRNA, mature mRNA and introns between isoginkgetin and control conditions, we input the summed exon-exon and exon-intron junction reads, exon-intron junction reads, exon-exon junction

reads and intron-body reads per transcript into the edgeR software (Robinson, McCarthy, & Smyth, 2010). Transcript features were filtered (CPM >1, detected in 4 out of 6 replicates) and library size adjusted. Model fitting and testing was performed using the exactTest function. A false discovery rate (FDR) of < 0.05 was used to determine differentially expressed events.

CircRNA identification and differential expression

To determine the expression of circRNAs after isoginkgetin treatment (M. Wang et al., 2019), we used a custom script. Chimeric aligments from the Chimeric.out.junction file were converted into BED12 files. The BEDTools software suit was employed to annotate the reads by intersecting their genomic coordinates with the Ensembl gene annotation for rat (rno5.0). If partial aligned segments within a chimeric read were i) at least 20bp long, ii) mapped to the same chromosome and strand, iii) showed the presence of a splice junction and iv) originated from the same gene but in reversed order, they were kept as head-to-tail junction read supporting the expression of a circRNA. Head-to-tail junction reads mapping to the X and Y chromosome, as well as mitochondrial chromosome were removed. Only circRNAs that were present with at least 1 unique read in all replicates and conditions were used for further analyses. To evaluate the differential expression of circRNAs between the isoginkgetin and control conditions, we input the head-to-tail junction reads and exon-exon junction reads of the parent mRNAs into the edgeR software. Model fitting and testing was performed using the exactTest function. Due to the low number of reads that were used as input, we decided to use a P value instead of false discovery rate (FDR) to determine differentially expressed events. The significance threshold value was set to 0.05.

Exon and intron feature analyses

The length of all rat exons and introns were determined using the Ensembl gene annotation for rat (rno5.0) and described in M. Wang et al. (2019). The identity of the exons spanning the head-to-tail junction was used i) to distinguish between

circRNAs comprised of a single exon or multiple exons, and ii) to identify the upstream and downstream flanking introns. A separate list of all introns located between the upstream and downstream flanking intron (a.k.a middle introns) was generated. The length of circRNA exons, flanking introns and middle introns were determined by cross-referencing their identity with the list containing the length of all rat exons and introns. Differentially expressed introns were identified as described above. However, instead of using intron-body reads per transcript, we applied the counts of each intron, together with all other transcript features as an input into the edgeR software. Length for up- and down-regulated introns was determined using the Ensembl gene annotation for rat (rno5.0).

Repeat feature and reverse complementary motif (RCM) analyses

As described in M. Wang et al. (2019). a list of repeat family and class, and their coordinates in the rat genome were obtained using the repeatMasker track of the UCSC table browser. Subsequently, the number of repeat families present in each circRNA flanking intron and the frequency of repeat family occurrence per 1kb intron length was determined. To calculated the average number of repeats per intron, we normalized the total number of each detected repeat family to the number of introns for up-regulated, un-changed and all circRNAs. Identification of reverse complementary motifs was conducted as previously described (Ivanov et al., 2015; X. O. Zhang et al., 2014). In short, intron alignments using BLAST (Altschul, Gish, Miller, Myers, & Lipman, 1990) were carried with the parameters "blastn -word_size 7 -gapopen 5 -gapextend 2 -penalty -3 -reward 2" and only local alignment with a BLAST score > 25 were kept.

Alu-repeat analysis

Orientation of Alu repeats in flanking intron pairs was determined as described previously (Jeck et al., 2013). In brief, paired flanking introns were analyzed for repeatMasker Alu elements using the BEDTools software suit. When at least one plus and one minus stranded Alu family element were detected on either side of the flanking introns a complementary Alu pair was identified. Alu repeats that

showed the same orientation were termed non-complementary. Single Alu repeats were designated as those that were found in one of the flanking introns but not both.

Minimum free energy calculation

RNA-fold was used to calculate the minimum free energy per intron sequence (Lorenz et al., 2011). Only sequences with a size ranging from 100-10,000nt were included into the analysis. Obtained MFE values were normalized to intron length.

Conservation and Gene Ontology enrichment analyses

Experiments were performed by Georgi Tushev as described in You et al. (2015). The position of rat circRNAs were converted to mouse (mm9) genome coordinates using UCSC liftOver tool and then intersected with mouse circRNA using BEDtools. To examine the evolutionary conservation score of the sequences around circRNA junctions the PhastCons scores for alignments of 29 vertebrate genomes with mouse (mm9) from http://hgdownload.soe.ucsc.edu/goldenPath/mm9/phastCons30way/vertebrate/. As control splice sites within same genes that do not participate in head-to-tail junction formation were analyzed. Gene Ontology enrichment analysis was performed using DAVID (Huang da, Sherman, & Lempicki, 2009a, 2009b). The background set consists of all expressed genes (TTO>0.01) and the test set consists of all expressed circRNA-hosting genes.

qRT-PCR work

RNase R treatment

Total RNA (1 – 3 μg) was incubated for 15 – 45 min at 37°C with 10 U of RNase R (Epicentre). RNA was subsequently purified using the RNA Clean and Concentrator kit (Zymo Research) according to manufacturer's protocol. Reverse

transcription was performed using the QuantiTect Reverse Transcription kit (QIAGEN). Quantitative RT-PCR was performed as described below.

cDNA synthesis and quantitative real-time PCR

The qRT-PCR experiments shown in Figure 12 were conducted by Ana Babic as described in You et al. (2015). For all the remaining qRT-PCR experiments, RNA was isolated as described above. Reverse transcription was performed using the QuantiTect Reverse Transcription kit (QIAGEN). For circRNA detection, the primers were designed to amplify the head-to-tail junction. To quantify the parent mRNA, the primers were designed to amplify the exon-exon junction upstream or downstream of the back-splicing exons. The following primers were used:

Table 6. List of circRNA and mRNA quantitative RT-PCR primers.

circRNA	**Primers**
cHomer1	AACACCCGATGTGACACAGA
	GCTCGAGTGCTGAAGATAGGTT
cKlhl2	TGGACCCTGAGGATGCTAAT
	TCTGATGACCCTGCTTTGTG
cGigyf2	AAAGATGTAGGCTCCGTGCT
	TCGGCCATATCGATAATCTGCT
cHook3	ACAAGAGACAGACTAGAAGCAG
	CATCGTTCTGTTGCCGAAGC
mRNA	**Primers**
pre-ActB (1)	GCCAGTGCTGAGAACGTTGTT
	CGCCCACGTAGGAGTCCTT
pre-ActB (2)	TGTGGCTTTAGGAGCTTGAC
	CTGGGGTGTTGAAGGTCTC
ActB	GGGTATGGGTCAGAAGGACT
	GGGTACTTCAGGGTCAGGAT
pre-Atp5i	CCGGTACTCCGCTCTGAT
	CCTCCCAATCCCCAAACT
Atp5i	GGCAGAGGAGGAGAGAAGAA
	TCTCTCAATCCGTTTCAACTCA
Homer1	GAGCTGGAAGAGACCCTAAAAG

	TCAAAGAGTCCCTCTGTTCTTG
Klhl2	TGTGAAGAAGACATGCTGTGAA
	TTTATTCAGGAGGTCTGTGCAT
Gigyf2	TTGCTGAAAACCTCTTGCTGTG
	TGCTGCCATTCTTCTCCGTA
Hook3	GACATTTGCAACTTCAGACCCA
	GCCATCCTGGCACCCTCTAT

Effect of global miR-181a depletion on Camk2a mRNA expression

Neurons cultured in 6 cm dishes, were transfected with Cy5-labelled anti-miR-181a oligonucleotides as described below. Neurons were scraped using Trizol (Invitrogen) and RNA was extracted following the manufacturer's protocol 48 h post-transfection. RNA clean up including the on-column DNase I digest was performed using the RNeasy Mini kit (QIAGEN). Reverse transcription was performed using the QuantiTect Reverse Transcription kit (QIAGEN). For Camk2a and housekeeping genes (18S rRNA and ActB) detection, the primers were designed to amplify an exon-exon junction. The following primers were used:

Table 8. List of quantitative real-time PCR primers.

mRNA	**Primers**
ActB	GGGTATGGGTCAGAAGGACT
	GGGTACTTCAGGGTCAGGAT
18S rRNA	CCGGTACTCCGCTCTGAT
	CCTCCCAATCCCCAAACT
Camk2a	Quantitect predesigned primers

AntimiR synthesis and fluorescence measurements

RNA probe synthesis and experiments described in this section were performed by Thomas Goldau and described in detail in his dissertation.

Table 9. Sequence details of antimiR probes.

AntimiR variant	Sequence 5' – 3'
Long hairpin probe	**L**G CGU **X**AA CAU **X**CA ACG C**X**G UCG GUG AGU **Q Q X F** ACU CAC CGA CAG CGU UGA AUG UU**F X**CG C**L**
Short hairpin probe	**L**AA CAU **X**CA ACG C**X**G UCG GUG AGU **Q Q X F** ACU CAC CGA CAG CGU UGA AUG UU**F L**
Molecular beacon probe	**F**CC GAC U*C*A *C*CG *AC*A G*C*G ***U****U*G *AA**U*** GUU CGG **Q Q**
Non-caged anti-miR-181a oligo	**F**A CUC ACC GAC AGC GUU GAA UGU U**L**

Legend: **L** = C3-spacer, **X** = photo-labile cleavable linker, **Q** = BBQ-650, **F** = Cy5.5, **F** = 6-FAM, **F** = Cy5, *CA* = nucleotide with photo-labile protective group, ***U*** = nucleotide with 6-FAM

Oligonucleotide synthesis

The synthesis of oligonucleotides was performed on an ABI 392 RNA/DNA Synthesizer (Applied Bipsystems) using polystyrol- or CPG columns (Applied Biosystems, Linktech, Glen Research). Phosphoramidite was used at a concentration of 0.11 M and as activator a 0.3 M BTT (5-Benzylthio-1*H*-tetrazole) solution in acetonitrile was used. To remove the triyl-protective groups TCA debloc (Proligo) was used. Free '5 OH groups were protected using capping reagents (Linktech) and for the oxidation reaction solutions of 3% iodine, 2% water and 20% pyridine in THF was used. If necessary, cyanoethyl protective groups were selectively removed after the synthesis by washing with 20% diethylamine solution (EMP Biotech) and acetonitrile, followed by drying step at high vacuum for 15 min. To remove any residual solvent concentrator 5301 (Eppendorf) was used.

Solid-phase synthesis of light-activatable antimiR probes

The synthesis was performed using an ABI392 Synthesizer (Applied Biosystems) in DMTr-ON mode and UltraMild conditions. Coupling times of 2'OMe-phosphoramidites (Linktech) was 6 min. To remove solid-phase material as well as protective groups, samples were incubated with aq. 32% NH_3 for 2 h at room temperature. To remove residual volatiles a vacuum concentrator (Eppendorf) was used. Sample clean-up was done using RP-HPLC and HFIP buffer (400 mM

HFIP, 16.3 mM TEA, pH 8) and MeOH on Xbridge BEH 300 columns (Waters) at 60°C. DMTr protective groups were removed by incubation with 80% acetic acid for 20 min at room temperature. After an additional round of volatile removal, oligo strands were purified using RP-HPLC. Mass spectrometric analysis of the oligo samples were preformed using micrOTOF-Q (Bruker). Oligos that were used for transfection into primary neurons, were pelleted using 3 M, 0.1 v/w $C_2H_3NaO_2$ (pH 5.6) and EtOH at -20°C for 16 h. This process was repeated 3-times.

Fluorescence measurements of antimiR probes under buffer conditions

To determine effect of photo-activation on antimiR probes, the molecular beacon or hairpin probes (1 μM probe in PBS) were photo-activated in a cuvette using 365nm UV-light at room temperature in presence (0.1 – 2.0 μM) or absence of miR-181a oligos. Changes in fluorescence intensity was determined using Platereader (Tecan).

AntimiR imaging experiments

Transfection of antimiR probes

Cultured neurons (DIV 3-4 weeks) were transfected with non-caged anti-miR-181a oligonucleotides (20 pmol) using either Lipofectamine 2000, RNAiMAX or Messenger Max (Thermofisher) according to manufacturer's protocol. To compare the transfection efficiency between the transfection reagents, neurons were fixed 4 h post-transfection using 4% paraformaldehyde/PBS for 20 min, stained with an anti-MAP2 antibody (Millipore AB5622, 1:1000 dilution) and imaged. For all subsequent experiments, molecular beacon or hairpin probes (20 pmol) were transfected using Lipofectamine Messenger Max (Thermofisher). Live-cell imaging was performed after transfection.

Co-localization of antimiR clusters with organelle markers

Neurons were fixed for 25 min in 4% paraformaldehyde/PBS 12 h after the transfection and stained with anti-EEA1 (Abcam ab2900, 1: 1000 dilution), anti-LAMP1 (Sigma L1418, 1:200 dilution) or anti-PABP antibody (Abcam ab21060, 1:500 dilution). After staining soma and dendrites with an anti-MAP2 antibody (Millipore AB5622, 1:1000 dilution) and cells were imaged.

Determine photo-activation settings

Cultured hippocampal neurons were transfected with antimiR variants as described above. Between 2 h – 12 h post-transfection, neurons were imaged in E4 Buffer supplemented with essential amino acids (Gibco). Live-cell imaging was performed in airy scan modus using a Zeiss LSM880 confocal laser fluorescence microscope system. The incubator was set to 37°C and a 40x water immersion objective were used. The entire soma or a dendritic stretch of 105 μm x 10 μm were selected. Photoactivation was performed using a multi-photon laser set-up at 355 nm with either 1.48, 2.18 or 3.58 mW laser power. Images were acquired every 5 sec for 250 sec or 300 sec from a single plane. Following the acquisition of the pre-photo-activation fluorescence images (“baseline”) for the first 10 frames (50 sec), a single photo-activation pulse was given at the 11st frame and then the imaging continued. Alternatively, consecutive photo-activation pulses were given starting from the 11st frame and repeated every 5 frames (8 pluses in total).

Quantification of Cy5.5 and 6-FAM intensity changes

To determine the changes in hybridization and tracking fluorophore intensity after photo-activation the following analysis pipeline was performed in ImageJ: After background subtraction, Cy5.5 and 6-FAM intensity of soma or dendritic stretch was determined for each frame. Fluorescence intensities were normalized to the average Cy5.5 or 6-FAM intensity of the first 10 pre-photo-activation frames and plotted.

Local photo-activation of short hairpin probe in distal dendrites

To investigate the effect of miR-181a inactivation on local Camk2a protein synthesis, neurons were transfected with the short hairpin probe (20 pmol) as described above. A distal dendritic stretch of 105 μm x 10 μm was photo-activated using a multi-photon laser set-up at 355 nm with 1.48 mW laser power. Images were acquired every 5 sec for a total of 250 sec. Photo-activation was performed starting with the 11th frame and repeated every 5 frames for a total of 8-times. Per culture dish 3 – 4 dendritic stretches were imaged consecutively in this manner.

Labelling of newly synthesized protein

Newly synthesized protein was visualized using the Puro-PLA protocol (tom Dieck et al., 2015). After the photo-activation of the last dendritic stretch, 1 μM puromycin (Sigma) was bath applied to the neuronal culture medium for 10 min. Neurons were washed and fixed for 25 min in 4% paraformaldehyde/PBS. Neurons were incubated with anti-puromycin antibody (Kerafast Equation 0001, 1:2500) and anti-Camk2a antibody (Millipore 04-1079, 1:1000) or anti-ActB protein (Abcam ab8227, 1:300 dilution) to visualize newly synthesized Camk2a or ActB protein, respectively. After staining soma and dendrites with an anti-MAP2 antibody (Millipore AB5622, 1:1000 dilution), the photo-activated dendritic stretches were re-imaged. In another set of experiments, neurons were incubated for 48 h using non-caged anti-miR-181a oligos and 1 μM puromycin was added to the medium in the last 10min to label for newly synthesized protein.

Puro-PLA image acquisition

Confocal microscopy was performed using a Zeiss LSM880 confocal laser fluorescence microscope system. Maximum intensity projections of image series of 20-32 confocal planes taken at 0.38 μm intervals using a 40x water immersion objective. Pixel size was matched to the pixel size of the live-cell images.

Quantification of Puro-PLA signal around hybridization spots

Customized ImageJ macro was applied to obtain a binary image of the hybridization spots. In brief, an average intensity projection of the Cy5.5 channel was obtained for frames before photo-activation ("baseline") and photo-activation frames ("photo-activation"). After background removal, the "baseline" image was subtracted from the "photo-activation" image. A common threshold was chosen and a binary image containing the Cy5.5 spots was generated. To count the number of newly synthesized protein puncta within a defined radius around each hybridization spot, a customized MATLAB script was used. First, all Cy5.5 spots that overlapped with 6-FAM spots were identified. The same number of 6-FAM spots that did not overlap with Cy5.5 spots were randomly selected and used as control spots. Within a user defined radius (μm) around each hybridization and control spot, the number of newly synthesized protein puncta were counted.

LITERATURE CITED

Abdelmohsen, K., Panda, A. C., Munk, R., Grammatikakis, I., Dudekula, D. B., De, S., . . . Gorospe, M. (2017). Identification of HuR target circular RNAs uncovers suppression of PABPN1 translation by CircPABPN1. *RNA Biol, 14*(3), 361-369. doi:10.1080/15476286.2017.1279788

Agranoff, B. W., Davis, R. E., & Brink, J. J. (1965). Memory fixation in the goldfish. *Proc Natl Acad Sci U S A, 54*(3), 788-793. doi:10.1073/pnas.54.3.788

Agranoff, B. W., Davis, R. E., Casola, L., & Lim, R. (1967). Actinomycin D blocks formation of memory of shock-avoidance in goldfish. *Science, 158*(3808), 1600-1601. doi:10.1126/science.158.3808.1600

Agranoff, B. W., & Klinger, P. D. (1964). PUROMYCIN EFFECT ON MEMORY FIXATION IN THE GOLDFISH. *Science, 146*(3646), 952-953. doi:10.1126/science.146.3646.952

Ai, J., Sun, L. H., Che, H., Zhang, R., Zhang, T. Z., Wu, W. C., . . . Yang, B. F. (2013). MicroRNA-195 protects against dementia induced by chronic brain hypoperfusion via its anti-amyloidogenic effect in rats. *J Neurosci, 33*(9), 3989-4001. doi:10.1523/jneurosci.1997-12.2013

Aksoy-Aksel, A., Zampa, F., & Schratt, G. (2014). MicroRNAs and synaptic plasticity--a mutual relationship. *Philos Trans R Soc Lond B Biol Sci, 369*(1652). doi:10.1098/rstb.2013.0515

Aktaş, T., Avşar Ilık, İ., Maticzka, D., Bhardwaj, V., Pessoa Rodrigues, C., Mittler, G., . . . Akhtar, A. (2017). DHX9 suppresses RNA processing defects originating from the Alu invasion of the human genome. *Nature, 544*(7648), 115-119. doi:10.1038/nature21715

Altschul, S. F., Gish, W., Miller, W., Myers, E. W., & Lipman, D. J. (1990). Basic local alignment search tool. *J Mol Biol, 215*(3), 403-410. doi:10.1016/s0022-2836(05)80360-2

Ameres, S. L., & Zamore, P. D. (2013). Diversifying microRNA sequence and function. *Nat Rev Mol Cell Biol, 14*(8), 475-488. doi:10.1038/nrm3611

Anderson, P., & Kedersha, N. (2006). RNA granules. *J Cell Biol, 172*(6), 803-808. doi:10.1083/jcb.200512082

Anderson, P., & Kedersha, N. (2008). Stress granules: the Tao of RNA triage. *Trends Biochem Sci, 33*(3), 141-150. doi:10.1016/j.tibs.2007.12.003

Ashraf, S. I., McLoon, A. L., Sclarsic, S. M., & Kunes, S. (2006). Synaptic protein synthesis associated with memory is regulated by the RISC pathway in Drosophila. *Cell, 124*(1), 191-205. doi:10.1016/j.cell.2005.12.017

Ashwal-Fluss, R., Meyer, M., Pamudurti, N. R., Ivanov, A., Bartok, O., Hanan, M., . . . Kadener, S. (2014). circRNA biogenesis competes with pre-mRNA splicing. *Mol Cell, 56*(1), 55-66. doi:10.1016/j.molcel.2014.08.019

Bachmayr-Heyda, A., Reiner, A. T., Auer, K., Sukhbaatar, N., Aust, S., Bachleitner-Hofmann, T., . . . Pils, D. (2015). Correlation of circular RNA abundance with proliferation--exemplified with colorectal and ovarian cancer, idiopathic lung fibrosis, and normal human tissues. *Sci Rep, 5*, 8057. doi:10.1038/srep08057

Bading, H. (2000). Transcription-dependent neuronal plasticity: The nuclear calcium hypothesis. *Eur J Biochem, 267*(17), 5280-5283. doi:10.1046/j.1432-1327.2000.01565.x

Bai, Y., Zhang, Y., Han, B., Yang, L., Chen, X., Huang, R., . . . Yao, H. (2018). Circular RNA DLGAP4 Ameliorates Ischemic Stroke Outcomes by Targeting miR-143 to Regulate Endothelial-Mesenchymal Transition Associated with Blood-Brain Barrier Integrity. *J Neurosci, 38*(1), 32-50. doi:10.1523/jneurosci.1348-17.2017

Ban, N., Nissen, P., Hansen, J., Moore, P. B., & Steitz, T. A. (2000). The complete atomic structure of the large ribosomal subunit at 2.4 A resolution. *Science, 289*(5481), 905-920. doi:10.1126/science.289.5481.905

Banko, J. L., Hou, L., Poulin, F., Sonenberg, N., & Klann, E. (2006). Regulation of eukaryotic initiation factor 4E by converging signaling pathways during metabotropic glutamate receptor-dependent long-term depression. *J Neurosci, 26*(8), 2167-2173. doi:10.1523/jneurosci.5196-05.2006

Barondes, S. H., & Cohen, H. D. (1966). Puromycin effect on successive phases of memory storage. *Science, 151*(3710), 594-595. doi:10.1126/science.151.3710.594

Barria, A., Muller, D., Derkach, V., Griffith, L. C., & Soderling, T. R. (1997). Regulatory phosphorylation of AMPA-type glutamate receptors by CaM-KII during long-term potentiation. *Science, 276*(5321), 2042-2045. doi:10.1126/science.276.5321.2042

Bartel, D. P. (2009). MicroRNAs: target recognition and regulatory functions. *Cell, 136*(2), 215-233. doi:10.1016/j.cell.2009.01.002

Bassell, G. J., Zhang, H., Byrd, A. L., Femino, A. M., Singer, R. H., Taneja, K. L., . . . Kosik, K. S. (1998). Sorting of beta-actin mRNA and protein to neurites and growth cones in culture. *J Neurosci, 18*(1), 251-265. doi:10.1523/jneurosci.18-01-00251.1998

Bennett, M. V. (2000). Electrical synapses, a personal perspective (or history). *Brain Res Brain Res Rev, 32*(1), 16-28. doi:10.1016/s0165-0173(99)00065-x

Berget, S. M., Moore, C., & Sharp, P. A. (1977). Spliced segments at the 5' terminus of adenovirus 2 late mRNA. *Proc Natl Acad Sci U S A, 74*(8), 3171-3175. doi:10.1073/pnas.74.8.3171

Bernard, D., Prasanth, K. V., Tripathi, V., Colasse, S., Nakamura, T., Xuan, Z., . . . Bessis, A. (2010). A long nuclear-retained non-coding RNA regulates synaptogenesis by modulating gene expression. *Embo j, 29*(18), 3082-3093. doi:10.1038/emboj.2010.199

Besse, F., & Ephrussi, A. (2008). Translational control of localized mRNAs: restricting protein synthesis in space and time. *Nat Rev Mol Cell Biol, 9*(12), 971-980. doi:10.1038/nrm2548

Bessonov, S., Anokhina, M., Will, C. L., Urlaub, H., & Lührmann, R. (2008). Isolation of an active step I spliceosome and composition of its RNP core. *Nature, 452*(7189), 846-850. doi:10.1038/nature06842

Béthune, J., Artus-Revel, C. G., & Filipowicz, W. (2012). Kinetic analysis reveals successive steps leading to miRNA-mediated silencing in mammalian cells. *EMBO Rep, 13*(8), 716-723. doi:10.1038/embor.2012.82

Bi, G., & Poo, M. (2001). Synaptic modification by correlated activity: Hebb's postulate revisited. *Annu Rev Neurosci, 24*, 139-166. doi:10.1146/annurev.neuro.24.1.139

Biever, A., Glock, C., Tushev, G., Ciirdaeva, E., Dalmay, T., Langer, J. D., & Schuman, E. M. (2020). Monosomes actively translate synaptic mRNAs in neuronal processes. *Science, 367*(6477). doi:10.1126/science.aay4991

Bingol, B., & Sheng, M. (2011). Deconstruction for reconstruction: the role of proteolysis in neural plasticity and disease. *Neuron, 69*(1), 22-32. doi:10.1016/j.neuron.2010.11.006

Black, D. L. (2003). Mechanisms of alternative pre-messenger RNA splicing. *Annu Rev Biochem, 72*, 291-336. doi:10.1146/annurev.biochem.72.121801.161720

Bliss, T. (2007). *The hippocampus book*. New York, NY, US: Oxford University Press.

Bliss, T. V., & Collingridge, G. L. (1993). A synaptic model of memory: long-term potentiation in the hippocampus. *Nature, 361*(6407), 31-39. doi:10.1038/361031a0

Bliss, T. V., & Lomo, T. (1973). Long-lasting potentiation of synaptic transmission in the dentate area of the anaesthetized rabbit following stimulation of the perforant path. *J Physiol, 232*(2), 331-356. doi:10.1113/jphysiol.1973.sp010273

Blow, M., Futreal, P. A., Wooster, R., & Stratton, M. R. (2004). A survey of RNA editing in human brain. *Genome Res, 14*(12), 2379-2387. doi:10.1101/gr.2951204

Böckers, T. M., Segger-Junius, M., Iglauer, P., Bockmann, J., Gundelfinger, E. D., Kreutz, M. R., . . . Kreienkamp, H. J. (2004). Differential expression and dendritic transcript localization of Shank family members: identification of a dendritic targeting element in the 3' untranslated region of Shank1 mRNA. *Mol Cell Neurosci, 26*(1), 182-190. doi:10.1016/j.mcn.2004.01.009

Bolshakov, V. Y., Golan, H., Kandel, E. R., & Siegelbaum, S. A. (1997). Recruitment of new sites of synaptic transmission during the cAMP-dependent late phase of LTP at CA3-CA1 synapses in the hippocampus. *Neuron, 19*(3), 635-651. doi:10.1016/s0896-6273(00)80377-3

Borah, S., Wong, A. C., & Steitz, J. A. (2009). Drosophila hnRNP A1 homologs Hrp36/Hrp38 enhance U2-type versus U12-type splicing to regulate alternative splicing of the prospero twintron. *Proc Natl Acad Sci U S A, 106*(8), 2577-2582. doi:10.1073/pnas.0812826106

Boswell, S. A., Snavely, A., Landry, H. M., Churchman, L. S., Gray, J. M., & Springer, M. (2017). Total RNA-seq to identify pharmacological effects on specific stages of mRNA synthesis. *Nat Chem Biol, 13*(5), 501-507. doi:10.1038/nchembio.2317

Bottai, D., Guzowski, J. F., Schwarz, M. K., Kang, S. H., Xiao, B., Lanahan, A., . . . Seeburg, P. H. (2002). Synaptic activity-induced conversion of intronic to exonic sequence in Homer 1 immediate early gene expression. *J Neurosci, 22*(1), 167-175. doi:10.1523/jneurosci.22-01-00167.2002

Boucard, A. A., Chubykin, A. A., Comoletti, D., Taylor, P., & Südhof, T. C. (2005). A splice code for trans-synaptic cell adhesion mediated by binding of neuroligin 1 to alpha- and beta-neurexins. *Neuron, 48*(2), 229-236. doi:10.1016/j.neuron.2005.08.026

Bradshaw, K. D., Emptage, N. J., & Bliss, T. V. (2003). A role for dendritic protein synthesis in hippocampal late LTP. *Eur J Neurosci, 18*(11), 3150-3152. doi:10.1111/j.1460-9568.2003.03054.x

Brennecke, J., Stark, A., Russell, R. B., & Cohen, S. M. (2005). Principles of microRNA-target recognition. *PLoS Biol, 3*(3), e85. doi:10.1371/journal.pbio.0030085

Brieke, C., Rohrbach, F., Gottschalk, A., Mayer, G., & Heckel, A. (2012). Light-controlled tools. *Angew Chem Int Ed Engl, 51*(34), 8446-8476. doi:10.1002/anie.201202134

Bruns, D., & Jahn, R. (1995). Real-time measurement of transmitter release from single synaptic vesicles. *Nature, 377*(6544), 62-65. doi:10.1038/377062a0

Buchan, J. R., & Parker, R. (2009). Eukaryotic stress granules: the ins and outs of translation. *Mol Cell, 36*(6), 932-941. doi:10.1016/j.molcel.2009.11.020

Bullock, S. L., Nicol, A., Gross, S. P., & Zicha, D. (2006). Guidance of bidirectional motor complexes by mRNA cargoes through control of dynein number and activity. *Curr Biol, 16*(14), 1447-1452. doi:10.1016/j.cub.2006.05.055

Burd, C. E., Jeck, W. R., Liu, Y., Sanoff, H. K., Wang, Z., & Sharpless, N. E. (2010). Expression of linear and novel circular forms of an INK4/ARF-associated non-coding RNA correlates with atherosclerosis risk. *PLoS Genet, 6*(12), e1001233. doi:10.1371/journal.pgen.1001233

Burgin, K. E., Waxham, M. N., Rickling, S., Westgate, S. A., Mobley, W. C., & Kelly, P. T. (1990). In situ hybridization histochemistry of Ca2+/calmodulin-dependent protein kinase in developing rat brain. *J Neurosci, 10*(6), 1788-1798. doi:10.1523/jneurosci.10-06-01788.1990

Busch, H., Reddy, R., Rothblum, L., & Choi, Y. C. (1982). SnRNAs, SnRNPs, and RNA processing. *Annu Rev Biochem, 51*, 617-654. doi:10.1146/annurev.bi.51.070182.003153

Cajigas, I. J., Tushev, G., Will, T. J., tom Dieck, S., Fuerst, N., & Schuman, E. M. (2012). The local transcriptome in the synaptic neuropil revealed by deep sequencing and high-resolution imaging. *Neuron, 74*(3), 453-466. doi:10.1016/j.neuron.2012.02.036

Campbell, D. S., & Holt, C. E. (2001). Chemotropic responses of retinal growth cones mediated by rapid local protein synthesis and degradation. *Neuron, 32*(6), 1013-1026. doi:10.1016/s0896-6273(01)00551-7

Carninci, P., Kasukawa, T., Katayama, S., Gough, J., Frith, M. C., Maeda, N., . . . Hayashizaki, Y. (2005). The transcriptional landscape of the mammalian genome. *Science, 309*(5740), 1559-1563. doi:10.1126/science.1112014

Cech, T. R., & Steitz, J. A. (2014). The noncoding RNA revolution-trashing old rules to forge new ones. *Cell, 157*(1), 77-94. doi:10.1016/j.cell.2014.03.008

Cesca, F., Baldelli, P., Valtorta, F., & Benfenati, F. (2010). The synapsins: key actors of synapse function and plasticity. *Prog Neurobiol, 91*(4), 313-348. doi:10.1016/j.pneurobio.2010.04.006

Chen, M., & Manley, J. L. (2009). Mechanisms of alternative splicing regulation: insights from molecular and genomics approaches. *Nat Rev Mol Cell Biol, 10*(11), 741-754. doi:10.1038/nrm2777

Chen, W., & Schuman, E. (2016). Circular RNAs in Brain and Other Tissues: A Functional Enigma. *Trends Neurosci, 39*(9), 597-604. doi:10.1016/j.tins.2016.06.006

Chi, S. W., Zang, J. B., Mele, A., & Darnell, R. B. (2009). Argonaute HITS-CLIP decodes microRNA-mRNA interaction maps. *Nature, 460*(7254), 479-486. doi:10.1038/nature08170

Chih, B., Gollan, L., & Scheiffele, P. (2006). Alternative splicing controls selective trans-synaptic interactions of the neuroligin-neurexin complex. *Neuron, 51*(2), 171-178. doi:10.1016/j.neuron.2006.06.005

Chou, M. Y., Rooke, N., Turck, C. W., & Black, D. L. (1999). hnRNP H is a component of a splicing enhancer complex that activates a c-src alternative exon in neuronal cells. *Mol Cell Biol, 19*(1), 69-77. doi:10.1128/mcb.19.1.69

Clark, B. D., Goldberg, E. M., & Rudy, B. (2009). Electrogenic tuning of the axon initial segment. *Neuroscientist, 15*(6), 651-668. doi:10.1177/1073858409341973

Clemson, C. M., Hutchinson, J. N., Sara, S. A., Ensminger, A. W., Fox, A. H., Chess, A., & Lawrence, J. B. (2009). An architectural role for a nuclear noncoding RNA: NEAT1 RNA is essential for the structure of paraspeckles. *Mol Cell, 33*(6), 717-726. doi:10.1016/j.molcel.2009.01.026

Cocquerelle, C., Daubersies, P., Majérus, M. A., Kerckaert, J. P., & Bailleul, B. (1992). Splicing with inverted order of exons occurs proximal to large introns. *Embo j, 11*(3), 1095-1098.

Cocquerelle, C., Mascrez, B., Hétuin, D., & Bailleul, B. (1993). Mis-splicing yields circular RNA molecules. *Faseb j, 7*(1), 155-160. doi:10.1096/fasebj.7.1.7678559

Cohen, H. D., Ervin, F., & Barondes, S. H. (1966). Puromycin and cycloheximide: different effects on hippocampal electrical activity. *Science, 154*(3756), 1557-1558. doi:10.1126/science.154.3756.1557

Colbert, C. M., & Johnston, D. (1996). Axonal action-potential initiation and Na+ channel densities in the soma and axon initial segment of subicular pyramidal neurons. *J Neurosci, 16*(21), 6676-6686. doi:10.1523/jneurosci.16-21-06676.1996

Collingridge, G. L., Isaac, J. T., & Wang, Y. T. (2004). Receptor trafficking and synaptic plasticity. *Nat Rev Neurosci, 5*(12), 952-962. doi:10.1038/nrn1556

Collingridge, G. L., Peineau, S., Howland, J. G., & Wang, Y. T. (2010). Long-term depression in the CNS. *Nat Rev Neurosci, 11*(7), 459-473. doi:10.1038/nrn2867

Condeelis, J., & Singer, R. H. (2005). How and why does beta-actin mRNA target? *Biol Cell, 97*(1), 97-110. doi:10.1042/bc20040063

Conn, S. J., Pillman, K. A., Toubia, J., Conn, V. M., Salmanidis, M., Phillips, C. A., . . . Goodall, G. J. (2015). The RNA binding protein quaking regulates formation of circRNAs. *Cell, 160*(6), 1125-1134. doi:10.1016/j.cell.2015.02.014

Costa-Mattioli, M., Sossin, W. S., Klann, E., & Sonenberg, N. (2009). Translational control of long-lasting synaptic plasticity and memory. *Neuron, 61*(1), 10-26. doi:10.1016/j.neuron.2008.10.055

Coultrap, S. J., & Bayer, K. U. (2012). CaMKII regulation in information processing and storage. *Trends Neurosci, 35*(10), 607-618. doi:10.1016/j.tins.2012.05.003

Cracco, J. B., Serrano, P., Moskowitz, S. I., Bergold, P. J., & Sacktor, T. C. (2005). Protein synthesis-dependent LTP in isolated dendrites of CA1 pyramidal cells. *Hippocampus, 15*(5), 551-556. doi:10.1002/hipo.20078

Craig, A. M., & Kang, Y. (2007). Neurexin-neuroligin signaling in synapse development. *Curr Opin Neurobiol, 17*(1), 43-52. doi:10.1016/j.conb.2007.01.011

Curti, S., Hoge, G., Nagy, J. I., & Pereda, A. E. (2012). Synergy between electrical coupling and membrane properties promotes strong synchronization of neurons of the mesencephalic trigeminal nucleus. *J Neurosci, 32*(13), 4341-4359. doi:10.1523/jneurosci.6216-11.2012

Czaplinski, K., & Singer, R. H. (2006). Pathways for mRNA localization in the cytoplasm. *Trends Biochem Sci, 31*(12), 687-693. doi:10.1016/j.tibs.2006.10.007

Darmanis, S., Sloan, S. A., Zhang, Y., Enge, M., Caneda, C., Shuer, L. M., . . . Quake, S. R. (2015). A survey of human brain transcriptome diversity at the single cell level. *Proc Natl Acad Sci U S A, 112*(23), 7285-7290. doi:10.1073/pnas.1507125112

Darnell, R. B. (2013). RNA protein interaction in neurons. *Annu Rev Neurosci, 36*, 243-270. doi:10.1146/annurev-neuro-062912-114322

Davis, H. P., & Squire, L. R. (1984). Protein synthesis and memory: a review. *Psychol Bull, 96*(3), 518-559.

Davis, S., Lollo, B., Freier, S., & Esau, C. (2006). Improved targeting of miRNA with antisense oligonucleotides. *Nucleic Acids Res, 34*(8), 2294-2304. doi:10.1093/nar/gkl183

de la Grange, P., Gratadou, L., Delord, M., Dutertre, M., & Auboeuf, D. (2010). Splicing factor and exon profiling across human tissues. *Nucleic Acids Res, 38*(9), 2825-2838. doi:10.1093/nar/gkq008

Deng, W., Aimone, J. B., & Gage, F. H. (2010). New neurons and new memories: how does adult hippocampal neurogenesis affect learning and memory? *Nat Rev Neurosci, 11*(5), 339-350. doi:10.1038/nrn2822

Derrien, T., Johnson, R., Bussotti, G., Tanzer, A., Djebali, S., Tilgner, H., . . . Guigó, R. (2012). The GENCODE v7 catalog of human long noncoding RNAs: analysis of their gene structure, evolution, and expression. *Genome Res, 22*(9), 1775-1789. doi:10.1101/gr.132159.111

Djebali, S., Davis, C. A., Merkel, A., Dobin, A., Lassmann, T., Mortazavi, A., . . . Gingeras, T. R. (2012). Landscape of transcription in human cells. *Nature, 489*(7414), 101-108. doi:10.1038/nature11233

Djuranovic, S., Nahvi, A., & Green, R. (2012). miRNA-mediated gene silencing by translational repression followed by mRNA deadenylation and decay. *Science, 336*(6078), 237-240. doi:10.1126/science.1215691

Dobin, A., Davis, C. A., Schlesinger, F., Drenkow, J., Zaleski, C., Jha, S., . . . Gingeras, T. R. (2013). STAR: ultrafast universal RNA-seq aligner. *Bioinformatics, 29*(1), 15-21. doi:10.1093/bioinformatics/bts635

Du, W. W., Yang, W., Liu, E., Yang, Z., Dhaliwal, P., & Yang, B. B. (2016). Foxo3 circular RNA retards cell cycle progression via forming ternary complexes with p21 and CDK2. *Nucleic Acids Res, 44*(6), 2846-2858. doi:10.1093/nar/gkw027

Dudek, S. M., & Bear, M. F. (1992). Homosynaptic long-term depression in area CA1 of hippocampus and effects of N-methyl-D-aspartate receptor blockade. *Proc Natl Acad Sci U S A, 89*(10), 4363-4367. doi:10.1073/pnas.89.10.4363

Ellison-Wright, I., & Bullmore, E. (2009). Meta-analysis of diffusion tensor imaging studies in schizophrenia. *Schizophr Res, 108*(1-3), 3-10. doi:10.1016/j.schres.2008.11.021

Engert, F., & Bonhoeffer, T. (1999). Dendritic spine changes associated with hippocampal long-term synaptic plasticity. *Nature, 399*(6731), 66-70. doi:10.1038/19978

Errichelli, L., Dini Modigliani, S., Laneve, P., Colantoni, A., Legnini, I., Capauto, D., . . . Bozzoni, I. (2017). FUS affects circular RNA expression in murine embryonic stem cell-derived motor neurons. *Nat Commun, 8*, 14741. doi:10.1038/ncomms14741

Eulalio, A., Huntzinger, E., & Izaurralde, E. (2008). Getting to the root of miRNA-mediated gene silencing. *Cell, 132*(1), 9-14. doi:10.1016/j.cell.2007.12.024

Fabian, M. R., Sonenberg, N., & Filipowicz, W. (2010). Regulation of mRNA translation and stability by microRNAs. *Annu Rev Biochem, 79*, 351-379. doi:10.1146/annurev-biochem-060308-103103

Faustino, N. A., & Cooper, T. A. (2003). Pre-mRNA splicing and human disease. *Genes Dev, 17*(4), 419-437. doi:10.1101/gad.1048803

Feig, S., & Lipton, P. (1993). Pairing the cholinergic agonist carbachol with patterned Schaffer collateral stimulation initiates protein synthesis in hippocampal CA1 pyramidal cell dendrites via a muscarinic, NMDA-dependent mechanism. *J Neurosci, 13*(3), 1010-1021. doi:10.1523/jneurosci.13-03-01010.1993

Filipowicz, W., Bhattacharyya, S. N., & Sonenberg, N. (2008). Mechanisms of post-transcriptional regulation by microRNAs: are the answers in sight? *Nat Rev Genet, 9*(2), 102-114. doi:10.1038/nrg2290

Fineberg, S. K., Kosik, K. S., & Davidson, B. L. (2009). MicroRNAs potentiate neural development. *Neuron, 64*(3), 303-309. doi:10.1016/j.neuron.2009.10.020

Fiore, R., Khudayberdiev, S., Christensen, M., Siegel, G., Flavell, S. W., Kim, T. K., . . . Schratt, G. (2009). Mef2-mediated transcription of the miR379-410 cluster regulates activity-dependent dendritogenesis by fine-tuning Pumilio2 protein levels. *Embo j, 28*(6), 697-710. doi:10.1038/emboj.2009.10

Fire, A., Xu, S., Montgomery, M. K., Kostas, S. A., Driver, S. E., & Mello, C. C. (1998). Potent and specific genetic interference by double-stranded RNA in Caenorhabditis elegans. *Nature, 391*(6669), 806-811. doi:10.1038/35888

Flavell, S. W., & Greenberg, M. E. (2008). Signaling mechanisms linking neuronal activity to gene expression and plasticity of the nervous system. *Annu Rev Neurosci, 31*, 563-590. doi:10.1146/annurev.neuro.31.060407.125631

Flexner, J. B., Flexner, L. B., & Stellar, E. (1963). Memory in mice as affected by intracerebral puromycin. *Science, 141*(3575), 57-59. doi:10.1126/science.141.3575.57

Fornerod, M., Ohno, M., Yoshida, M., & Mattaj, I. W. (1997). CRM1 is an export receptor for leucine-rich nuclear export signals. *Cell, 90*(6), 1051-1060. doi:10.1016/s0092-8674(00)80371-2

Frey, U., Krug, M., Reymann, K. G., & Matthies, H. (1988). Anisomycin, an inhibitor of protein synthesis, blocks late phases of LTP phenomena in the hippocampal CA1 region in vitro. *Brain Res, 452*(1-2), 57-65. doi:10.1016/0006-8993(88)90008-x

Frith, M. C., Pheasant, M., & Mattick, J. S. (2005). The amazing complexity of the human transcriptome. *Eur J Hum Genet, 13*(8), 894-897. doi:10.1038/sj.ejhg.5201459

Fu, X. D., & Ares, M., Jr. (2014). Context-dependent control of alternative splicing by RNA-binding proteins. *Nat Rev Genet, 15*(10), 689-701. doi:10.1038/nrg3778

Furlanis, E., Traunmüller, L., Fucile, G., & Scheiffele, P. (2019). Landscape of ribosome-engaged transcript isoforms reveals extensive neuronal-cell-class-specific alternative splicing programs. *Nat Neurosci, 22*(10), 1709-1717. doi:10.1038/s41593-019-0465-5

Fuzik, J., Zeisel, A., Máté, Z., Calvigioni, D., Yanagawa, Y., Szabó, G., . . . Harkany, T. (2016). Integration of electrophysiological recordings with single-cell RNA-seq data identifies neuronal subtypes. *Nat Biotechnol, 34*(2), 175-183. doi:10.1038/nbt.3443

Galarreta, M., & Hestrin, S. (2001). Spike transmission and synchrony detection in networks of GABAergic interneurons. *Science, 292*(5525), 2295-2299. doi:10.1126/science.1061395

Gao, J., Wang, W. Y., Mao, Y. W., Gräff, J., Guan, J. S., Pan, L., . . . Tsai, L. H. (2010). A novel pathway regulates memory and plasticity via SIRT1 and miR-134. *Nature, 466*(7310), 1105-1109. doi:10.1038/nature09271

Garner, C. C., Tucker, R. P., & Matus, A. (1988). Selective localization of messenger RNA for cytoskeletal protein MAP2 in dendrites. *Nature, 336*(6200), 674-677. doi:10.1038/336674a0

Geisler, S., & Coller, J. (2013). RNA in unexpected places: long non-coding RNA functions in diverse cellular contexts. *Nat Rev Mol Cell Biol, 14*(11), 699-712. doi:10.1038/nrm3679

Getting, P. A. (1974). Modification of neuron properties by electrotonic synapses. I. Input resistance, time constant, and integration. *J Neurophysiol, 37*(5), 846-857. doi:10.1152/jn.1974.37.5.846

Ghosal, S., Das, S., Sen, R., Basak, P., & Chakrabarti, J. (2013). Circ2Traits: a comprehensive database for circular RNA potentially associated with disease and traits. *Front Genet, 4*, 283. doi:10.3389/fgene.2013.00283

Gong, C., & Maquat, L. E. (2011). lncRNAs transactivate STAU1-mediated mRNA decay by duplexing with 3' UTRs via Alu elements. *Nature, 470*(7333), 284-288. doi:10.1038/nature09701

Graber, T. E., Hébert-Seropian, S., Khoutorsky, A., David, A., Yewdell, J. W., Lacaille, J. C., & Sossin, W. S. (2013). Reactivation of stalled polyribosomes in synaptic plasticity. *Proc Natl Acad Sci U S A, 110*(40), 16205-16210. doi:10.1073/pnas.1307747110

Graf, E. R., Kang, Y., Hauner, A. M., & Craig, A. M. (2006). Structure function and splice site analysis of the synaptogenic activity of the neurexin-1 beta LNS domain. *J Neurosci, 26*(16), 4256-4265. doi:10.1523/jneurosci.1253-05.2006

Granger, A. J., Shi, Y., Lu, W., Cerpas, M., & Nicoll, R. A. (2013). LTP requires a reserve pool of glutamate receptors independent of subunit type. *Nature, 493*(7433), 495-500. doi:10.1038/nature11775

Griepenburg, J. C., Ruble, B. K., & Dmochowski, I. J. (2013). Caged oligonucleotides for bidirectional photomodulation of let-7 miRNA in zebrafish embryos. *Bioorg Med Chem, 21*(20), 6198-6204. doi:10.1016/j.bmc.2013.04.082

Grosso, A. R., Gomes, A. Q., Barbosa-Morais, N. L., Caldeira, S., Thorne, N. P., Grech, G., . . . Carmo-Fonseca, M. (2008). Tissue-specific splicing factor gene expression signatures. *Nucleic Acids Res, 36*(15), 4823-4832. doi:10.1093/nar/gkn463

Gruner, H., Cortés-López, M., Cooper, D. A., Bauer, M., & Miura, P. (2016). CircRNA accumulation in the aging mouse brain. *Sci Rep, 6*, 38907. doi:10.1038/srep38907

Gumy, L. F., Yeo, G. S., Tung, Y. C., Zivraj, K. H., Willis, D., Coppola, G., . . . Fawcett, J. W. (2011). Transcriptome analysis of embryonic and adult sensory axons reveals changes in mRNA repertoire localization. *Rna, 17*(1), 85-98. doi:10.1261/rna.2386111

Guo, J. U., Agarwal, V., Guo, H., & Bartel, D. P. (2014). Expanded identification and characterization of mammalian circular RNAs. *Genome Biol, 15*(7), 409. doi:10.1186/s13059-014-0409-z

Guttman, M., Amit, I., Garber, M., French, C., Lin, M. F., Feldser, D., . . . Lander, E. S. (2009). Chromatin signature reveals over a thousand highly conserved large non-coding RNAs in mammals. *Nature, 458*(7235), 223-227. doi:10.1038/nature07672

Guttman, M., Donaghey, J., Carey, B. W., Garber, M., Grenier, J. K., Munson, G., . . . Lander, E. S. (2011). lincRNAs act in the circuitry controlling pluripotency and differentiation. *Nature, 477*(7364), 295-300. doi:10.1038/nature10398

Guttman, M., Russell, P., Ingolia, N. T., Weissman, J. S., & Lander, E. S. (2013). Ribosome profiling provides evidence that large noncoding RNAs do not encode proteins. *Cell, 154*(1), 240-251. doi:10.1016/j.cell.2013.06.009

Hafner, A. S., Donlin-Asp, P. G., Leitch, B., Herzog, E., & Schuman, E. M. (2019). Local protein synthesis is a ubiquitous feature of neuronal pre- and postsynaptic compartments. *Science, 364*(6441). doi:10.1126/science.aau3644

Hafting, T., Fyhn, M., Molden, S., Moser, M. B., & Moser, E. I. (2005). Microstructure of a spatial map in the entorhinal cortex. *Nature, 436*(7052), 801-806. doi:10.1038/nature03721

Hamilton, A. J., & Baulcombe, D. C. (1999). A species of small antisense RNA in posttranscriptional gene silencing in plants. *Science, 286*(5441), 950-952. doi:10.1126/science.286.5441.950

Han, B., Zhang, Y., Zhang, Y., Bai, Y., Chen, X., Huang, R., . . . Yao, H. (2018). Novel insight into circular RNA HECTD1 in astrocyte activation via autophagy by targeting MIR142-TIPARP: implications for cerebral ischemic stroke. *Autophagy, 14*(7), 1164-1184. doi:10.1080/15548627.2018.1458173

Hansen, T. B., Jensen, T. I., Clausen, B. H., Bramsen, J. B., Finsen, B., Damgaard, C. K., & Kjems, J. (2013). Natural RNA circles function as efficient microRNA sponges. *Nature, 495*(7441), 384-388. doi:10.1038/nature11993

He, X., Arslan, A. D., Pool, M. D., Ho, T. T., Darcy, K. M., Coon, J. S., & Beck, W. T. (2011). Knockdown of splicing factor SRp20 causes apoptosis in ovarian cancer cells and its expression is associated with malignancy of epithelial ovarian cancer. *Oncogene, 30*(3), 356-365. doi:10.1038/onc.2010.426

Hegele, A., Kamburov, A., Grossmann, A., Sourlis, C., Wowro, S., Weimann, M., . . . Stelzl, U. (2012). Dynamic protein-protein interaction wiring of the human spliceosome. *Mol Cell, 45*(4), 567-580. doi:10.1016/j.molcel.2011.12.034

Hentze, M. W., & Preiss, T. (2013). Circular RNAs: splicing's enigma variations. *Embo j, 32*(7), 923-925. doi:10.1038/emboj.2013.53

Hoagland, M. B., Keller, E. B., & Zamecnik, P. C. (1956). Enzymatic carboxyl activation of amino acids. *J Biol Chem, 218*(1), 345-358.

Holdt, L. M., Stahringer, A., Sass, K., Pichler, G., Kulak, N. A., Wilfert, W., . . . Teupser, D. (2016). Circular non-coding RNA ANRIL modulates ribosomal RNA maturation and atherosclerosis in humans. *Nat Commun, 7*, 12429. doi:10.1038/ncomms12429

Holt, C. E., Martin, K. C., & Schuman, E. M. (2019). Local translation in neurons: visualization and function. *Nat Struct Mol Biol, 26*(7), 557-566. doi:10.1038/s41594-019-0263-5

Holt, C. E., & Schuman, E. M. (2013). The central dogma decentralized: new perspectives on RNA function and local translation in neurons. *Neuron, 80*(3), 648-657. doi:10.1016/j.neuron.2013.10.036

Hsu, M. T., & Coca-Prados, M. (1979). Electron microscopic evidence for the circular form of RNA in the cytoplasm of eukaryotic cells. *Nature, 280*(5720), 339-340. doi:10.1038/280339a0

Hu, Z., & Li, Z. (2017). miRNAs in synapse development and synaptic plasticity. *Curr Opin Neurobiol, 45*, 24-31. doi:10.1016/j.conb.2017.02.014

Huang, C., Liang, D., Tatomer, D. C., & Wilusz, J. E. (2018). A length-dependent evolutionarily conserved pathway controls nuclear export of circular RNAs. *Genes Dev, 32*(9-10), 639-644. doi:10.1101/gad.314856.118

Huang da, W., Sherman, B. T., & Lempicki, R. A. (2009a). Bioinformatics enrichment tools: paths toward the comprehensive functional analysis of large gene lists. *Nucleic Acids Res, 37*(1), 1-13. doi:10.1093/nar/gkn923

Huang da, W., Sherman, B. T., & Lempicki, R. A. (2009b). Systematic and integrative analysis of large gene lists using DAVID bioinformatics resources. *Nat Protoc, 4*(1), 44-57. doi:10.1038/nprot.2008.211

Huang, G., Zhu, H., Shi, Y., Wu, W., Cai, H., & Chen, X. (2015). cir-ITCH plays an inhibitory role in colorectal cancer by regulating the Wnt/β-catenin pathway. *PLoS One, 10*(6), e0131225. doi:10.1371/journal.pone.0131225

Huang, Y. Y., & Kandel, E. R. (2005). Theta frequency stimulation induces a local form of late phase LTP in the CA1 region of the hippocampus. *Learn Mem, 12*(6), 587-593. doi:10.1101/lm.98905

Huber, K. M., Kayser, M. S., & Bear, M. F. (2000). Role for rapid dendritic protein synthesis in hippocampal mGluR-dependent long-term depression. *Science, 288*(5469), 1254-1257. doi:10.1126/science.288.5469.1254

Hughes, J. R. (1958). Post-tetanic potentiation. *Physiol Rev, 38*(1), 91-113. doi:10.1152/physrev.1958.38.1.91

Huntzinger, E., & Izaurralde, E. (2011). Gene silencing by microRNAs: contributions of translational repression and mRNA decay. *Nat Rev Genet, 12*(2), 99-110. doi:10.1038/nrg2936

Hüttelmaier, S., Zenklusen, D., Lederer, M., Dictenberg, J., Lorenz, M., Meng, X., . . . Singer, R. H. (2005). Spatial regulation of beta-actin translation by Src-dependent phosphorylation of ZBP1. *Nature, 438*(7067), 512-515. doi:10.1038/nature04115

Ishizuka, N., Cowan, W. M., & Amaral, D. G. (1995). A quantitative analysis of the dendritic organization of pyramidal cells in the rat hippocampus. *J Comp Neurol, 362*(1), 17-45. doi:10.1002/cne.903620103

Ivanov, A., Memczak, S., Wyler, E., Torti, F., Porath, H. T., Orejuela, M. R., . . . Rajewsky, N. (2015). Analysis of intron sequences reveals hallmarks of circular RNA biogenesis in animals. *Cell Rep, 10*(2), 170-177. doi:10.1016/j.celrep.2014.12.019

Izaurralde, E., Lewis, J., McGuigan, C., Jankowska, M., Darzynkiewicz, E., & Mattaj, I. W. (1994). A nuclear cap binding protein complex involved in pre-mRNA splicing. *Cell, 78*(4), 657-668. doi:10.1016/0092-8674(94)90530-4

Jackson, R. J., & Standart, N. (2007). How do microRNAs regulate gene expression? *Sci STKE, 2007*(367), re1. doi:10.1126/stke.3672007re1

Jang, S., Lee, H., & Kim, E. (2017). Synaptic adhesion molecules and excitatory synaptic transmission. *Curr Opin Neurobiol, 45*, 45-50. doi:10.1016/j.conb.2017.03.005

Jeck, W. R., & Sharpless, N. E. (2014). Detecting and characterizing circular RNAs. *Nat Biotechnol, 32*(5), 453-461. doi:10.1038/nbt.2890

Jeck, W. R., Sorrentino, J. A., Wang, K., Slevin, M. K., Burd, C. E., Liu, J., . . . Sharpless, N. E. (2013). Circular RNAs are abundant, conserved, and associated with ALU repeats. *Rna, 19*(2), 141-157. doi:10.1261/rna.035667.112

Joshi, K. B., Vlachos, A., Mikat, V., Deller, T., & Heckel, A. (2012). Light-activatable molecular beacons with a caged loop sequence. *Chem Commun (Camb), 48*(22), 2746-2748. doi:10.1039/c2cc16654b

Jurica, M. S., & Moore, M. J. (2003). Pre-mRNA splicing: awash in a sea of proteins. *Mol Cell, 12*(1), 5-14. doi:10.1016/s1097-2765(03)00270-3

Kang, H., & Schuman, E. M. (1996). A requirement for local protein synthesis in neurotrophin-induced hippocampal synaptic plasticity. *Science, 273*(5280), 1402-1406. doi:10.1126/science.273.5280.1402

Kiebler, M. A., & Bassell, G. J. (2006). Neuronal RNA granules: movers and makers. *Neuron, 51*(6), 685-690. doi:10.1016/j.neuron.2006.08.021

Kim, E., & Sheng, M. (2004). PDZ domain proteins of synapses. *Nat Rev Neurosci, 5*(10), 771-781. doi:10.1038/nrn1517

Kino, T., Hurt, D. E., Ichijo, T., Nader, N., & Chrousos, G. P. (2010). Noncoding RNA gas5 is a growth arrest- and starvation-associated repressor of the glucocorticoid receptor. *Sci Signal, 3*(107), ra8. doi:10.1126/scisignal.2000568

Kleaveland, B., Shi, C. Y., Stefano, J., & Bartel, D. P. (2018). A Network of Noncoding Regulatory RNAs Acts in the Mammalian Brain. *Cell, 174*(2), 350-362.e317. doi:10.1016/j.cell.2018.05.022

Knowles, R. B., Sabry, J. H., Martone, M. E., Deerinck, T. J., Ellisman, M. H., Bassell, G. J., & Kosik, K. S. (1996). Translocation of RNA granules in living neurons. *J Neurosci, 16*(24), 7812-7820. doi:10.1523/jneurosci.16-24-07812.1996

Kramer, M. C., Liang, D., Tatomer, D. C., Gold, B., March, Z. M., Cherry, S., & Wilusz, J. E. (2015). Combinatorial control of Drosophila circular RNA expression by intronic repeats, hnRNPs, and SR proteins. *Genes Dev, 29*(20), 2168-2182. doi:10.1101/gad.270421.115

Krichevsky, A. M., King, K. S., Donahue, C. P., Khrapko, K., & Kosik, K. S. (2003). A microRNA array reveals extensive regulation of microRNAs during brain development. *Rna, 9*(10), 1274-1281. doi:10.1261/rna.5980303

Krichevsky, A. M., & Kosik, K. S. (2001). Neuronal RNA granules: a link between RNA localization and stimulation-dependent translation. *Neuron, 32*(4), 683-696. doi:10.1016/s0896-6273(01)00508-6

Krol, J., Busskamp, V., Markiewicz, I., Stadler, M. B., Ribi, S., Richter, J., . . . Filipowicz, W. (2010). Characterizing light-regulated retinal microRNAs reveals rapid turnover as a common property of neuronal microRNAs. *Cell, 141*(4), 618-631. doi:10.1016/j.cell.2010.03.039

Kubicki, M., McCarley, R., Westin, C. F., Park, H. J., Maier, S., Kikinis, R., . . . Shenton, M. E. (2007). A review of diffusion tensor imaging studies in schizophrenia. *J Psychiatr Res, 41*(1-2), 15-30. doi:10.1016/j.jpsychires.2005.05.005

Kye, M. J., Liu, T., Levy, S. F., Xu, N. L., Groves, B. B., Bonneau, R., . . . Kosik, K. S. (2007). Somatodendritic microRNAs identified by laser capture and multiplex RT-PCR. *Rna, 13*(8), 1224-1234. doi:10.1261/rna.480407

La Manno, G., Gyllborg, D., Codeluppi, S., Nishimura, K., Salto, C., Zeisel, A., . . . Linnarsson, S. (2016). Molecular Diversity of Midbrain Development in Mouse, Human, and Stem Cells. *Cell, 167*(2), 566-580.e519. doi:10.1016/j.cell.2016.09.027

Lagos-Quintana, M., Rauhut, R., Lendeckel, W., & Tuschl, T. (2001). Identification of novel genes coding for small expressed RNAs. *Science, 294*(5543), 853-858. doi:10.1126/science.1064921

Lagos-Quintana, M., Rauhut, R., Yalcin, A., Meyer, J., Lendeckel, W., & Tuschl, T. (2002). Identification of tissue-specific microRNAs from mouse. *Curr Biol, 12*(9), 735-739. doi:10.1016/s0960-9822(02)00809-6

Lai, E. C. (2002). Micro RNAs are complementary to 3' UTR sequence motifs that mediate negative post-transcriptional regulation. *Nat Genet, 30*(4), 363-364. doi:10.1038/ng865

Lamond, A. I., & Spector, D. L. (2003). Nuclear speckles: a model for nuclear organelles. *Nat Rev Mol Cell Biol, 4*(8), 605-612. doi:10.1038/nrm1172

Latos, P. A., Pauler, F. M., Koerner, M. V., Şenergin, H. B., Hudson, Q. J., Stocsits, R. R., . . . Barlow, D. P. (2012). Airn transcriptional overlap, but not its lncRNA products, induces imprinted Igf2r silencing. *Science, 338*(6113), 1469-1472. doi:10.1126/science.1228110

Lau, C. G., & Zukin, R. S. (2007). NMDA receptor trafficking in synaptic plasticity and neuropsychiatric disorders. *Nat Rev Neurosci, 8*(6), 413-426. doi:10.1038/nrn2153

Lau, N. C., Lim, L. P., Weinstein, E. G., & Bartel, D. P. (2001). An abundant class of tiny RNAs with probable regulatory roles in Caenorhabditis elegans. *Science, 294*(5543), 858-862. doi:10.1126/science.1065062

Lee, R. C., & Ambros, V. (2001). An extensive class of small RNAs in Caenorhabditis elegans. *Science, 294*(5543), 862-864. doi:10.1126/science.1065329

Lee, R. C., Feinbaum, R. L., & Ambros, V. (1993). The C. elegans heterochronic gene lin-4 encodes small RNAs with antisense complementarity to lin-14. *Cell, 75*(5), 843-854. doi:10.1016/0092-8674(93)90529-y

Legnini, I., Di Timoteo, G., Rossi, F., Morlando, M., Briganti, F., Sthandier, O., . . . Bozzoni, I. (2017). Circ-ZNF609 Is a Circular RNA that Can Be Translated and Functions in Myogenesis. *Mol Cell, 66*(1), 22-37.e29. doi:10.1016/j.molcel.2017.02.017

Lein, E. S., Hawrylycz, M. J., Ao, N., Ayres, M., Bensinger, A., Bernard, A., . . . Jones, A. R. (2007). Genome-wide atlas of gene expression in the adult mouse brain. *Nature, 445*(7124), 168-176. doi:10.1038/nature05453

Leung, A. K. L. (2015). The Whereabouts of microRNA Actions: Cytoplasm and Beyond. *Trends Cell Biol, 25*(10), 601-610. doi:10.1016/j.tcb.2015.07.005

Lewis, B. P., Burge, C. B., & Bartel, D. P. (2005). Conserved seed pairing, often flanked by adenosines, indicates that thousands of human genes are microRNA targets. *Cell, 120*(1), 15-20. doi:10.1016/j.cell.2004.12.035

Lewis, B. P., Shih, I. H., Jones-Rhoades, M. W., Bartel, D. P., & Burge, C. B. (2003). Prediction of mammalian microRNA targets. *Cell, 115*(7), 787-798. doi:10.1016/s0092-8674(03)01018-3

Li, H., & Durbin, R. (2009). Fast and accurate short read alignment with Burrows-Wheeler transform. *Bioinformatics, 25*(14), 1754-1760. doi:10.1093/bioinformatics/btp324

Li, Q., Lee, J. A., & Black, D. L. (2007). Neuronal regulation of alternative pre-mRNA splicing. *Nat Rev Neurosci, 8*(11), 819-831. doi:10.1038/nrn2237

Li, Y., Zheng, F., Xiao, X., Xie, F., Tao, D., Huang, C., . . . Jiang, G. (2017). CircHIPK3 sponges miR-558 to suppress heparanase expression in bladder cancer cells. *EMBO Rep, 18*(9), 1646-1659. doi:10.15252/embr.201643581

Liang, D., Tatomer, D. C., Luo, Z., Wu, H., Yang, L., Chen, L. L., . . . Wilusz, J. E. (2017). The Output of Protein-Coding Genes Shifts to Circular RNAs When the Pre-mRNA Processing Machinery Is Limiting. *Mol Cell, 68*(5), 940-954.e943. doi:10.1016/j.molcel.2017.10.034

Liang, D., & Wilusz, J. E. (2014). Short intronic repeat sequences facilitate circular RNA production. *Genes Dev, 28*(20), 2233-2247. doi:10.1101/gad.251926.114

Licatalosi, D. D., Mele, A., Fak, J. J., Ule, J., Kayikci, M., Chi, S. W., . . . Darnell, R. B. (2008). HITS-CLIP yields genome-wide insights into brain alternative RNA processing. *Nature, 456*(7221), 464-469. doi:10.1038/nature07488

Lim, S., Naisbitt, S., Yoon, J., Hwang, J. I., Suh, P. G., Sheng, M., & Kim, E. (1999). Characterization of the Shank family of synaptic proteins. Multiple genes, alternative splicing, and differential expression in brain and development. *J Biol Chem, 274*(41), 29510-29518. doi:10.1074/jbc.274.41.29510

Lipscombe, D. (2005). Neuronal proteins custom designed by alternative splicing. *Curr Opin Neurobiol, 15*(3), 358-363. doi:10.1016/j.conb.2005.04.002

Lisman, J., Schulman, H., & Cline, H. (2002). The molecular basis of CaMKII function in synaptic and behavioural memory. *Nat Rev Neurosci, 3*(3), 175-190. doi:10.1038/nrn753

Liu, J., Valencia-Sanchez, M. A., Hannon, G. J., & Parker, R. (2005). MicroRNA-dependent localization of targeted mRNAs to mammalian P-bodies. *Nat Cell Biol, 7*(7), 719-723. doi:10.1038/ncb1274

Lonskaya, I., Shekoyan, A. R., Hebron, M. L., Desforges, N., Algarzae, N. K., & Moussa, C. E. (2013). Diminished parkin solubility and co-localization with intraneuronal amyloid-β are associated with autophagic defects in Alzheimer's disease. *J Alzheimers Dis, 33*(1), 231-247. doi:10.3233/jad-2012-121141

Lorenz, R., Bernhart, S. H., Höner Zu Siederdissen, C., Tafer, H., Flamm, C., Stadler, P. F., & Hofacker, I. L. (2011). ViennaRNA Package 2.0. *Algorithms Mol Biol, 6*, 26. doi:10.1186/1748-7188-6-26

Lucchesi, W., Mizuno, K., & Giese, K. P. (2011). Novel insights into CaMKII function and regulation during memory formation. *Brain Res Bull, 85*(1-2), 2-8. doi:10.1016/j.brainresbull.2010.10.009

Lugli, G., Larson, J., Martone, M. E., Jones, Y., & Smalheiser, N. R. (2005). Dicer and eIF2c are enriched at postsynaptic densities in adult mouse brain and are modified by neuronal activity in a calpain-dependent manner. *J Neurochem, 94*(4), 896-905. doi:10.1111/j.1471-4159.2005.03224.x

Lugli, G., Torvik, V. I., Larson, J., & Smalheiser, N. R. (2008). Expression of microRNAs and their precursors in synaptic fractions of adult mouse forebrain. *J Neurochem, 106*(2), 650-661. doi:10.1111/j.1471-4159.2008.05413.x

Lukiw, W. J. (2013). Circular RNA (circRNA) in Alzheimer's disease (AD). *Front Genet, 4*, 307. doi:10.3389/fgene.2013.00307

Lynch, G. S., Dunwiddie, T., & Gribkoff, V. (1977). Heterosynaptic depression: a postsynaptic correlate of long-term potentiation. *Nature, 266*(5604), 737-739. doi:10.1038/266737a0

Madhani, H. D., & Guthrie, C. (1994). Dynamic RNA-RNA interactions in the spliceosome. *Annu Rev Genet, 28*, 1-26. doi:10.1146/annurev.ge.28.120194.000245

Martens, S., & McMahon, H. T. (2008). Mechanisms of membrane fusion: disparate players and common principles. *Nat Rev Mol Cell Biol, 9*(7), 543-556. doi:10.1038/nrm2417

Martin, K. C., Casadio, A., Zhu, H., Yaping, E., Rose, J. C., Chen, M., . . . Kandel, E. R. (1997). Synapse-specific, long-term facilitation of aplysia sensory to motor synapses: a function for local protein synthesis in memory storage. *Cell, 91*(7), 927-938. doi:10.1016/s0092-8674(00)80484-5

Massenet, S., Pellizzoni, L., Paushkin, S., Mattaj, I. W., & Dreyfuss, G. (2002). The SMN complex is associated with snRNPs throughout their cytoplasmic assembly pathway. *Mol Cell Biol, 22*(18), 6533-6541. doi:10.1128/mcb.22.18.6533-6541.2002

Matera, A. G., Terns, R. M., & Terns, M. P. (2007). Non-coding RNAs: lessons from the small nuclear and small nucleolar RNAs. *Nat Rev Mol Cell Biol, 8*(3), 209-220. doi:10.1038/nrm2124

Matera, A. G., & Wang, Z. (2014). A day in the life of the spliceosome. *Nat Rev Mol Cell Biol, 15*(2), 108-121. doi:10.1038/nrm3742

Mattick, J. S. (2001). Non-coding RNAs: the architects of eukaryotic complexity. *EMBO Rep, 2*(11), 986-991. doi:10.1093/embo-reports/kve230

Mayer, G., & Heckel, A. (2006). Biologically active molecules with a "light switch". *Angew Chem Int Ed Engl, 45*(30), 4900-4921. doi:10.1002/anie.200600387

Mayford, M., Baranes, D., Podsypanina, K., & Kandel, E. R. (1996). The 3'-untranslated region of CaMKII alpha is a cis-acting signal for the localization and translation of mRNA in dendrites. *Proc Natl Acad Sci U S A, 93*(23), 13250-13255. doi:10.1073/pnas.93.23.13250

Mayr, C. (2016). Evolution and Biological Roles of Alternative 3'UTRs. *Trends Cell Biol, 26*(3), 227-237. doi:10.1016/j.tcb.2015.10.012

McCullough, A. J., & Berget, S. M. (1997). G triplets located throughout a class of small vertebrate introns enforce intron borders and regulate splice site selection. *Mol Cell Biol, 17*(8), 4562-4571. doi:10.1128/mcb.17.8.4562

McGaugh, J. L., & Izquierdo, I. (2000). The contribution of pharmacology to research on the mechanisms of memory formation. *Trends Pharmacol Sci, 21*(6), 208-210. doi:10.1016/s0165-6147(00)01473-5

Meister, G., Eggert, C., & Fischer, U. (2002). SMN-mediated assembly of RNPs: a complex story. *Trends Cell Biol, 12*(10), 472-478. doi:10.1016/s0962-8924(02)02371-1

Memczak, S., Jens, M., Elefsinioti, A., Torti, F., Krueger, J., Rybak, A., . . . Rajewsky, N. (2013). Circular RNAs are a large class of animal RNAs with regulatory potency. *Nature, 495*(7441), 333-338. doi:10.1038/nature11928

Memczak, S., Papavasileiou, P., Peters, O., & Rajewsky, N. (2015). Identification and Characterization of Circular RNAs As a New Class of Putative Biomarkers in Human Blood. *PLoS One, 10*(10), e0141214. doi:10.1371/journal.pone.0141214

Mercer, T. R., Dinger, M. E., Sunkin, S. M., Mehler, M. F., & Mattick, J. S. (2008). Specific expression of long noncoding RNAs in the mouse brain. *Proc Natl Acad Sci U S A, 105*(2), 716-721. doi:10.1073/pnas.0706729105

Mercer, T. R., Qureshi, I. A., Gokhan, S., Dinger, M. E., Li, G., Mattick, J. S., & Mehler, M. F. (2010). Long noncoding RNAs in neuronal-glial fate specification and oligodendrocyte lineage maturation. *BMC Neurosci, 11*, 14. doi:10.1186/1471-2202-11-14

Miller, S., Yasuda, M., Coats, J. K., Jones, Y., Martone, M. E., & Mayford, M. (2002). Disruption of dendritic translation of CaMKIIalpha impairs stabilization of synaptic plasticity and memory consolidation. *Neuron, 36*(3), 507-519. doi:10.1016/s0896-6273(02)00978-9

Missler, M., Südhof, T. C., & Biederer, T. (2012). Synaptic cell adhesion. *Cold Spring Harb Perspect Biol, 4*(4), a005694. doi:10.1101/cshperspect.a005694

Morris, R. G., Garrud, P., Rawlins, J. N., & O'Keefe, J. (1982). Place navigation impaired in rats with hippocampal lesions. *Nature, 297*(5868), 681-683. doi:10.1038/297681a0

Moss, E. G., Lee, R. C., & Ambros, V. (1997). The cold shock domain protein LIN-28 controls developmental timing in C. elegans and is regulated by the lin-4 RNA. *Cell, 88*(5), 637-646. doi:10.1016/s0092-8674(00)81906-6

Mu, Y., Otsuka, T., Horton, A. C., Scott, D. B., & Ehlers, M. D. (2003). Activity-dependent mRNA splicing controls ER export and synaptic delivery of NMDA receptors. *Neuron, 40*(3), 581-594. doi:10.1016/s0896-6273(03)00676-7

Müller, P., Seyfried, P., Frühauf, A., & Heckel, A. (2019). Phosphodiester photo-tethers for the (multi-)cyclic conformational caging of oligonucleotides. *Methods Enzymol, 624*, 89-111. doi:10.1016/bs.mie.2019.04.019

Ngô, H., Tschudi, C., Gull, K., & Ullu, E. (1998). Double-stranded RNA induces mRNA degradation in Trypanosoma brucei. *Proc Natl Acad Sci U S A, 95*(25), 14687-14692. doi:10.1073/pnas.95.25.14687

Nguyen, P. V., Abel, T., & Kandel, E. R. (1994). Requirement of a critical period of transcription for induction of a late phase of LTP. *Science, 265*(5175), 1104-1107. doi:10.1126/science.8066450

Nigro, J. M., Cho, K. R., Fearon, E. R., Kern, S. E., Ruppert, J. M., Oliner, J. D., . . . Vogelstein, B. (1991). Scrambled exons. *Cell, 64*(3), 607-613. doi:10.1016/0092-8674(91)90244-s

Nilsen, T. W., & Graveley, B. R. (2010). Expansion of the eukaryotic proteome by alternative splicing. *Nature, 463*(7280), 457-463. doi:10.1038/nature08909

Noller, H. F., Hoffarth, V., & Zimniak, L. (1992). Unusual resistance of peptidyl transferase to protein extraction procedures. *Science, 256*(5062), 1416-1419. doi:10.1126/science.1604315

Norris, A. D., & Calarco, J. A. (2012). Emerging Roles of Alternative Pre-mRNA Splicing Regulation in Neuronal Development and Function. *Front Neurosci, 6*, 122. doi:10.3389/fnins.2012.00122

Nover, L., Scharf, K. D., & Neumann, D. (1989). Cytoplasmic heat shock granules are formed from precursor particles and are associated with a specific set of mRNAs. *Mol Cell Biol, 9*(3), 1298-1308. doi:10.1128/mcb.9.3.1298

Nudelman, A. S., DiRocco, D. P., Lambert, T. J., Garelick, M. G., Le, J., Nathanson, N. M., & Storm, D. R. (2010). Neuronal activity rapidly induces transcription of the CREB-regulated microRNA-132, in vivo. *Hippocampus, 20*(4), 492-498. doi:10.1002/hipo.20646

O'Brien, K., Matlin, A. J., Lowell, A. M., & Moore, M. J. (2008). The biflavonoid isoginkgetin is a general inhibitor of Pre-mRNA splicing. *J Biol Chem, 283*(48), 33147-33154. doi:10.1074/jbc.M805556200

O'Keefe, J., & Dostrovsky, J. (1971). The hippocampus as a spatial map. Preliminary evidence from unit activity in the freely-moving rat. *Brain Res, 34*(1), 171-175. doi:10.1016/0006-8993(71)90358-1

Ohno, M., Segref, A., Bachi, A., Wilm, M., & Mattaj, I. W. (2000). PHAX, a mediator of U snRNA nuclear export whose activity is regulated by phosphorylation. *Cell, 101*(2), 187-198. doi:10.1016/s0092-8674(00)80829-6

Okazaki, Y., Furuno, M., Kasukawa, T., Adachi, J., Bono, H., Kondo, S., . . . Hayashizaki, Y. (2002). Analysis of the mouse transcriptome based on functional annotation of 60,770 full-length cDNAs. *Nature, 420*(6915), 563-573. doi:10.1038/nature01266

Omi, K., Tokunaga, K., & Hohjoh, H. (2004). Long-lasting RNAi activity in mammalian neurons. *FEBS Lett, 558*(1-3), 89-95. doi:10.1016/s0014-5793(04)00017-1

Padgett, R. A. (2012). New connections between splicing and human disease. *Trends Genet, 28*(4), 147-154. doi:10.1016/j.tig.2012.01.001

Palade, G. E. (1955). A small particulate component of the cytoplasm. *J Biophys Biochem Cytol, 1*(1), 59-68. doi:10.1083/jcb.1.1.59

Palazzo, A. F., & Lee, E. S. (2015). Non-coding RNA: what is functional and what is junk? *Front Genet, 6*, 2. doi:10.3389/fgene.2015.00002

Pamudurti, N. R., Bartok, O., Jens, M., Ashwal-Fluss, R., Stottmeister, C., Ruhe, L., . . . Kadener, S. (2017). Translation of CircRNAs. *Mol Cell, 66*(1), 9-21.e27. doi:10.1016/j.molcel.2017.02.021

Pan, Q., Shai, O., Lee, L. J., Frey, B. J., & Blencowe, B. J. (2008). Deep surveying of alternative splicing complexity in the human transcriptome by high-throughput sequencing. *Nat Genet, 40*(12), 1413-1415. doi:10.1038/ng.259

Park, C. S., & Tang, S. J. (2009). Regulation of microRNA expression by induction of bidirectional synaptic plasticity. *J Mol Neurosci, 38*(1), 50-56. doi:10.1007/s12031-008-9158-3

Pasquinelli, A. E., Reinhart, B. J., Slack, F., Martindale, M. Q., Kuroda, M. I., Maller, B., . . . Ruvkun, G. (2000). Conservation of the sequence and temporal expression of let-7 heterochronic regulatory RNA. *Nature, 408*(6808), 86-89. doi:10.1038/35040556

Pellizzoni, L., Yong, J., & Dreyfuss, G. (2002). Essential role for the SMN complex in the specificity of snRNP assembly. *Science, 298*(5599), 1775-1779. doi:10.1126/science.1074962

Pereda, A. E. (2014). Electrical synapses and their functional interactions with chemical synapses. *Nat Rev Neurosci, 15*(4), 250-263. doi:10.1038/nrn3708

Piwecka, M., Glažar, P., Hernandez-Miranda, L. R., Memczak, S., Wolf, S. A., Rybak-Wolf, A., . . . Rajewsky, N. (2017). Loss of a mammalian circular RNA locus causes miRNA deregulation and affects brain function. *Science, 357*(6357). doi:10.1126/science.aam8526

Poon, M. M., Choi, S. H., Jamieson, C. A., Geschwind, D. H., & Martin, K. C. (2006). Identification of process-localized mRNAs from cultured rodent

hippocampal neurons. *J Neurosci, 26*(51), 13390-13399. doi:10.1523/jneurosci.3432-06.2006

Protter, D. S. W., & Parker, R. (2016). Principles and Properties of Stress Granules. *Trends Cell Biol, 26*(9), 668-679. doi:10.1016/j.tcb.2016.05.004

Qin, M., Liu, G., Huo, X., Tao, X., Sun, X., Ge, Z., . . . Qin, W. (2016). Hsa_circ_0001649: A circular RNA and potential novel biomarker for hepatocellular carcinoma. *Cancer Biomark, 16*(1), 161-169. doi:10.3233/cbm-150552

Qu, S., Yang, X., Li, X., Wang, J., Gao, Y., Shang, R., . . . Li, H. (2015). Circular RNA: A new star of noncoding RNAs. *Cancer Lett, 365*(2), 141-148. doi:10.1016/j.canlet.2015.06.003

Quesnel-Vallières, M., Irimia, M., Cordes, S. P., & Blencowe, B. J. (2015). Essential roles for the splicing regulator nSR100/SRRM4 during nervous system development. *Genes Dev, 29*(7), 746-759. doi:10.1101/gad.256115.114

Quinlan, A. R., & Hall, I. M. (2010). BEDTools: a flexible suite of utilities for comparing genomic features. *Bioinformatics, 26*(6), 841-842. doi:10.1093/bioinformatics/btq033

Ramsköld, D., Wang, E. T., Burge, C. B., & Sandberg, R. (2009). An abundance of ubiquitously expressed genes revealed by tissue transcriptome sequence data. *PLoS Comput Biol, 5*(12), e1000598. doi:10.1371/journal.pcbi.1000598

Rao, A., & Steward, O. (1991). Evidence that protein constituents of postsynaptic membrane specializations are locally synthesized: analysis of proteins synthesized within synaptosomes. *J Neurosci, 11*(9), 2881-2895. doi:10.1523/jneurosci.11-09-02881.1991

Reinhart, B. J., Slack, F. J., Basson, M., Pasquinelli, A. E., Bettinger, J. C., Rougvie, A. E., . . . Ruvkun, G. (2000). The 21-nucleotide let-7 RNA regulates developmental timing in Caenorhabditis elegans. *Nature, 403*(6772), 901-906. doi:10.1038/35002607

Remenyi, J., van den Bosch, M. W., Palygin, O., Mistry, R. B., McKenzie, C., Macdonald, A., . . . Pankratov, Y. (2013). miR-132/212 knockout mice reveal roles for these miRNAs in regulating cortical synaptic transmission and plasticity. *PLoS One, 8*(4), e62509. doi:10.1371/journal.pone.0062509

Rheaume, B. A., Jereen, A., Bolisetty, M., Sajid, M. S., Yang, Y., Renna, K., . . . Trakhtenberg, E. F. (2018). Single cell transcriptome profiling of retinal ganglion cells identifies cellular subtypes. *Nat Commun, 9*(1), 2759. doi:10.1038/s41467-018-05134-3

Rinn, J. L., & Chang, H. Y. (2012). Genome regulation by long noncoding RNAs. *Annu Rev Biochem, 81*, 145-166. doi:10.1146/annurev-biochem-051410-092902

Robinson, M. D., McCarthy, D. J., & Smyth, G. K. (2010). edgeR: a Bioconductor package for differential expression analysis of digital gene expression data. *Bioinformatics, 26*(1), 139-140. doi:10.1093/bioinformatics/btp616

Rosonina, E., & Blencowe, B. J. (2004). Analysis of the requirement for RNA polymerase II CTD heptapeptide repeats in pre-mRNA splicing and 3'-end cleavage. *Rna, 10*(4), 581-589. doi:10.1261/rna.5207204

Roxo, M. R., Franceschini, P. R., Zubaran, C., Kleber, F. D., & Sander, J. W. (2011). The limbic system conception and its historical evolution. *ScientificWorldJournal, 11*, 2428-2441. doi:10.1100/2011/157150

Ruble, B. K., Yeldell, S. B., & Dmochowski, I. J. (2015). Caged oligonucleotides for studying biological systems. *J Inorg Biochem, 150*, 182-188. doi:10.1016/j.jinorgbio.2015.03.010

Rybak-Wolf, A., Stottmeister, C., Glažar, P., Jens, M., Pino, N., Giusti, S., . . . Rajewsky, N. (2015). Circular RNAs in the Mammalian Brain Are Highly Abundant, Conserved, and Dynamically Expressed. *Mol Cell, 58*(5), 870-885. doi:10.1016/j.molcel.2015.03.027

Sala, C., Vicidomini, C., Bigi, I., Mossa, A., & Verpelli, C. (2015). Shank synaptic scaffold proteins: keys to understanding the pathogenesis of autism and other synaptic disorders. *J Neurochem, 135*(5), 849-858. doi:10.1111/jnc.13232

Salzman, J., Chen, R. E., Olsen, M. N., Wang, P. L., & Brown, P. O. (2013). Cell-type specific features of circular RNA expression. *PLoS Genet, 9*(9), e1003777. doi:10.1371/journal.pgen.1003777

Salzman, J., Gawad, C., Wang, P. L., Lacayo, N., & Brown, P. O. (2012). Circular RNAs are the predominant transcript isoform from hundreds of human genes in diverse cell types. *PLoS One, 7*(2), e30733. doi:10.1371/journal.pone.0030733

Sambandan, S., Akbalik, G., Kochen, L., Rinne, J., Kahlstatt, J., Glock, C., . . . Schuman, E. M. (2017). Activity-dependent spatially localized miRNA maturation in neuronal dendrites. *Science, 355*(6325), 634-637. doi:10.1126/science.aaf8995

Sanger, H. L., Klotz, G., Riesner, D., Gross, H. J., & Kleinschmidt, A. K. (1976). Viroids are single-stranded covalently closed circular RNA molecules existing as highly base-paired rod-like structures. *Proc Natl Acad Sci U S A, 73*(11), 3852-3856. doi:10.1073/pnas.73.11.3852

Schaffert, N., Hossbach, M., Heintzmann, R., Achsel, T., & Lührmann, R. (2004). RNAi knockdown of hPrp31 leads to an accumulation of U4/U6 di-snRNPs in Cajal bodies. *Embo j, 23*(15), 3000-3009. doi:10.1038/sj.emboj.7600296

Scheiffele, P. (2003). Cell-cell signaling during synapse formation in the CNS. *Annu Rev Neurosci, 26*, 485-508. doi:10.1146/annurev.neuro.26.043002.094940

Schratt, G. M., Tuebing, F., Nigh, E. A., Kane, C. G., Sabatini, M. E., Kiebler, M., & Greenberg, M. E. (2006). A brain-specific microRNA regulates dendritic spine development. *Nature, 439*(7074), 283-289. doi:10.1038/nature04367

Scoville, W. B., & Milner, B. (1957). Loss of recent memory after bilateral hippocampal lesions. *J Neurol Neurosurg Psychiatry, 20*(1), 11-21. doi:10.1136/jnnp.20.1.11

Sempere, L. F., Freemantle, S., Pitha-Rowe, I., Moss, E., Dmitrovsky, E., & Ambros, V. (2004). Expression profiling of mammalian microRNAs uncovers a subset of brain-expressed microRNAs with possible roles in murine and human neuronal differentiation. *Genome Biol, 5*(3), R13. doi:10.1186/gb-2004-5-3-r13

Sevignani, C., Calin, G. A., Siracusa, L. D., & Croce, C. M. (2006). Mammalian microRNAs: a small world for fine-tuning gene expression. *Mamm Genome, 17*(3), 189-202. doi:10.1007/s00335-005-0066-3

Seyfried, P., Eiden, L., Grebenovsky, N., Mayer, G., & Heckel, A. (2017). Photo-Tethers for the (Multi-)Cyclic, Conformational Caging of Long Oligonucleotides. *Angew Chem Int Ed Engl, 56*(1), 359-363. doi:10.1002/anie.201610025

Sheffield, M. E., & Dombeck, D. A. (2015). Calcium transient prevalence across the dendritic arbour predicts place field properties. *Nature, 517*(7533), 200-204. doi:10.1038/nature13871

Sheffield, M. E. J., Adoff, M. D., & Dombeck, D. A. (2017). Increased Prevalence of Calcium Transients across the Dendritic Arbor during Place Field Formation. *Neuron, 96*(2), 490-504.e495. doi:10.1016/j.neuron.2017.09.029

Sheng, M., & Hoogenraad, C. C. (2007). The postsynaptic architecture of excitatory synapses: a more quantitative view. *Annu Rev Biochem, 76*, 823-847. doi:10.1146/annurev.biochem.76.060805.160029

Sheng, M., & Kim, E. (2011). The postsynaptic organization of synapses. *Cold Spring Harb Perspect Biol, 3*(12). doi:10.1101/cshperspect.a005678

Sheth, U., & Parker, R. (2003). Decapping and decay of messenger RNA occur in cytoplasmic processing bodies. *Science, 300*(5620), 805-808. doi:10.1126/science.1082320

Siegel, G., Obernosterer, G., Fiore, R., Oehmen, M., Bicker, S., Christensen, M., . . . Schratt, G. M. (2009). A functional screen implicates microRNA-138-dependent regulation of the depalmitoylation enzyme APT1 in dendritic spine morphogenesis. *Nat Cell Biol, 11*(6), 705-716. doi:10.1038/ncb1876

Singh, R. K., & Cooper, T. A. (2012). Pre-mRNA splicing in disease and therapeutics. *Trends Mol Med, 18*(8), 472-482. doi:10.1016/j.molmed.2012.06.006

Sjöström, P. J., Rancz, E. A., Roth, A., & Häusser, M. (2008). Dendritic excitability and synaptic plasticity. *Physiol Rev, 88*(2), 769-840. doi:10.1152/physrev.00016.2007

Sleeman, J. E., & Lamond, A. I. (1999). Newly assembled snRNPs associate with coiled bodies before speckles, suggesting a nuclear snRNP maturation pathway. *Curr Biol, 9*(19), 1065-1074. doi:10.1016/s0960-9822(99)80475-8

Smalheiser, N. R., & Lugli, G. (2009). microRNA regulation of synaptic plasticity. *Neuromolecular Med, 11*(3), 133-140. doi:10.1007/s12017-009-8065-2

Smith, K. P., & Lawrence, J. B. (2000). Interactions of U2 gene loci and their nuclear transcripts with Cajal (coiled) bodies: evidence for PreU2 within Cajal bodies. *Mol Biol Cell, 11*(9), 2987-2998. doi:10.1091/mbc.11.9.2987

Smith, W. B., Starck, S. R., Roberts, R. W., & Schuman, E. M. (2005). Dopaminergic stimulation of local protein synthesis enhances surface expression of GluR1 and synaptic transmission in hippocampal neurons. *Neuron, 45*(5), 765-779. doi:10.1016/j.neuron.2005.01.015

Squire, L. R., & Zola-Morgan, S. (1991). The medial temporal lobe memory system. *Science, 253*(5026), 1380-1386. doi:10.1126/science.1896849

St Johnston, D. (1995). The intracellular localization of messenger RNAs. *Cell, 81*(2), 161-170. doi:10.1016/0092-8674(95)90324-0

Starke, S., Jost, I., Rossbach, O., Schneider, T., Schreiner, S., Hung, L. H., & Bindereif, A. (2015). Exon circularization requires canonical splice signals. *Cell Rep, 10*(1), 103-111. doi:10.1016/j.celrep.2014.12.002

Stegeman, R., Hall, H., Escobedo, S. E., Chang, H. C., & Weake, V. M. (2018). Proper splicing contributes to visual function in the aging Drosophila eye. *Aging Cell, 17*(5), e12817. doi:10.1111/acel.12817

Steward, O., & Levy, W. B. (1982). Preferential localization of polyribosomes under the base of dendritic spines in granule cells of the dentate gyrus. *J Neurosci, 2*(3), 284-291. doi:10.1523/jneurosci.02-03-00284.1982

Stuart, G., Spruston, N., Sakmann, B., & Häusser, M. (1997). Action potential initiation and backpropagation in neurons of the mammalian CNS. *Trends Neurosci, 20*(3), 125-131. doi:10.1016/s0166-2236(96)10075-8

Sun, W., You, X., Gogol-Döring, A., He, H., Kise, Y., Sohn, M., . . . Chen, W. (2013). Ultra-deep profiling of alternatively spliced Drosophila Dscam isoforms by circularization-assisted multi-segment sequencing. *Embo j, 32*(14), 2029-2038. doi:10.1038/emboj.2013.144

Sutton, M. A., Ito, H. T., Cressy, P., Kempf, C., Woo, J. C., & Schuman, E. M. (2006). Miniature neurotransmission stabilizes synaptic function via tonic suppression of local dendritic protein synthesis. *Cell, 125*(4), 785-799. doi:10.1016/j.cell.2006.03.040

Sutton, M. A., & Schuman, E. M. (2006). Dendritic protein synthesis, synaptic plasticity, and memory. *Cell, 127*(1), 49-58. doi:10.1016/j.cell.2006.09.014

Sutton, M. A., Taylor, A. M., Ito, H. T., Pham, A., & Schuman, E. M. (2007). Postsynaptic decoding of neural activity: eEF2 as a biochemical sensor coupling miniature synaptic transmission to local protein synthesis. *Neuron, 55*(4), 648-661. doi:10.1016/j.neuron.2007.07.030

Sutton, M. A., Wall, N. R., Aakalu, G. N., & Schuman, E. M. (2004). Regulation of dendritic protein synthesis by miniature synaptic events. *Science, 304*(5679), 1979-1983. doi:10.1126/science.1096202

Suzuki, T., Izumi, H., & Ohno, M. (2010). Cajal body surveillance of U snRNA export complex assembly. *J Cell Biol, 190*(4), 603-612. doi:10.1083/jcb.201004109

Taft, R. J., Pheasant, M., & Mattick, J. S. (2007). The relationship between non-protein-coding DNA and eukaryotic complexity. *Bioessays, 29*(3), 288-299. doi:10.1002/bies.20544

Tan, W., Wang, K., & Drake, T. J. (2004). Molecular beacons. *Curr Opin Chem Biol, 8*(5), 547-553. doi:10.1016/j.cbpa.2004.08.010

Tanackovic, G., Ransijn, A., Thibault, P., Abou Elela, S., Klinck, R., Berson, E. L., . . . Rivolta, C. (2011). PRPF mutations are associated with generalized defects in spliceosome formation and pre-mRNA splicing in patients with retinitis pigmentosa. *Hum Mol Genet, 20*(11), 2116-2130. doi:10.1093/hmg/ddr094

Tian, B., & Manley, J. L. (2017). Alternative polyadenylation of mRNA precursors. *Nat Rev Mol Cell Biol, 18*(1), 18-30. doi:10.1038/nrm.2016.116

Tiedge, H., Fremeau, R. T., Jr., Weinstock, P. H., Arancio, O., & Brosius, J. (1991). Dendritic location of neural BC1 RNA. *Proc Natl Acad Sci U S A, 88*(6), 2093-2097. doi:10.1073/pnas.88.6.2093

Tiruchinapalli, D. M., Oleynikov, Y., Kelic, S., Shenoy, S. M., Hartley, A., Stanton, P. K., . . . Bassell, G. J. (2003). Activity-dependent trafficking and dynamic localization of zipcode binding protein 1 and beta-actin mRNA in dendrites and spines of hippocampal neurons. *J Neurosci, 23*(8), 3251-3261. doi:10.1523/jneurosci.23-08-03251.2003

tom Dieck, S., Kochen, L., Hanus, C., Heumüller, M., Bartnik, I., Nassim-Assir, B., . . . Schuman, E. M. (2015). Direct visualization of newly synthesized target proteins in situ. *Nat Methods, 12*(5), 411-414. doi:10.1038/nmeth.3319

Trinkle-Mulcahy, L., Boulon, S., Lam, Y. W., Urcia, R., Boisvert, F. M., Vandermoere, F., . . . Lamond, A. (2008). Identifying specific protein interaction partners using quantitative mass spectrometry and bead proteomes. *J Cell Biol, 183*(2), 223-239. doi:10.1083/jcb.200805092

Tripathi, V., Ellis, J. D., Shen, Z., Song, D. Y., Pan, Q., Watt, A. T., . . . Prasanth, K. V. (2010). The nuclear-retained noncoding RNA MALAT1 regulates alternative splicing by modulating SR splicing factor phosphorylation. *Mol Cell, 39*(6), 925-938. doi:10.1016/j.molcel.2010.08.011

Tsai, M. C., Manor, O., Wan, Y., Mosammaparast, N., Wang, J. K., Lan, F., . . . Chang, H. Y. (2010). Long noncoding RNA as modular scaffold of histone modification complexes. *Science, 329*(5992), 689-693. doi:10.1126/science.1192002

Tseng, Y. Y., Moriarity, B. S., Gong, W., Akiyama, R., Tiwari, A., Kawakami, H., . . . Bagchi, A. (2014). PVT1 dependence in cancer with MYC copy-number increase. *Nature, 512*(7512), 82-86. doi:10.1038/nature13311

Tsien, J. Z., Huerta, P. T., & Tonegawa, S. (1996). The essential role of hippocampal CA1 NMDA receptor-dependent synaptic plasticity in spatial memory. *Cell, 87*(7), 1327-1338. doi:10.1016/s0092-8674(00)81827-9

Tushev, G., Glock, C., Heumüller, M., Biever, A., Jovanovic, M., & Schuman, E. M. (2018). Alternative 3' UTRs Modify the Localization, Regulatory Potential, Stability, and Plasticity of mRNAs in Neuronal Compartments. *Neuron, 98*(3), 495-511.e496. doi:10.1016/j.neuron.2018.03.030

Tyagi, S., & Kramer, F. R. (1996). Molecular beacons: probes that fluoresce upon hybridization. *Nat Biotechnol, 14*(3), 303-308. doi:10.1038/nbt0396-303

Ule, J., Stefani, G., Mele, A., Ruggiu, M., Wang, X., Taneri, B., . . . Darnell, R. B. (2006). An RNA map predicting Nova-dependent splicing regulation. *Nature, 444*(7119), 580-586. doi:10.1038/nature05304

Usoskin, D., Furlan, A., Islam, S., Abdo, H., Lönnerberg, P., Lou, D., . . . Ernfors, P. (2015). Unbiased classification of sensory neuron types by large-scale single-cell RNA sequencing. *Nat Neurosci, 18*(1), 145-153. doi:10.1038/nn.3881

Venø, M. T., Hansen, T. B., Venø, S. T., Clausen, B. H., Grebing, M., Finsen, B., . . . Kjems, J. (2015). Spatio-temporal regulation of circular RNA expression during porcine embryonic brain development. *Genome Biol, 16*, 245. doi:10.1186/s13059-015-0801-3

Vessey, J. P., Vaccani, A., Xie, Y., Dahm, R., Karra, D., Kiebler, M. A., & Macchi, P. (2006). Dendritic localization of the translational repressor Pumilio 2 and its contribution to dendritic stress granules. *J Neurosci, 26*(24), 6496-6508. doi:10.1523/jneurosci.0649-06.2006

Vickers, C. A., Dickson, K. S., & Wyllie, D. J. (2005). Induction and maintenance of late-phase long-term potentiation in isolated dendrites of rat hippocampal CA1 pyramidal neurones. *J Physiol, 568*(Pt 3), 803-813. doi:10.1113/jphysiol.2005.092924

Vo, N., Klein, M. E., Varlamova, O., Keller, D. M., Yamamoto, T., Goodman, R. H., & Impey, S. (2005). A cAMP-response element binding protein-induced microRNA regulates neuronal morphogenesis. *Proc Natl Acad Sci U S A, 102*(45), 16426-16431. doi:10.1073/pnas.0508448102

Voorhees, R. M., & Ramakrishnan, V. (2013). Structural basis of the translational elongation cycle. *Annu Rev Biochem, 82*, 203-236. doi:10.1146/annurev-biochem-113009-092313

Wang, E. T., Sandberg, R., Luo, S., Khrebtukova, I., Zhang, L., Mayr, C., . . . Burge, C. B. (2008). Alternative isoform regulation in human tissue transcriptomes. *Nature, 456*(7221), 470-476. doi:10.1038/nature07509

Wang, H., Iacoangeli, A., Lin, D., Williams, K., Denman, R. B., Hellen, C. U., & Tiedge, H. (2005). Dendritic BC1 RNA in translational control mechanisms. *J Cell Biol, 171*(5), 811-821. doi:10.1083/jcb.200506006

Wang, H., Iacoangeli, A., Popp, S., Muslimov, I. A., Imataka, H., Sonenberg, N., . . . Tiedge, H. (2002). Dendritic BC1 RNA: functional role in regulation of translation initiation. *J Neurosci, 22*(23), 10232-10241. doi:10.1523/jneurosci.22-23-10232.2002

Wang, M., Hou, J., Müller-McNicoll, M., Chen, W., & Schuman, E. M. (2019). Long and Repeat-Rich Intronic Sequences Favor Circular RNA Formation under Conditions of Reduced Spliceosome Activity. *iScience, 20*, 237-247. doi:10.1016/j.isci.2019.08.058

Wang, R. Y., Phang, R. Z., Hsu, P. H., Wang, W. H., Huang, H. T., & Liu, I. Y. (2013). In vivo knockdown of hippocampal miR-132 expression impairs memory acquisition of trace fear conditioning. *Hippocampus, 23*(7), 625-633. doi:10.1002/hipo.22123

Wang, Y., Gogol-Döring, A., Hu, H., Fröhler, S., Ma, Y., Jens, M., . . . Chen, W. (2013). Integrative analysis revealed the molecular mechanism underlying RBM10-mediated splicing regulation. *EMBO Mol Med, 5*(9), 1431-1442. doi:10.1002/emmm.201302663

Weinberg, R. A., & Penman, S. (1968). Small molecular weight monodisperse nuclear RNA. *J Mol Biol, 38*(3), 289-304. doi:10.1016/0022-2836(68)90387-2

Westholm, J. O., Miura, P., Olson, S., Shenker, S., Joseph, B., Sanfilippo, P., . . . Lai, E. C. (2014). Genome-wide analysis of drosophila circular RNAs reveals their structural and sequence properties and age-dependent neural accumulation. *Cell Rep, 9*(5), 1966-1980. doi:10.1016/j.celrep.2014.10.062

Wightman, B., Bürglin, T. R., Gatto, J., Arasu, P., & Ruvkun, G. (1991). Negative regulatory sequences in the lin-14 3'-untranslated region are necessary to generate a temporal switch during Caenorhabditis elegans development. *Genes Dev, 5*(10), 1813-1824. doi:10.1101/gad.5.10.1813

Wightman, B., Ha, I., & Ruvkun, G. (1993). Posttranscriptional regulation of the heterochronic gene lin-14 by lin-4 mediates temporal pattern formation in C. elegans. *Cell, 75*(5), 855-862. doi:10.1016/0092-8674(93)90530-4

Will, C. L., & Lührmann, R. (2011). Spliceosome structure and function. *Cold Spring Harb Perspect Biol, 3*(7). doi:10.1101/cshperspect.a003707

Wimberly, B. T., Brodersen, D. E., Clemons, W. M., Jr., Morgan-Warren, R. J., Carter, A. P., Vonrhein, C., . . . Ramakrishnan, V. (2000). Structure of the 30S ribosomal subunit. *Nature, 407*(6802), 327-339. doi:10.1038/35030006

Yamagata, M., Sanes, J. R., & Weiner, J. A. (2003). Synaptic adhesion molecules. *Curr Opin Cell Biol, 15*(5), 621-632. doi:10.1016/s0955-0674(03)00107-8

Yang, Y., Fan, X., Mao, M., Song, X., Wu, P., Zhang, Y., . . . Wang, Z. (2017). Extensive translation of circular RNAs driven by N(6)-methyladenosine. *Cell Res, 27*(5), 626-641. doi:10.1038/cr.2017.31

Yang, Y., Shu, X., Liu, D., Shang, Y., Wu, Y., Pei, L., . . . Lu, Y. (2012). EPAC null mutation impairs learning and social interactions via aberrant regulation of miR-124 and Zif268 translation. *Neuron, 73*(4), 774-788. doi:10.1016/j.neuron.2012.02.003

Yekta, S., Shih, I. H., & Bartel, D. P. (2004). MicroRNA-directed cleavage of HOXB8 mRNA. *Science, 304*(5670), 594-596. doi:10.1126/science.1097434

Yeo, G., & Burge, C. B. (2004). Maximum entropy modeling of short sequence motifs with applications to RNA splicing signals. *J Comput Biol, 11*(2-3), 377-394. doi:10.1089/1066527041410418

Yeo, G., Holste, D., Kreiman, G., & Burge, C. B. (2004). Variation in alternative splicing across human tissues. *Genome Biol, 5*(10), R74. doi:10.1186/gb-2004-5-10-r74

You, X., Vlatkovic, I., Babic, A., Will, T., Epstein, I., Tushev, G., . . . Chen, W. (2015). Neural circular RNAs are derived from synaptic genes and regulated by development and plasticity. *Nat Neurosci, 18*(4), 603-610. doi:10.1038/nn.3975

Yu, C. Y., Li, T. C., Wu, Y. Y., Yeh, C. H., Chiang, W., Chuang, C. Y., & Kuo, H. C. (2017). The circular RNA circBIRC6 participates in the molecular

circuitry controlling human pluripotency. *Nat Commun, 8*(1), 1149. doi:10.1038/s41467-017-01216-w

Yusupov, M. M., Yusupova, G. Z., Baucom, A., Lieberman, K., Earnest, T. N., Cate, J. H., & Noller, H. F. (2001). Crystal structure of the ribosome at 5.5 A resolution. *Science, 292*(5518), 883-896. doi:10.1126/science.1060089

Zalfa, F., Giorgi, M., Primerano, B., Moro, A., Di Penta, A., Reis, S., . . . Bagni, C. (2003). The fragile X syndrome protein FMRP associates with BC1 RNA and regulates the translation of specific mRNAs at synapses. *Cell, 112*(3), 317-327. doi:10.1016/s0092-8674(03)00079-5

Zamecnik, P. C., & Keller, E. B. (1954). Relation between phosphate energy donors and incorporation of labeled amino acids into proteins. *J Biol Chem, 209*(1), 337-354.

Zhang, X. O., Wang, H. B., Zhang, Y., Lu, X., Chen, L. L., & Yang, L. (2014). Complementary sequence-mediated exon circularization. *Cell, 159*(1), 134-147. doi:10.1016/j.cell.2014.09.001

Zhang, Y., Xue, W., Li, X., Zhang, J., Chen, S., Zhang, J. L., . . . Chen, L. L. (2016). The Biogenesis of Nascent Circular RNAs. *Cell Rep, 15*(3), 611-624. doi:10.1016/j.celrep.2016.03.058

Zheng, G., Cochella, L., Liu, J., Hobert, O., & Li, W. H. (2011). Temporal and spatial regulation of microRNA activity with photoactivatable cantimirs. *ACS Chem Biol, 6*(12), 1332-1338. doi:10.1021/cb200290e

Zhong, J., Zhang, T., & Bloch, L. M. (2006). Dendritic mRNAs encode diversified functionalities in hippocampal pyramidal neurons. *BMC Neurosci, 7*, 17. doi:10.1186/1471-2202-7-17

Zhou, Z., Licklider, L. J., Gygi, S. P., & Reed, R. (2002). Comprehensive proteomic analysis of the human spliceosome. *Nature, 419*(6903), 182-185. doi:10.1038/nature01031

Ziv, N. E., & Garner, C. C. (2004). Cellular and molecular mechanisms of presynaptic assembly. *Nat Rev Neurosci, 5*(5), 385-399. doi:10.1038/nrn1370

Zivraj, K. H., Tung, Y. C., Piper, M., Gumy, L., Fawcett, J. W., Yeo, G. S., & Holt, C. E. (2010). Subcellular profiling reveals distinct and developmentally regulated repertoire of growth cone mRNAs. *J Neurosci, 30*(46), 15464-15478. doi:10.1523/jneurosci.1800-10.2010

Zovoilis, A., Agbemenyah, H. Y., Agis-Balboa, R. C., Stilling, R. M., Edbauer, D., Rao, P., . . . Fischer, A. (2011). microRNA-34c is a novel target to treat dementias. *Embo j, 30*(20), 4299-4308. doi:10.1038/emboj.2011.327

APPENDICES

A. LIST OF FIGURES

B. LIST OF TABLES

C. ABBREVIATIONS

ACSF	Artificial cerebrospinal fluid
ActB	Beta actin
AMPA	α-amino-3-hydroxy-5-methyl-4-isoxazolepropionic acid
ATP	Adenosine triphosphate
ATP5I	ATP synthetase membrane subunit
BDNF	Brain-derived neurotrophic facto
CA	Cornu ammonis
Camk2a	Ca^{2+}/calmodulin-dependent kinase alpha subunit
cDNA	complementary DNA
ciRNA	Circular RNA
CNS	Central nervous system
CREB	cAMP response element-binding protein
CTD	Carboxy terminal domain
DAPI	4′,6-Diamidin-2-phenylindol
DG	Dentate gyrus
DMSO	Dimethyl sulfoxide
DNA	Deoxyribonucleic acid
EC	Entorhinal cortex
EEA1	early endosome antigen 1
EM	Electron microcopy
EPSC	Excitatory postsynpatic current
FAM	Fluorescein amidites
FC	Fold change
FDR	False discovery rate
FISH	Fluorescence *in situ* hybridization
FPKM	Fragments per kilobase million
GABA	γ-aminobutyric acid
hnRNA	Heterogeneous nuclear RNA

hnRNP	Heterogeneous nuclear ribonucleoprotein
IPSC	Inhibitory postsynaptic current
L-LTP	Late long-term depression
LAMP1	lysosomal-associated membrane protein 1
LNA	Locked nucleic acid
lncRNA	long noncoding RNA
LTD	Long-term depression
LTP	Long-term potentiation
MEF2	Myocyte enhancer factor-2
mEPSC	Mini excitatory postsynaptic current
mGluR	Metabotropic glutamate receptor
miRNA	micro RNA
mRNA	Messenger RNA
mRNP	messenger ribonucleoproteins
ncRNA	Non-coding RNA
NMDA	N-Methyl-d-aspartic acid
P-body	Processing body
PABP1	poly(A)-binding protein 1
PBS	Phosphate-buffered saline
PC-linker	Photo-cleavable linker
PCR	Polymerase chain reaction
PFA	Paraformaldehyd
piRNA	PIWI-associated RNA
PSD	Post-synaptic density
Puro-PLA	Puromycin proximity ligation assay
qRT-PCR	Quantitative real-time PCR
RBP	RNA-binding protein
RISC	RNA-induced silencing complex
RNA	Ribonucleic acid
RNAi	RNA interference
RP	Retinitis pigmentosa

rRNA	Ribosomal RNA
S	Subiculum
SEM	Standard error of the mean
SG	Stress granules
SH3 domain	SRC Homology 3 Domain
SMA	Spinal muscular atrophy
SMN	Survival of motor neuron
SNARE	Snap receptor
snoRNA	Small nucleolar RNA
snRNA	Small nuclear RNA
snRNP	small nuclear ribonucleoproteins
STAR	Spliced transcripts alignment to a reference
TBS	Tris-buffered saline
TPM	Transcript per million
tRNA	Transfer RNA
TTO	Total transcriptional output
UTR	Untranslated region
VGCC	Voltage-gated calcium channel
Xist	X-inactive-specific transcript RNA

D. CURRICULUM VITAE

Mantian Wang

Max Planck Institute for Brain Research
Max-von-Laue-Str. 4, 60438 Frankfurt, Germany
mantian.wang@brain.mpg.de | D.O.B: 22.02.1989
Nationality: Austrian

EDUCATION AND RESEARCH EXPERIENCE

Since 2015	**Max Planck Institute for Brain Research, Frankfurt, Germany** Ph.D. Student Group of Prof. Erin M. Schuman, Department of Synaptic Plasticity Topic: Role of circular and micro RNAs in the establishment and maintenance of synaptic plasticity in hippocampal neurons.
2011 – 2015	**University of Vienna, Austria** **M.Sc. in Molecular Biology** | Major in Neuroscience *Obtained with highest honors* Faculty of Life Sciences
2013 – 2014	**Max Planck Institute for Brain Research, Frankfurt, Germany** Master's thesis Group of Prof. Erin M. Schuman, Department of Synaptic Plasticity Topic: Expression of long non-coding RNAs in neuronal compartments and their role in homeostatic plasticity.
2013	**Max F. Perutz Laboratories (MFPL), Vienna** Research internship Group of Prof. Johann Rotheneder, Department of Medical Biochemistry Topic: Effect of nuclear phosphor-protein EAPP on cell proliferation and cell cycle arrest.
2012	**Max F. Perutz Laboratories (MFPL), Vienna** Research internship Group of Prof. Roland Foisner, Department of Medical Biochemistry Topic: Role of LEM-domain proteins on nuclear structure and DNA damage repair.

2007 – 2011 **University of Vienna, Austria**
B.Sc. in Biology | Major in Microbiology and Genetics
Faculty of Life Sciences

1999 – 2007 **Bundesgymnasium Werndlpark Steyr**
Matura | Focus on Biology and English
Obtained with highest honors

PUBLICATIONS

Wang M, Hou J, Müller-McNicoll M, Chen W, Schuman EM. Long and repeat-rich intronic sequences favor circRNA formation under conditions of reduced spliceosome activity. *iScience* 2019

Poorthuis RB, Muhammad K, **Wang M**, Verhoog MB, Junek S, Wrana A, Mansvelder HD and Letzkus JJ. Rapid neuromodulation of Layer 1 interneurons in human neocortex. *Cell Reports* 2018

You X*, Vlatkovic I*, Babic A*, Will T*, Epstein I*, Tushev G*, Akbalik G*, **Wang M**, Glock C, Quedenau C, Wang X, Hou J, Liu H, Sun W, Sambandan S, Chen T, Schuman EM, Chen W. Neural circular RNAs are derived from synaptic genes and regulated by development and plasticity. *Authors contributed equally, *Nature Neuroscience* 2015

CONFERENCES AND COURSES

2019 Society for Neuroscience Meeting, Chicago, United States – Poster: "Spatio-temporal dynamics of miRNA-mediated regulation of local protein synthesis"

2019 WireUp Symposium, Max Planck Institute of Neurobiology, Martinsried, Germany – Poster: "Long and repeat-rich intronic sequences favor circRNA formation under conditions of reduced spliceosome activity"

2018 MPI Brain Research Retreat, Oberwesel, Germany

2016 EMBL Course, Heidelberg, Germany – "Analysis and Integration of Transcriptome and Proteome data"

2015 The EMBO Conference on RNA localization and local translation, Hersonissos, Greece – Poster: "Regulation of alternative splicing in rat hippocampal neurons"

2015 FELASA B Course, Frankfurt, Germany